

System Identification, Design and Flight Testing H_∞ Controllers for Heave Dynamics of RUAV

Manuel Keppler



Die approbierte Originalversion dieser Diplom-/
Masterarbeit ist in der Hauptbibliothek der Tech-
nischen Universität Wien aufgestellt und zugänglich.

<http://www.ub.tuwien.ac.at>



The approved original version of this diploma or
master thesis is available at the main library of the
Vienna University of Technology.

<http://www.ub.tuwien.ac.at/eng>

DIPLOMARBEIT

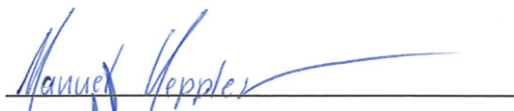
SYSTEM IDENTIFICATION, DESIGN AND FLIGHT TESTING H-INFINITY CONTROLLERS FOR HEAVE DYNAMICS OF RUAV

Freigabe:

Der Bearbeiter:


Unterschriften

Manuel Keppler



Betreuer:

Dr. Konstantin Kondak



Der Institutsdirektor

Dr. Alin Albu-Schäffer



Dieser Bericht enthält 125 Seiten, 44 Abbildungen und 9 Tabellen

Die approbierte Originalversion dieser Diplom-/Masterarbeit ist in der Hauptbibliothek der Technischen Universität Wien aufgestellt und zugänglich.

<http://www.ub.tuwien.ac.at>



The approved original version of this diploma or master thesis is available at the main library of the Vienna University of Technology.

<http://www.ub.tuwien.ac.at/eng>

Diplomarbeit

System Identification, Design and Flight Testing of H_∞ Controllers for Heave Dynamics of RUAV

ausgeführt zum Zwecke der Erlangung des akademischen Grades eines
Diplom-Ingenieurs
unter der Leitung von

Univ. Prof. Dr. Stefan Jakubek
E325 Institut für Mechanik und Mechatronik
Regelungstechnik und Prozessautomatisierung

eingereicht an der Technischen Universität Wien

Fakultät für Maschinenwesen und Betriebswissenschaften

von

Manuel Keppler
Matr. Nr.: 0406126
Tannenbergstr. 3
82234 Wessling

Wien, am November 30, 2014

Manuel Keppler

SYSTEM IDENTIFICATION, DESIGN AND FLIGHT TESTING OF H_∞ CONTROLLERS FOR HEAVE DYNAMICS OF RUAV

MANUEL KEPPLER



November 2014 – version 1.0

ABSTRACT

Focus of this thesis was the improvement of the vertical flight performance of the small-scaled, unmanned, autonomous DLR helicopters HE-1 and HE-2 by employing an advanced model-based controller. The success of the final design was to be analyzed in flight experiments and benchmarked against the original flight controller.

We cover the development of a basic three rigid body model for the helicopter HE-1. The heave (vertical) dynamics of the mechanical model was extended by the aerodynamic effect called *heave dampening*. Unknown parameters of the heave dynamics model were determined with the *Prediction Error Minimization* (PEM) system identification method. Necessary flight data was recorded in specially designed test flights.

The decision for the controller concept was made in favor of H_∞ control due to its desirable characteristics, such as MIMO capability and its *robustness* performance for systems subject to (parameter) uncertainties and external disturbances. Based on the final heave dynamics model, various H_∞ controller designs, such as (i) *S/KS/T mixed sensitivity optimization*, (ii) *signal-based H_∞ control*, (iii) *1 degree-of-freedom loop shaping design*, (iv) *2 degree-of-freedom loop shaping design* were realized and compared in simulation. The most promising design (iv) was then implemented on the HE-2 on-board flight controller and benchmarked in flight experiments versus the original cascaded PID controller. Based on the analyzed data, suggestions on how to further improve the controller are given.

ACKNOWLEDGMENTS

I would like to thank Dr. Konstantin Kondak for giving me the unique opportunity to write my master thesis at the Robotics and Mechatronics Center (RMC) at the German Space and Aerospace Center (DLR) in Oberpfaffenhofen. I would furthermore like to thank my colleagues of the DLR Flying Robots team who made my stay enjoyable and for all the support they provided. It was a pleasure to work with all of you! Thanks also go to Grob Aircraft AG who provided us with the opportunity to perform test flights on their airfield.

I am equally grateful to Prof. Jakubek for giving the opportunity to work at the Christian Doppler Laboratory for Model Based Calibration Methodologies and supporting me in writing my Master Thesis at the DLR.

Many thanks go to Prof. Schmiedmayer and Prof. Plöchl for giving me the opportunity to work as mechanics tutors for several years throughout my studies, which helped consolidating my mechanics knowledge immensely and gave me valuable experience in teaching. Last but not least I enjoyed assisting other students a lot.

I also want to thank Alexander Schirrer who gave me invaluable support during my bachelor thesis, projects works etc. and always took the time for in-depth discussions about control theory.

My parents who supported me unconditionally throughout my entire studies deserve the highest gratitude. Dear V. Gavino, I want to thank you for the sacrifices you made so I could afford to spend time to complete my studies.

CONTENTS

1	INTRODUCTION	1
1.1	Challenges	1
1.2	Mechanical Model	3
i	MODELING	5
2	KINEMATICS	7
2.1	Coordinate Systems	7
2.1.1	Inertial Frame (Earth Frame)	7
2.1.2	Body Frame	7
2.2	Attitude Description	9
2.2.1	Coordinate System Transformation	9
3	DYNAMICS	11
3.1	Preliminaries	11
3.1.1	Generalized Coordinates	11
3.1.2	Generalized Velocities	12
3.1.3	System Description	12
3.1.4	Kinematic equations	15
3.1.5	Kane's Equations of Motion	16
3.2	Kane's Method	18
3.2.1	Non-Contributing Forces	19
3.2.2	Contributing Forces	19
3.3	Step-by-Step Procedure to Construct Kane's Dynamical Equation	19
3.4	Estimating the Contribution of each Component of the Mechanical Model	21
3.4.1	Conclusion	23
3.5	Equations of Motion	23
3.6	Linearization	26
3.6.1	Linearization about an arbitrary Trim State	26
3.7	Heave Dynamics	30
3.7.1	Change in Angle of Attack due to Induced Inflow v_i	32
3.7.2	Ground Effect	34
3.7.3	Analytical Determination of Z_w	34
3.7.4	Interpretation of the Heave Dampening Derivative Z_w	35
3.7.5	Z_w and its Relation to Vertical Gust Response in hover	37
3.7.6	Vertical Gust Response in Forward Flight	37
3.7.7	Modeling Vertical Wind Disturbance	38
3.8	Scaling	38
4	SYSTEM IDENTIFICATION	41
4.1	Frequency-Domain System Identification	42

ii	CONTROL	45
5	MATHEMATICAL PRELIMINARIES	47
5.1	Gain of a System $G(s)$	47
5.1.1	Measuring the Gain of MIMO Systems	47
5.2	Singular Values	48
5.2.1	Singular Value Decomposition	48
5.2.2	Role of Singular Values in Control Theory	49
5.2.3	Singular Values as a Measure for Performance	50
5.3	\mathcal{H}_∞ norm	51
5.3.1	Definition	51
5.3.2	Interpretation	52
6	H INFINITY CONTROL	53
6.1	Design Goals and Trade-offs in MIMO Feedback Design	53
6.1.1	Closed Loop Transfer Functions	53
6.2	Closed Loop Stability	54
6.3	Performance Criteria	55
6.3.1	Time Domain Performance	55
6.3.2	Frequency Domain Performance	56
6.3.3	Maximum Peak Performance Criteria	57
6.3.4	Trade-offs of Loop-shaping in terms of L	57
6.3.5	Trade-offs of Loop-shaping in Terms of Closed-Loop Transfer Functions	58
6.4	General Control Configuration	59
6.4.1	Closed Loop Transfer Function N	59
6.5	$S/KS/T$ Mixed Sensitivity Optimization	60
6.5.1	Weight Selection	62
6.5.2	Selection of W_U	63
6.5.3	Analysis of the Controller	64
6.6	Signal-based H_∞ Control	65
6.7	H_∞ loop-shaping design (1 DoF)	66
6.7.1	Shaped System G_s	67
6.7.2	Robust Stabilization	67
6.7.3	Plant Shaping and Final Controller	70
6.8	Two Degrees of Freedom Loop-Shaping Design	71
7	SIMULATION RESULTS (CONTROLLER COMPARISONS)	77
7.1	Simulink Model	77
7.1.1	Step Response	77
7.1.2	Disturbance Rejection	77
iii	FLIGHT EXPERIMENTS	83
8	FLIGHT EXPERIMENTS	85
8.1	Implementation of the H_∞ Controller into the existing Flight Controller	86
8.2	Results	86
8.3	Conclusion	90

iv	APPENDIX	91
A	MATHEMATICAL BACKGROUND	93
A.1	General H_∞ algorithm	93
A.2	Essentials of Linear System Theory	94
A.3	Coprime Factorization	94
A.4	Matrix Norm	95
B	FILE LIST	97
B.1	Maple	97
B.2	MATLAB	97
B.3	Simulink	98
	BIBLIOGRAPHY	99

LIST OF FIGURES

Figure 1	Helicopter HE-1 of the DLR Oberpfaffenhofen Flying Robots group	1
Figure 2	Helicopter HE-1 of the DLR Oberpfaffenhofen Flying Robots group	2
Figure 3	Ground reference frame: NED system (North, East, Down)	7
Figure 4	Exchange Figure or add source	8
Figure 5	Orientation problem	9
Figure 6	Forces, Torques, coordinate system	14
Figure 7	Turbine powered Flettner helicopter with spray attachment	23
Figure 8	Angle of attack, rotational and resultant relative wind, induced flow, [5]	32
Figure 9	Components of relative wind and how they affect the angle of attack [5]	33
Figure 10	Ground effect, [25]	34
Figure 11	Step response of $G_{w,\delta coll}(s)$	36
Figure 12	Step response of $G_{z,\delta coll}(s)$	36
Figure 13	Heave dampening derivative in forward flight, [25]	38
Figure 14	Pulse width modulated input signal	39
Figure 15	41
Figure 16	System Identification Results	43
Figure 17	Variation of Z_w about plus minus $\pm 20\%$ of its nominal value of 0.5 s^{-1} in equidistant intervals	44
Figure 18	Variation of Z_{θ_0} about plus minus $\pm 20\%$ of its nominal value of $-0.0230 \text{ m/s}^2/\text{ms}$ in equidistant intervals	44
Figure 19	Random variation of Z_w and Z_{θ_0} about plus minus $\pm 20\%$; of their nominal values	44
Figure 20	Standard 1 DoF feedback control system	54
Figure 21	General Control Configuration	59
Figure 22	$S/KS/T$ mixed-sensitivity optimization	60
Figure 23	Bode plots of weights for mixed sensitivity optimization	63
Figure 24	Singular value plot showing the results of the H_∞ mixed sensitivity controller design	65
Figure 25	Signal-based H_∞ control problem	66
Figure 26	1 DoF H_∞ loop-shaping setup	67
Figure 27	H_∞ robust stabilization of a normalized left coprime factor plant G	68
Figure 28	$M\Delta$ -structure for robust stability analysis	68
Figure 29	Singular value plots original plant G , the shaped plant G_s and the disturbance transfer function G_d	70

Figure 30	Singular value plots of the shaped plant G_s and the final loop transfer functions with their respective boundaries	71
Figure 31	2 DoF H_∞ loop-shaping design problem with pre-filter K_1 and feedback controller K_2	72
Figure 32	Singular value bode plots of the loop transfer function, the input/output sensitivity $S = (I - K_2G)^{-1}$ and input/output complementary sensitivity $K_2G(I - K_2G)^{-1}$	75
Figure 33	Simulink model for comparison of the different controller designs	78
Figure 34	Unit step response and control input, climbing 1 m .	79
Figure 35	Comparison of the disturbance rejection capabilities; output noise, wind disturbances	80
Figure 36	Temporal course of $ e ^2$ and the MSE. The helicopter system is affected by output noise and wind disturbances	81
Figure 37	Test flight of HE-2 with controller version FE03 . .	85
Figure 38	General scheme of the helicopter control [18] . . .	86
Figure 39	Flight Experiments with original PID controller . .	87
Figure 40	Flight Experiments with H_∞ controller (FE02) . . .	88
Figure 41	Flight Experiments with H_∞ controller (FE03) . . .	89
Figure 42	MSE overall	89
Figure 43	MSE in hovering	89
Figure 44	Autonomous helicopter with 7 DoF manipulator . .	90

LIST OF TABLES

Table 1	Generalized coordinates and velocities	13
Table 2	Trade-offs in feedback control in terms of open-loop objectives L and K	57
Table 3	Trade-offs in feedback control in terms of closed-loop transfer functions	58
Table 4	Performance parameters of the H_∞ mixed sensitivity design	64
Table 5	Parameters of the desired heave dynamics response	73
Table 6	Comparison of the disturbance and output noise rejection capabilities of the different controller designs in terms of MSE and maximum squared error. Simulation time: 100 s.	82
Table 7	Performance comparison of different H_∞ -optimization based controller designs. * indicates that $\gamma = \gamma_{min}$. .	82

Table 8	Design parameters for the H_∞ 2 DoF controllers used in flight experiments	87
Table 9	Flight performance in terms of mean squared errors (MSE)	89

PREFACE

A short overview of the notation used, which is mostly consistent with that in Jazar [13].

- Bold lower case letters indicate vectors, e.g.:

r

- Bold uppercase letters indicate matrices, e.g.:

J

- Calligraphic letters denote coordinate frame, e.g:

\mathcal{N} Earth-fixed coordinate frame \mathcal{N}

- Right subscript on a transformation matrix denotes the *departure* frame and the left superscript the *destination* frame

${}^A\mathbf{T}_B$ Transformation matrix from frame \mathcal{B}
to frame \mathcal{A}

- Left superscript on a vector denotes the frame in which the vector is expressed, e.g.:

${}^N\mathbf{r}$ position vector \mathbf{r} expressed in frame \mathcal{N}

in other words, the vector is described as a linear combination of the respective frames basis vectors e.g.:

$${}^N\mathbf{r} = r_1\mathbf{n}_1 + r_2\mathbf{n}_2 + r_3\mathbf{n}_3$$

- First right subscript letter denotes the tip point of a position vector, e.g.:

${}^N\mathbf{r}_C$ position of point C ,
expressed in frame \mathcal{N}

- Second right subscript letters denote the shaft point of a position vector, e.g.:

${}^N\mathbf{r}_{CD}$ position vector pointing from D to C ,
expressed in frame \mathcal{N}

if the vector points from the origin of a frame it is expressed in, the second letter will be left out, e.g:

${}^N\mathbf{r}_C$ position vector pointing from origin of \mathcal{N} to C ,
expressed in \mathcal{N}

- Left subscript on a velocity vector denotes the frame the velocity is measured with respect to, e.g.:

$${}^N_B \mathbf{v}_P \quad \begin{array}{l} \text{velocity of point } P \\ \text{with respect to frame } \mathcal{B}, \\ \text{expressed in frame } \mathcal{N} \end{array}$$

- Right subscript on a angular velocity vector denotes the frame it is referred to, e.g.:

$${}^N \omega_B \quad \begin{array}{l} \text{angular velocity of frame } \mathcal{B}, \\ \text{expressed in frame } \mathcal{N} \end{array}$$

- Left subscript on a angular velocity vector denotes the frame the angular velocity is measured with respect to, e.g.:

$${}^N_{B_2} \omega_{B_1} \quad \begin{array}{l} \text{angular velocity of frame } \mathcal{B}_1 \\ \text{with respect to frame } \mathcal{B}_2, \\ \text{expressed in frame } \mathcal{N} \end{array}$$

- The left superscript on derivative operators indicates the frame in which the derivative of the variable is taken, e.g.:

$$\frac{{}^N d_N}{dt} \mathbf{r}_A$$

NOTATION

HELICOPTER

α_0	main rotor blade lift curve slope (1/rad)
A_b	blade area
A_d	rotor disc area
\mathcal{B}	fuselage-fixed frame
$\mathbf{b}_1, \mathbf{b}_2, \mathbf{b}_3$	basis vectors of coordinate frame \mathcal{B} (also denoted by $\mathbf{X}, \mathbf{Y}, \mathbf{Z}$)
C	center of gravity of the entire helicopter
C_F	center of gravity of the fuselage
C_{MR}	center of gravity of the main rotor (also denoted as MR)
C_T	lift coefficient
C_{TR}	center of gravity of the tail rotor (also denoted as TR)
F_{MR}	rotor thrust of main rotor
F_{TR}	rotor thrust of tail rotor
g	acceleration due to gravity (m/s^2)
I_{xx}, I_{yy}, I_{zz}	fuselage fixed axes x, y and z (kg m^2)
λ_i	induced downwash
\mathcal{N}	earth-fixed inertial frame
$\mathbf{n}_1, \mathbf{n}_2, \mathbf{n}_3$	basis vectors of coordinate frame \mathcal{N} (also denoted by $\mathbf{x}, \mathbf{y}, \mathbf{z}$)
ω	rpm of the main rotor
p, q, r	angular velocity components of helicopter about fuselage fix axes x, y and z (rad/s)
ρ	air density (kg/kg^3)
θ_0	main rotor collective pitch angle
θ_{0T}	tail rotor collective pitch angle
θ_{1s}	longitudinal cyclic pitch
θ_{1c}	lateral cyclic pitch
$\mathbf{u}(t)$	control vector
u, v, w	translational velocity components of helicopter about fuselage fix axes x, y and z ; for linearized models p, q, r represent the deviations from the trim state ($\delta u \equiv u$), e.g. hovering state (m/s)
s	blade solidity
V_c	rotor climb velocity
V_d	rotor descent velocity
z_g	distance of ground below rotor (m)

CONTROL

A	system matrix
B	control matrix
C	output matrix
D	feedthrough matrix
G_d	disturbance transfer function
$G_{w,\delta coll}(s)$	transfer function from collective pitch input (PWM) to vertical velocity component w
$G_{z,\delta coll}(s)$	transfer function from collective pitch input (PWM) to height z
$\sigma(s)$	unit step in frequency domain
	collective pitch input
Z_{θ_0}	control sensitivity derivative
Z_w	Heave dampening derivative

ACRONYMS

CIFER	Comprehensive Identification from FrEQUENCY Responses
CAMRAD II	Comprehensive Analytical Model of Rotorcraft Aerodynamics
CoG	Center of Gravity
DoF	Degrees of Freedom
EoM	Equation of Motion
EV	Eigen Values
GM	Gain Margin
LSD	Loop Shaping Design
MSE	Mean Squared Error
PM	Phase Margin
PID	Proportional-Integral-Derivative
rpm	rounds per minute
RUAV	Rotor Craft UAV
UAV	Unmanned Aerial Vehicle

INTRODUCTION

1.1 CHALLENGES

Goal of this thesis was the improvement of the vertical flight performance of the unmanned, autonomous DLR helicopter HE-1 and HE-2, respectively, see figure 1. One major research field of the Flying Robots group at the DLR Oberpfaffenhofen is aerial manipulation, [11]. For the success of these missions the helicopters' set-point tracking performances are critical. Of utmost importance is the helicopter's capability to hover at constant height while interacting with objects on the ground. To achieve this, it was intended to develop model-based controller concepts for the heave dynamics, test them in simulation and benchmark the most promising candidate against the original flight controller in flight experiments. At first a basic three rigid bodies heli-



Figure 1: Helicopter HE-1 of the DLR Oberpfaffenhofen Flying Robots group

copter model was derived and then extended by heave dampening. Helicopter modeling is quite challenging. The underlying physical phenomena are complex and a plethora of couplings between the numerous subsystems make an engineer's life hard. Modeling the primary rotor dynamic effects of the main rotor, such as flapping, lead-lag and coning already requires complex models with plenty of parameters. What makes life even harder is the fact, that pure analytical approaches promise very little success. All reliable helicopter models that are used for the development of commercial flight controllers are derived with special simulation software such as CAMRAD II, these „raw“ models are then fine-tuned in an iterative process of flight testing and system identification for a vast array of different flight conditions, [24], [15], which covers a time span of years. That makes it clear that the model had to be kept simple, even though we were primarily interested in just the heave dynamics. Yet, it



Figure 2: Helicopter HE-1 of the DLR Oberpfaffenhofen Flying Robots group

had to be precise enough to achieve flight performance improvements with a model-based controller. The focus was set on extending the rigid-body model by heave dampening. The Prediction Error Minimization (PEM) system identification method was used to determine unknown parameters of the heave dynamics model, using log data of special test flights that were performed at the airfield of Grob Aircraft AG and at the DLR Oberpfaffenhofen area. The high vibrations that are inherent with airborne helicopters result in noisy velocity, and especially acceleration data. A lot of care has to be taken when fixing the IMUs on the helicopter. Good dampening and decoupling from the main frame is mandatory to gain any usable flight data.

The helicopters used are the HE-1 and HE-2 from DLR, Oberpfaffenhofen. Their mechanical parts are both based on a customized Maxi Joker 3. They mostly differ in on-board electronic components and battery capacity, nevertheless the total lift off weight is equal. As a result their flight behavior is expected to be similar, which is backed up by manual flight experience. Figure 1 shows helicopter HE-1 with an adapter on the bottom to pick up ground based robots. Figure 2 shows helicopter HE-2 with the additional battery packs mounted right under the main rotor. More information about the helicopters can be found in [Kondak et al. \[16\], \[18\], \[19\]](#).

Based on the heave dynamics model, several H_∞ control schemes, such as

- S/KS/T mixed sensitivity optimization
- signal-based H_∞ control
- 1 degree-of-freedom loop shaping design
- 2 degree-of-freedom loop shaping design

were realized and compared in simulation. The most promising design (2 DoF LSD) was then implemented on the HE-2 on-board flight controller and benchmarked in flight experiments versus the original *cascaded PID controller*. The H_∞ based approach was chosen due to its excellent robustness performance which is superior to that of other robust methods such as LQR techniques when it comes to parametric and unstructured uncertainties, [37]. The provided robustness performance to system models inherent parametric uncertainties, unmodeled uncertainties and external disturbances such

as wind gusts has made H_∞ a prominent choice in flight control design for helicopter control, [33]. The success of this method in real-life flight control application was shown by Postlethwaite and Yue [28], [27] and many others.

1.2 MECHANICAL MODEL

Helicopter HE-1 is approximated by three rigid bodies: fuselage, main and tail rotor.

FUSELAGE The fuselage with a mass of m_F is assumed to have a vertical plane of symmetry, therefore the entries I_{xy}, I_{yz} of its inertia tensor I_F are zero

$$I_F = \begin{bmatrix} I_{F_{xx}} & 0 & I_{F_{xz}} \\ 0 & I_{F_{yy}} & 0 \\ I_{F_{xz}} & 0 & I_{F_{zz}} \end{bmatrix}. \quad (1.1)$$

See chapter 2 for definition of the coordinate axes.

MAIN ROTOR The main rotor is modeled as a solid disc with a mass of $m_{MR} = 246.5$ g and a radius of $r_{MR} = 892$ mm.

The main reason behind this simplification is the fact that the rotational equation of motion becomes more compact, since the moment of inertia tensor of the main rotor becomes time-invariant with respect to the fuselage-fixed frame, see eq. (3.15).

TAIL ROTOR The tail rotor with a mass of $m_{TR} = 5$ g and a radius of $r_{TR} = 133$ mm is modeled in analog fashion to the main rotor.

The entire mass m of the fully equipped helicopter is given by:

$$m = m_F + m_{MR} + m_{TR} \quad (1.2)$$

and equals 101 N.

Part I

MODELING

"Helicopter vertical motion in hover is probably the simplest to analyze, but even here our simplifying approximations break down at higher frequencies and amplitudes, as unsteady aerodynamics, blade stall and rotor dynamic effects alter the details of the motion considerably."

— Gareth D. Padfield [25]

KINEMATICS

2.1 COORDINATE SYSTEMS

As it is common practice in the aerospace field, two reference frames are introduced to describe the position and orientation of the helicopter, including the earth-fixed inertial frame \mathcal{N} and the fuselage-fixed body frame \mathcal{B} .

2.1.1 Inertial Frame (Earth Frame)

The earth-fixed frame \mathcal{N} with the standard basis $\mathbf{n}_1, \mathbf{n}_2, \mathbf{n}_3$ is assumed to be inertial¹. Its origin O_N is located on the earth's local tangential surface at some arbitrary point. According to aeronautic convention the three axis are defined as follows:

- n_1 -axis pointing north
- n_2 -axis pointing east
- n_3 -axis positive towards the center of the earth

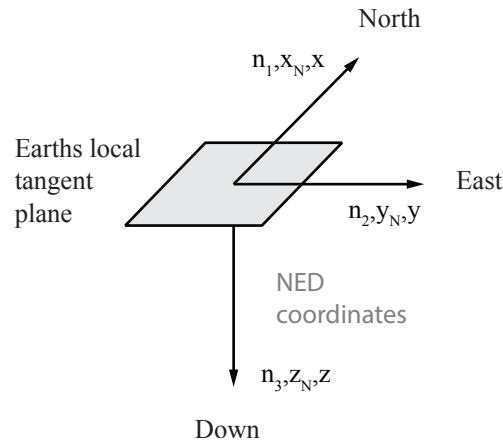


Figure 3: Ground reference frame: NED system (North, East, Down)

Often it is also referred to as NED (North, East, Down) system.

2.1.2 Body Frame

The origin O_B of the orthogonal body axes system \mathcal{B} , with basis vectors $\mathbf{b}_1, \mathbf{b}_2, \mathbf{b}_3$ ², is fixed at the center of gravity (cog) C of the entire helicopter.

¹ $\mathbf{n}_1, \mathbf{n}_2, \mathbf{n}_3$ and $\mathbf{x}, \mathbf{y}, \mathbf{z}$ are used interchangeably throughout this thesis

² $\mathbf{b}_1, \mathbf{b}_2, \mathbf{b}_3$ and $\mathbf{X}, \mathbf{Y}, \mathbf{Z}$ are used interchangeably throughout this thesis

The movement of the cog due to flapping of the rotor blades is neglected and a mean position relative to a particular trim state is assumed. Again, according to aeronautic convention the three axis are defined as follows:

- b_1 -axis positive out the nose of the aircraft in the plane of symmetry of the aircraft³
- b_3 -axis perpendicular to the b_1 -axis, in the plane of symmetry of the aircraft, positive below the aircraft
- b_2 -axis perpendicular to the b_1, b_3 -plane, positive determined by the right-hand rule (generally, positive out the right wing)

Any orientation of a rigid body can be achieved by three successive *elemental*⁴ rotations. In aeronautics three *intrinsic* rotations z, y', x'' are used to describe a change of orientation of an aircraft, with the following sequence of rotation:

1. rotation about the b_3 -axis by the *yaw* angle (ψ)
2. rotation about the first intermediary b_2 -axis by *pitch* angle (θ)
3. rotation about the 2nd intermediary b_1 -axis by *roll* angle (ϕ)

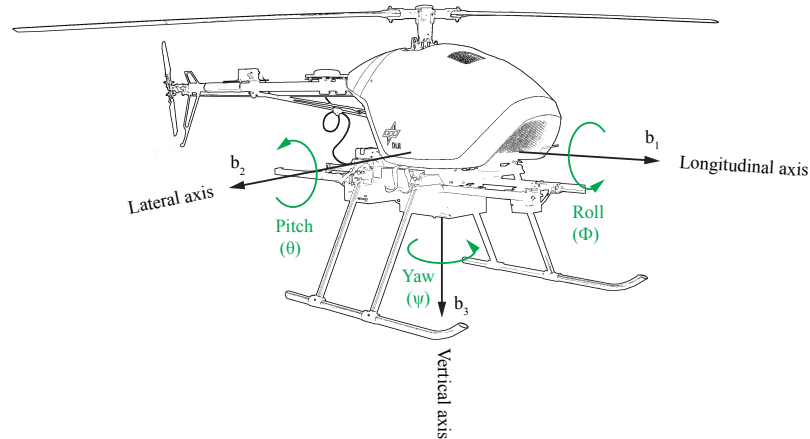


Figure 4: Body-fixed coordinate system

The angular velocity of a rotating frame (body) can be described by either an angular velocity vector or an angular velocity tensor. They can be derived from each other.

It is often easier to set up equations of motions by using a body frame to express certain vectors, especially when angular momentum or rotational kinetic energy are involved in the calculations, since the moment of inertia tensor is time invariant for rigid bodies when expressed in a body-fixed frame.

³ The helicopter HE-1 is assumed to be symmetric with respect to the b_1, b_3 -plane.

⁴ A rotation about one of the axes of a Coordinate system.

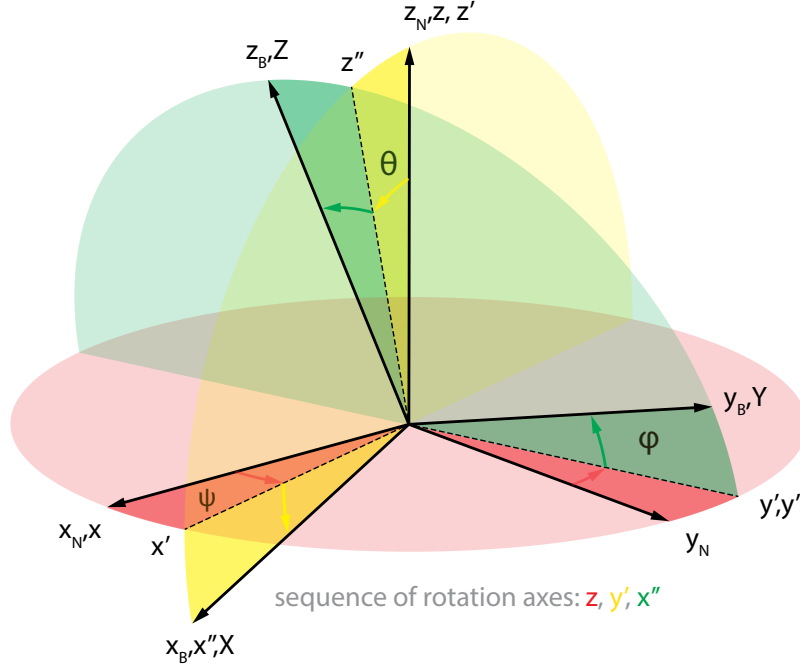


Figure 5: Orientation problem

2.2 ATTITUDE DESCRIPTION

The orientation of an aircraft is usually referred to as *attitude*. It can be described by the relative orientation of the aircraft-fixed frame to the earth frame, which will be used as the reference frame. In this thesis the relative orientation will be expressed with rotation matrices or Euler angles. A popular alternative form would be Quaternions (no gimbal lock problematics).

2.2.1 Coordinate System Transformation

To transform the Earth frame \mathcal{N} to the body frame we will use three intrinsic rotations z, y', x'' about the Euler angles ψ, θ, ϕ . Figure 5 visualizes this process. x', y', z' , with $z' = z_N$, denote the axes of the first intermediary frame which results from rotating the Earth Frame \mathcal{N} around the z_N -axis by the yaw angle ψ . Consecutive rotation about the y' axis by the pitch angle θ yields the second intermediary frame. x'', y'', z'' denote its axes, with $y'' = y'$. Finally, the body frame results by rotating the second intermediary frame around the x'' -axis by the roll angle ϕ .

The single, elemental yaw, pitch and roll rotations of the coordinate frames can also be described by the following rotation matrices:

$$\mathbf{R}_x(\phi) = {}^B\mathbf{R}_2(\phi) = \begin{bmatrix} 1 & 0 & 0 \\ 0 & \cos(\phi) & \sin(\phi) \\ 0 & \sin(\phi) & \cos(\phi) \end{bmatrix} \quad (2.1)$$

$$\mathbf{R}_y(\theta) = {}^2\mathbf{R}_1(\theta) = \begin{bmatrix} \cos(\theta) & 0 & -\sin(\theta) \\ 0 & 1 & 0 \\ \sin(\theta) & 0 & \cos(\theta) \end{bmatrix} \quad (2.2)$$

$$\mathbf{R}_z(\psi) = {}^1\mathbf{R}_N(\psi) = \begin{bmatrix} \cos(\psi) & \sin(\psi) & 0 \\ -\sin(\psi) & \cos(\psi) & 0 \\ 0 & 0 & 1 \end{bmatrix}. \quad (2.3)$$

Rotation matrices are orthogonal with determinant 1, i.e. its columns and rows are orthogonal unit vectors or equivalently $\mathbf{R}^T = \mathbf{R}^{-1}$ and $\det(\mathbf{R}) = 1$.

2.2.1.1 Transformations between frame \mathcal{N} and \mathcal{B}

By composing three elemental rotations (2.1)-(2.3) in the correct order, the resulting rotation matrix ${}^B\mathbf{R}_N$ – which again is orthogonal – describes the transformation from frame \mathcal{N} to \mathcal{B}

$$\begin{aligned} {}^B\mathbf{R}_N(\phi, \psi, \theta) &= {}^B\mathbf{R}(\phi) {}^2\mathbf{R}(\theta) {}^1\mathbf{R}(\psi)_N \\ &= \begin{bmatrix} c(\psi)c(\theta) & c(\theta)s(\psi) & -s(\theta) \\ c(\psi)s(\phi)s(\theta) - c(\phi)s(\psi) & c(\phi)c(\psi) + s(\phi)s(\psi)s(\theta) & c(\theta)s(\phi) \\ s(\phi)s(\psi) + c(\phi)c(\psi)s(\theta) & c(\phi)s(\psi)s(\theta) - c(\psi)s(\phi) & c(\phi)c(\theta) \end{bmatrix}. \end{aligned} \quad (2.4)$$

Transformation in the opposite direction can be achieved by pre-multiplying with

$$\begin{aligned} {}^N\mathbf{R}_B &= {}^B\mathbf{R}_N^{-1} = {}^B\mathbf{R}_N^T = \\ &= \begin{bmatrix} c(\psi)c(\theta) & c(\psi)s(\phi)s(\theta) - c(\phi)s(\psi) & s(\phi)s(\psi) + c(\phi)c(\psi)s(\theta) \\ c(\theta)s(\psi) & c(\phi)c(\psi) + s(\phi)s(\psi)s(\theta) & c(\phi)s(\psi)s(\theta) - c(\psi)s(\phi) \\ -s(\theta) & c(\theta)s(\phi) & c(\phi)c(\theta) \end{bmatrix}. \end{aligned} \quad (2.5)$$

Remark. Certain orientations cannot be uniquely represented by Euler Angles; so called *Gimbal lock* might occur. For the rotations above, this will happen when the pitch angle reaches the following values: $\theta = \pi/2 + n\pi$, $n \in \mathbb{Z}$.

Kane's method (sometimes called „Lagrange's form of d'Alembert's principle“, „Joudain's principle“, or the „principle of virtual power, “[12]) is employed to derive the helicopter's rigid body equations of motions.

The development in this chapter can be found in more detail in [14].

3.1 PRELIMINARIES

To employ Kanes Algorithm it is necessary to understand the meaning of generalized coordinates and speeds, kinematic constraints and kinematic motion equations. Therefore we start this chapter with an introduction to those concepts. Other important concepts are partial (angular) velocities and contributing and non-contributing forces, which will be introduced later in this chapter.

3.1.1 Generalized Coordinates

The configuration (position and orientation) of a system with a *dimension of configuration space* of p , consisting of N rigid bodies, can be completely described by a minimum set of p independent scalar values, the so called *independent generalized coordinates*

$$\mathbf{q} = [q_1, q_2, \dots, q_p]^T. \quad (3.1)$$

Sometimes, the configuration of a system can be described more conveniently with a non-minimum set of n *generalized coordinates*

$$\mathbf{q} = [q_1, q_2, \dots, q_n]^T. \quad (3.2)$$

3.1.1.1 Equations of Constraints

For $n > p$ a subset of these generalized coordinates are non-independent and kinematic relations in form of constraint equations describe their dependencies. The number of constraints μ depends on the number of generalized coordinates n and the total degrees of freedom (dimension of configuration space) p of the system

$$\mu = n - p. \quad (3.3)$$

Constraints of the form

$$f_j(q_1, q_2, \dots, q_n, t) = 0, \quad j = 1, \dots, \mu \quad (3.4)$$

are called *holonomic constraints*. If the constraints are dependent on the generalized coordinates and their first derivatives are non-integrable,

$$g_j(q_1, q_2, \dots, q_n, \dot{q}_1, \dot{q}_2, \dots, \dot{q}_n, t) = 0 \quad (3.5)$$

they are called first-order *non-holonomic* constraints.

3.1.2 Generalized Velocities

The motion of a system can be completely described by a minimum set of m independent scalars, the so called *independent generalized velocities*

$$\mathbf{u} = [u_1, u_2, \dots, u_m]^T. \quad (3.6)$$

They can always be expressed as functions η, κ of the generalized coordinates q_i and are linear in \dot{q}_i

$$u_j = \sum_{i=1}^n \eta_i(q_1, \dots, q_n) \dot{q}_i + \kappa_j(q_1, \dots, q_n), \quad j = 1, \dots, l. \quad (3.7)$$

The number of independent generalized velocities m will be denoted as the systems *degrees of freedom*.

3.1.2.1 Motion Constraints

For a non-minimal set of l generalized velocities $l - m$ *motion constraints* describe their dependencies. The generalized velocities can always be chosen such that the motion constraints f_i can be expressed as linear functions $\xi_{i,j}$ of the generalized speeds [17]

$$f_i(q_1, q_2, \dots, q_n, u_1, u_2, \dots, u_m, t) = \sum_{j=1}^m \xi_{i,j}(q_1, q_2, \dots, q_n, t) u_j = 0, \quad (3.8)$$

$$i = 1, \dots, l - m, \quad j = 1, \dots, l.$$

m is said to be the *controllable degrees of freedom* of the system. For holonomic systems the controllable is equal to the total degrees of freedom, i.e. $p = m$.

3.1.3 System Description

The helicopter is approximated to be composed of three rigid bodies; fuselage, main rotor and tail rotor. To completely describe the systems configuration and motion we introduce the following two sets of variables \mathbf{q} and \mathbf{u} . The robot is assumed to be able to move freely in space. Therefore six independent scalar values ($q_1 - q_6$) are needed to describe the pose of the fuselage. Two additional independent scalars are needed to describe the relative orientation of both rotors with respect to the fuselage (q_7, q_8).

- *generalized coordinates* \mathbf{q}

$$\begin{aligned} \mathbf{q} &= [q_1, q_2, q_3, q_4, q_5, q_6, q_7, q_8]^T \\ &= [x, y, z, \phi, \theta, \psi, \alpha, \beta]^T \end{aligned} \quad (3.9)$$

q_1, \dots, q_2	position of the center of gravity of the entire helicopter C , expressed in \mathcal{N}	${}^N\mathbf{r}_C = q_1\mathbf{n}_1 + q_2\mathbf{n}_2 + q_3\mathbf{n}_3$
$q_4 \dots q_6$	orientation of the fuselage with respect to frame \mathcal{N} (Euler angles)	see ${}^N\mathbf{T}_B$ in (2.4)
$u_1 \dots u_3$	translational vel. of C with respect to frame \mathcal{N} , expressed in \mathcal{N}	${}^N\mathbf{v}_B = u_1\mathbf{n}_1 + u_2\mathbf{n}_2 + u_3\mathbf{n}_3$
$u_4 \dots u_6$	rotational vel. of the fuselage with respect to earth frame \mathcal{N} , expressed in \mathcal{B}	${}^B_N\boldsymbol{\omega}_B = u_4\mathbf{b}_1 + u_5\mathbf{b}_2 + u_6\mathbf{b}_3$
α, β	angular pos. of the main and tail rotor relative to the fuselage	
$\dot{\alpha}, \dot{\beta}$	angular vel. of the main and tail rotor relative to the fuselage, expressed in frame \mathcal{B}	${}^B\boldsymbol{\omega}_{MR} = \dot{\alpha}\mathbf{b}_3, {}^B\boldsymbol{\omega}_{TR} = \dot{\beta}\mathbf{b}_3$

Table 1: Generalized coordinates and velocities

- and the *generalized speeds* \mathbf{u}

$$\begin{aligned}\mathbf{u} &= [u_1, u_2, u_3, u_4, u_5, u_6, u_7, u_8]^T \\ &= [u, v, w, p, q, r, \dot{\alpha}, \dot{\beta}]^T.\end{aligned}\quad (3.10)$$

Check figure 6 to see how they are defined. Table 1 summarizes their definitions.

The translational motion of the helicopter's combined center of gravity ${}^N\mathbf{v}_C$ is expressed in the Earth frame, which is advantageous when deriving the translational dynamics since the gravitational force has only a vertical component in \mathcal{N}

$${}^N\mathbf{v}_O = u_1\mathbf{n}_1 + u_2\mathbf{n}_2 + u_3\mathbf{n}_3 = \dot{q}_1\mathbf{n}_1 + \dot{q}_2\mathbf{n}_2 + \dot{q}_3\mathbf{n}_3. \quad (3.11)$$

In good accordance with reality the angular velocities of the two rotors are assumed to be constant, which eliminates the last two entries of \mathbf{u} .

We express the rotational motions of each of the three bodies ${}^B\boldsymbol{\omega}_i$ in Body frame \mathcal{B} .

$${}^B_N\boldsymbol{\omega}_B = p\mathbf{b}_1 + q\mathbf{b}_2 + r\mathbf{b}_3 \quad (3.12)$$

$${}^B_N\boldsymbol{\omega}_{MR} = p\mathbf{b}_1 + q\mathbf{b}_2 + (r + \dot{\alpha})\mathbf{b}_3 \quad (3.13)$$

$${}^B_N\boldsymbol{\omega}_{TR} = p\mathbf{b}_1 + (q + \dot{\beta})\mathbf{b}_2 + r\mathbf{b}_3 \quad (3.14)$$

Thereby, when deriving the rotational dynamics we can make advantage of the fact that the inertial tensors are time-invariant. Generally the inertial tensor of a body is only time-invariant when expressed in a frame fixed to it.

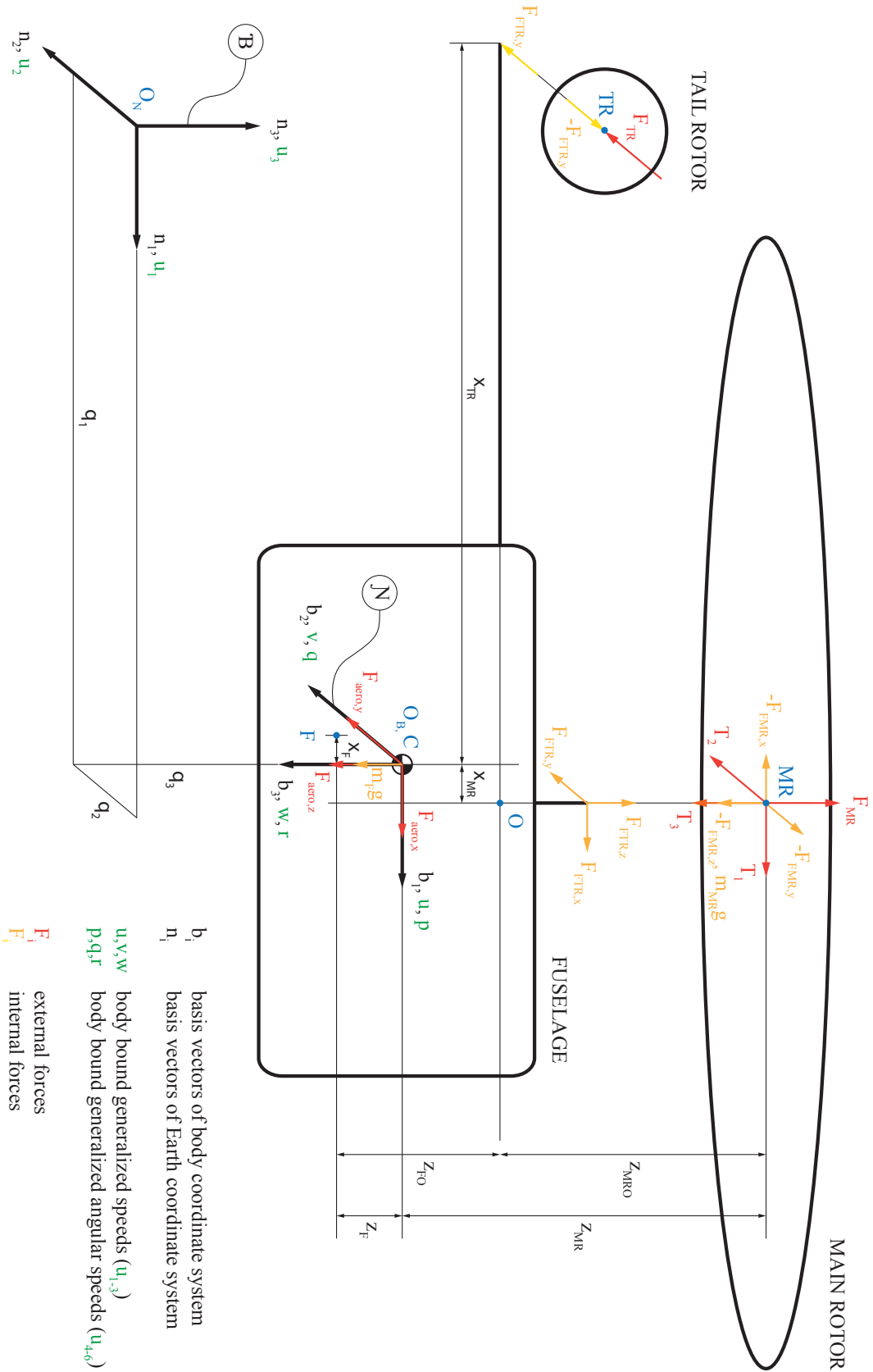


Figure 6: Forces, Torques, coordinate system

But in this case, the axes of rotation of the main rotor is fixed in \mathcal{B} and the moment of inertias about axes normal to its axis of rotation are equal – recall, we modeled the rotor as disc which is an axially symmetric body. Under these conditions the inertial tensor of the main rotor, expressed in \mathcal{B} , is time-variant. As a result the time derivative of the angular momentum simplifies to

$$\frac{{}^B d^B L_{MR}}{dt} = {}^B I_{MR} \frac{{}^B d_N^B \omega_{MR}}{dt},$$

which can be exploited when setting up Euler's equation. The same is true for the tail rotor. This simplifies the rotational dynamics significantly and is the main reason for modeling the rotor as described in section 1.2. The axial symmetry and time-invariant inertia tensors of the rotors result in equations of motions independent of α and β , see eq. (3.5)-(3.5). Therefore the last two entries of \mathbf{q} can be eliminated as well.

3.1.4 Kinematic equations

By solving equations (3.8) for \dot{q}_i we receive n linear equations for \dot{q}_i with respect to the generalized velocities u_j of the following form

$$\dot{q}_i = \sum_{j=1}^l \alpha_j(q_1, \dots, q_n) u_j + \beta_i(q_1, \dots, q_n), \quad i = 1, \dots, n \quad (3.15)$$

Note, the kinematic equations are always linear in generalized speeds and their number is dependent on the chosen set of generalized coordinates.

3.1.4.1 Kinematic Relations between the General Coordinates and the Linear and Rotational Generalized Velocities

We set up kinematic equations (compare eq. (3.15)) to relate the generalized velocities \mathbf{u} to the first order derivatives of the generalized coordinates. For the translational motion these relations are trivial

$${}^N \mathbf{v}_{O_B}^T = \begin{bmatrix} \mathbf{n}_1 & \mathbf{n}_2 & \mathbf{n}_3 \end{bmatrix} \begin{bmatrix} u \\ v \\ w \end{bmatrix} = \begin{bmatrix} \mathbf{n}_1 & \mathbf{n}_2 & \mathbf{n}_3 \end{bmatrix} \begin{bmatrix} \dot{q}_1 \\ \dot{q}_2 \\ \dot{q}_3 \end{bmatrix} = \dot{\mathbf{q}}_{trans}, \quad (3.16)$$

the same is true for u_7

$${}^B \omega_{MR} = \dot{q}_7 \mathbf{b}_3 = u_7 \mathbf{b}_3 \quad (3.17)$$

and u_8

$${}^B \omega_{TR} = \dot{q}_8 \mathbf{b}_3 = u_8 \mathbf{b}_3, \quad (3.18)$$

respectively.

Transformation of the Euler angular rates $\dot{\mathbf{q}}_{rot} = [\dot{\phi}, \dot{\theta}, \dot{\psi}]$ into \mathcal{B} and the generalized angular velocities p, q, r .

$${}^B_N\omega_B^T = \begin{bmatrix} \mathbf{b}_1 & \mathbf{b}_2 & \mathbf{b}_3 \end{bmatrix} \begin{bmatrix} p \\ q \\ r \end{bmatrix} = \begin{bmatrix} \dot{\phi} \\ 0 \\ 0 \end{bmatrix} + {}^B\mathbf{R}_2(\phi) \begin{bmatrix} 0 \\ \dot{\theta} \\ 0 \end{bmatrix} + {}^B\mathbf{R}_2(\phi) {}^2\mathbf{R}_1(\theta) \begin{bmatrix} 0 \\ 0 \\ \dot{\psi} \end{bmatrix}$$

which yields

$$\begin{bmatrix} p \\ q \\ r \end{bmatrix} = \underbrace{\begin{bmatrix} 1 & 0 & -\sin(\theta) \\ 0 & \cos(\phi) & \sin(\phi)\cos(\theta) \\ 0 & -\sin(\phi) & \cos(\phi)\cos(\theta) \end{bmatrix}}_{\mathbf{K}} \begin{bmatrix} \dot{\phi} \\ \dot{\theta} \\ \dot{\psi} \end{bmatrix}, \quad (3.19)$$

inversion of \mathbf{K} leads to

$$\begin{bmatrix} \dot{\phi} \\ \dot{\theta} \\ \dot{\psi} \end{bmatrix} = \underbrace{\begin{bmatrix} 1 & \sin(\phi)\tan(\theta) & \cos(\phi)\tan(\theta) \\ 0 & \cos(\phi) & -\sin(\phi) \\ 0 & \sin(\phi)/\cos(\theta) & \cos(\phi)/\cos(\theta) \end{bmatrix}}_{\mathbf{K}^{-1}} \begin{bmatrix} p \\ q \\ r \end{bmatrix}, \quad (3.20)$$

which relates the aircrafts local rotational rates to the Euler angular velocities. Matrix \mathbf{K}^{-1} makes the Gimbal lock problematics apparent. As expected, \mathbf{K} and \mathbf{K}^{-1} have unit matrix form for small Euler angles.

Now, we can relate the angular velocity vector ${}^B_N\omega_B$ to the Euler angular rates $\dot{\mathbf{q}}_{rot}$ by the following relation:

$${}^B_N\omega_B = \begin{bmatrix} \omega_x \\ \omega_y \\ \omega_z \end{bmatrix} = \mathbf{K} \dot{\mathbf{q}}_{rot} \quad (3.21)$$

And ${}^N_N\omega_B$ in terms of yaw-pitch-roll angular velocities equals:

$${}^N_N\omega_B = \begin{bmatrix} \omega_X \\ \omega_Y \\ \omega_Z \end{bmatrix} = {}^N\mathbf{R}_B \mathbf{K} \dot{\mathbf{q}}_{rot}. \quad (3.22)$$

Matrix \mathbf{K} as well as ${}^E\mathbf{R}_B\mathbf{K}$ are not/non orthogonal matrices. This is because the Euler angles frame is not an orthogonal basis.

3.1.5 Kane's Equations of Motion

This section presents a way to derive Kane's equations of motion via Newton's second law (3.23) and Euler's equations (3.26). First, a summary of both laws is given. One alternative way to arrive at Kane's equations is via *d'Alembert's principle*, see [Purushotham and J. \[29\]](#).

Theorem 3.1 (Newton's 2nd Law). *The translational equations of motion for a rigid body can be derived by Newton's second law:*

$${}^N\mathbf{F} = \frac{{}^N d {}^N \mathbf{p}}{dt} = m \frac{{}^N d {}^N \mathbf{v}}{dt} \quad (3.23)$$

expression in frame \mathcal{B} yields, [13]:

$${}^B\mathbf{F} = \frac{{}^B d {}^B \mathbf{p}}{dt} = m \frac{{}^B d {}^B \mathbf{v}}{dt} + {}^B_N \boldsymbol{\omega}_B \times {}^B \mathbf{v} \quad (3.24)$$

which states, the net force \mathbf{F} acting on a rigid body is equal to the temporal derivative of the body's linear momentum \mathbf{p} with respect to an inertial frame \mathcal{N} . ${}^N \mathbf{v}$ is the velocity of the body's center of gravity expressed in \mathcal{N} .

This law is also applicable to a mechanical multi body system whose center of gravity moves like a point mass with equal mass, see Jazar [13] for example. The resulting external force can be conveniently expressed in the body frame, but then has to be transformed into inertial frame \mathcal{N} .

$${}^N\mathbf{F} = {}^N\mathbf{R}_B {}^B\mathbf{F} \quad (3.25)$$

Theorem 3.2 (Euler's Equation's). *The rotational dynamics of a rigid body can be derived with Euler's Law*

$${}^N\mathbf{M}_A = \frac{{}^N d {}^N \mathbf{L}_A}{dt} + \mathbf{r}_{CA} \times m \mathbf{a}_A \quad (3.26)$$

where A is an arbitrary point on the body and C its center of gravity.

$${}^j\mathbf{L}_i = {}^j\mathbf{I}_i {}^j\boldsymbol{\omega}_j \quad (3.27)$$

denotes the angular momentum of the i -th body, expressed in frame j . Usually the inertia matrix can be more conveniently expressed in a body fixed frame, \mathcal{B} in this case, leading to

$${}^B\mathbf{M}_A = \frac{{}^B d {}^B \mathbf{L}_A}{dt} + {}^B_N \boldsymbol{\omega}_B \times {}^B \mathbf{L}_A + \mathbf{r}_{CA} \times m \mathbf{a}_A. \quad (3.28)$$

Choosing the center of mass m as reference point yields

$$\begin{aligned} {}^B\mathbf{M}_C &= \frac{{}^B d {}^B \mathbf{L}_C}{dt} + {}^B_N \boldsymbol{\omega}_B \times {}^B \mathbf{L}_C \\ &= {}^B\mathbf{I}_{CN} \dot{\boldsymbol{\omega}}_B + {}^B_N \boldsymbol{\omega}_B \times ({}^B\mathbf{I}_{CN} {}^B\boldsymbol{\omega}_B) \end{aligned} \quad (3.29)$$

since \mathbf{I} is constant in frame \mathcal{B} .

1 Equality is true under the assumption of constant mass.

3.2 KANE'S METHOD

First we set up the Euler equations and Newton's 2nd law for each body k . For each of the N bodies the respective center of mass C_k is chosen as point of reference. By post-multiplying these equations with vectors called *partial velocities* $\tilde{\mathbf{v}}_r^{C_k}$

$$\mathbf{F}_k^{C_k} \tilde{\mathbf{v}}_r^{C_k} = m_k \mathbf{a}_{C_k} \tilde{\mathbf{v}}_r^{C_k} \quad (3.30)$$

and *partial angular velocities* $\tilde{\boldsymbol{\omega}}_r^k$

$$\mathbf{T}_k^{C_k} \tilde{\boldsymbol{\omega}}_r^k = (\mathbf{I}_k \dot{\boldsymbol{\omega}}_k + \boldsymbol{\omega}_k \times (\mathbf{I}_k \boldsymbol{\omega}_k)) \tilde{\boldsymbol{\omega}}_r^k \quad (3.31)$$

we project those vector equations from \mathbb{R}^3 to \mathbb{R} . By superposing force (3.30) and moment equations (3.31) and summing up over all bodies we arrive at Kane's equations

$$\sum_k^N \left(\mathbf{F}_k^{C_k} \tilde{\mathbf{v}}_r^{C_k} + \mathbf{T}_k^{C_k} \tilde{\boldsymbol{\omega}}_r^k \right) = \sum_k^N \left(m_k \mathbf{a}_{C_k} \tilde{\mathbf{v}}_r^{C_k} + (\mathbf{I}_k \dot{\boldsymbol{\omega}}_k + \boldsymbol{\omega}_k \times (\mathbf{I}_k \boldsymbol{\omega}_k)) \tilde{\boldsymbol{\omega}}_r^k \right). \quad (3.32)$$

In total we get r scalar equations, one for each degree-of-freedom. We consider holonomic systems only, i.e. $p = m$.

Theorem 3.3 (Partial velocities and partial angular velocities [12]). *Consider a multi-body system of N interconnected rigid bodies whose kinematics is completely described by a set of generalized coordinates q_i and a set of generalized velocities u_r . The velocity of any body-fixed point of interest P and angular velocity of any body k can be expressed as follows*

$$\mathbf{v}^P = \sum_{r=1}^m \tilde{\mathbf{v}}_r^P u_r + \tilde{\mathbf{v}}_t^P, \quad (3.33)$$

$$\boldsymbol{\omega}^k = \sum_{r=1}^m \tilde{\boldsymbol{\omega}}_r^k u_r + \tilde{\boldsymbol{\omega}}_t^k, \quad (3.34)$$

where

$$\tilde{\mathbf{v}}_r^P, \quad r = 1, \dots, p$$

is denoted as *constrained partial velocities* and

$$\tilde{\boldsymbol{\omega}}_r, \quad r = 1, \dots, p$$

as the *constrained partial angular velocities*.

Definition 3.1 (Generalized active forces [14]). The scalar values on the left hand side for each of the p equations (3.32)

$$\tilde{F}_r = \sum_k^N \left(\mathbf{F}_k^{C_k} \tilde{\mathbf{v}}_r^{C_k} + \mathbf{T}_k^{C_k} \tilde{\boldsymbol{\omega}}_r^k \right), \quad r = 1, \dots, p \quad (3.35)$$

are denoted as *generalized active forces*.

Definition 3.2 (Generalized inertia forces [14]). The scalar values on the right hand side for each of the p equations (3.32)

$$\tilde{F}_r^* = \sum_k^N \left(m_k \mathbf{a}_{C_k} \tilde{\mathbf{v}}_r^{C_k} + (\mathbf{I}_k \dot{\boldsymbol{\omega}}_k + \boldsymbol{\omega}_k \times (\mathbf{I}_k \boldsymbol{\omega}_k)) \tilde{\boldsymbol{\omega}}_r^k \right), \quad r = 1, \dots, p \quad (3.36)$$

are denoted as *generalized inertia forces*.

Using the definitions above Kane's equations simplify to

$$\tilde{F}_r^*(q, u, \dot{u}, t) + \tilde{F}_r(q, u, t) = 0, \quad r = 1, \dots, p. \quad (3.37)$$

Remark. It is important to remember that $\mathbf{R}_k^{C_k}$ is the resultant force acting on the center of gravity of body k . Which means, in order to calculate the generalized active forces using equation (3.35) the actual load on each of the N bodies has to be transformed, to an equivalent one, by moving the points of action for all the forces acting on body k to its center of gravity C_k .

Similarly, $\mathbf{T}_k^{C_k}$ denotes the sum of all moments about the center of mass of body k and all torques acting on it.

3.2.1 Non-Contributing Forces

Definition 3.3. Some summands of sum (3.35) have zero contribution to the generalized forces. The corresponding forces $\mathbf{F}_k^{C_k}$ or torques $\mathbf{T}_k^{C_k}$ of these terms are denoted *non-contributing forces*. They can be neglected when setting up the equations of motions via Kane's method.

3.2.2 Contributing Forces

Definition 3.4. Forces and $\mathbf{F}_k^{C_k}$ and torques $\mathbf{T}_k^{C_k}$ that have a non-zero contribution to at least one of the generalized active forces are denoted as *contributing forces*.

Most *contact forces* such as reaction forces whose line of action are perpendicular to contact surfaces, static friction and rolling friction are non-contributing forces. One exception are sliding forces, which do contribute to the generalized active force.

Additionally, all forces whose points of attack have zero velocity with respect to an inertial frame are non-contributing, as well as torques acting on a body whose angular velocity relative to an inertial frame is zero.

3.3 STEP-BY-STEP PROCEDURE TO CONSTRUCT KANE'S DYNAMICAL EQUATION

1. **SYSTEM DESCRIPTION.** Define a set of generalized coordinates q_i ($i = 1, \dots, n$) and a set of independent generalized velocities u_j ($j = 1, \dots, p$) to completely describe the systems configuration and motion, see fig. 6.

2. KINEMATICS. Describe \dot{q}_i as functions of u_j and q_i by setting up n kinematic equations of motion, see 3.1.4.
3. CONTRIBUTING AND TORQUES. Define the points of action of all contributing forces. Express all contributing forces $\mathbf{F}_k^{P_i}$ and torques \mathbf{T}_k as functions of q_i and u_j
4. VELOCITIES & ACCELERATIONS. Determine the velocities \mathbf{v}^{C_k} and accelerations \mathbf{a}^{C_k} for each of the N bodies centers of gravity. For every contributing force $\mathbf{F}_k^{P_i}$, acting on a point P_i on body k , calculate the velocities \mathbf{v}^{P_i} for each of the points P_i .

- a) Write down the velocities \mathbf{v}^{C_k} in the form shown in eq. (3.33)

$$\mathbf{v}^{C_k} = \sum_{r=1}^m \tilde{\mathbf{v}}_r^{C_k} u_r + \tilde{\mathbf{v}}_t^{C_k}$$

and determine the linear vector coefficient of the generalized speeds u_j which correspond to the partial velocities $\tilde{\mathbf{v}}_r^{C_k}$, p in total.

- b) Write down the velocities \mathbf{v}^{P_i} in the form shown in eq. (3.33)

$$\mathbf{v}^{P_i} = \sum_{r=1}^m \tilde{\mathbf{v}}_r^{P_i} u_r + \tilde{\mathbf{v}}_t^{P_i}$$

and proceed as in the previous step to determine the partial velocities $\tilde{\mathbf{v}}_r^{P_i}$.

- c) The accelerations \mathbf{a}^{C_k} are of the form

$$\mathbf{a}^{C_k} = f(\mathbf{q}, t) \dot{\mathbf{u}} + g(\mathbf{q}, \mathbf{u}, t).$$

5. ANGULAR VELOCITIES & ACCELERATIONS. Determine the angular velocities $\boldsymbol{\omega}_k$ for each of the K bodies and express them as functions of q_i and u_j . Similarly, calculate the angular accelerations $\boldsymbol{\alpha}_k$ for each of the K bodies and express them as functions of q_i , u_j and \dot{u}_j .

- a) Write down the angular velocities $\boldsymbol{\omega}_k$ in the form shown in (3.34)

$$\boldsymbol{\omega}^k = \sum_{r=1}^m \tilde{\boldsymbol{\omega}}_r^k u_r + \tilde{\boldsymbol{\omega}}_t^k,$$

- b) Angular accelerations are of the form

$$\boldsymbol{\alpha}_k = r(\mathbf{q}, t) \dot{\mathbf{u}} + t(\mathbf{q}, \mathbf{u}, t).$$

6. GENERALIZED ACTIVE FORCES. Calculate the p generalized active forces using equation (3.35)

$$\tilde{F}_r = \sum_k^N \left(m_k \mathbf{a}_{C_k} \tilde{\mathbf{v}}_r^{C_k} + \left(\mathbf{I}_k \dot{\boldsymbol{\omega}}_k + \boldsymbol{\omega}_k \times (\mathbf{I}_k \boldsymbol{\omega}_k) \right) \tilde{\boldsymbol{\omega}}_r^k \right)$$

where $\mathbf{R}_k^{C_k}$ is the resultant force acting on the center of gravity of body k and $\mathbf{T}_k^{C_k}$ is the sum of all moments about the center of mass and all torques acting on body k . Alternatively, equation

$$\tilde{F}_r = \sum_k \sum_i \mathbf{F}_k^{P_i} \tilde{\mathbf{v}}_r^{P_i} * \sum_k \mathbf{T}_k \tilde{\omega}_r \quad r = 1, \dots, m \quad (3.37)$$

can be used, which requires no reduction of all external forces to the respective centers of gravity, but demand calculation of additional partial velocities $\tilde{\mathbf{v}}_r^{P_i}$.

7. GENERALIZED INERTIAL FORCES. Calculate the p generalized inertia forces using equation (3.36)

$$\tilde{F}_r^* = \sum_k^N \left(\mathbf{F}_k^{C_k} \tilde{\mathbf{v}}_r^{C_k} + \mathbf{T}_k^{C_k} \tilde{\omega}_r^k \right)$$

8. DYNAMIC EQUATIONS OF MOTION. As shown in (3.37) set up the p differential equations (linear in u_j) which describe the dynamics of the entire system

$$\tilde{F}_r^*(q, u, \dot{u}, t) + \tilde{F}_r(q, u, t) = 0, \quad r = 1, \dots, p.$$

3.4 ESTIMATING THE CONTRIBUTION OF EACH COMPONENT OF THE MECHANICAL MODEL

Before we derive the equations of motion we estimate the contribution of each of the three rigid bodies to the total torque requirements for rotational motions. Thereby we can check whether any of the three rigid bodies might be reduced to a point mass without significantly altering the total dynamics. To analyze the contributions we consider the most straining flight condition, i.e. maximal allowed angular velocities and accelerations, and then, calculate the required torques to realize this motion for each body.

The maximal angular velocity of the fuselage is assumed to be

$${}^N \boldsymbol{\omega}_B = [\omega_{max}, \omega_{max}, \omega_{max}]^T,$$

where $\omega_{max} = 3.14 \text{ rad/s}$ and the maximal angular acceleration is assumed to be

$${}^N \boldsymbol{\alpha}_B = [\alpha_{max}, \alpha_{max}, \alpha_{max}]^T,$$

where $\alpha_{max} = 3.14 \text{ rad/s}^2$. The angular velocities of both rotors are kept at constant speeds

$$\begin{aligned} {}^B_N \boldsymbol{\omega}_{MR} &= \begin{bmatrix} 0 & 0 & 1400 \end{bmatrix}^T \text{ rpm} \\ {}^B_N \boldsymbol{\omega}_{TR} &= \begin{bmatrix} 0 & 0 & 6720 \end{bmatrix}^T \text{ rpm.} \end{aligned}$$

The tail rotor is driven by the main motor. The gear ratio between main and tail rotor is 4.8. In good approximation, the angular accelerations of both rotors with respect to the fuselage are assumed to be zero

$${}^B_B\alpha_{MR} = {}^B_B\alpha_{TR} = \begin{bmatrix} 0 & 0 & 0 \end{bmatrix}^T \text{ rad/s}^2.$$

The fuselage is roughly approximated by a rectangular parallelepiped with constant density of the dimensions $m_F = 10 \text{ N}$, $l_1 = 0.5 \text{ m}$, $l_2 = 0.15 \text{ m}$ and $l_3 = 0.3 \text{ m}$. For the specified movement above, the following torque is required for the fuselage:

$$T_F = \begin{bmatrix} 0.85 & -1.2 & 2.2 \end{bmatrix}^T, \quad |T_F| = 2.6 \text{ N m}$$

To simplify the EoM the main and tail rotor are approximated by solid discs. The mass per circular ring of infinitesimal thickness dr and constant radius $r \in [0, R]$ is assumed to be constant, therefore the mass density decreases linearly with increasing radius. The polar principal moment of inertia can be calculated as

$$I_{rotor,33} = \int_0^R r^2 dm, \quad (3.36)$$

where

$$dm = \frac{m}{R} dr.$$

The resulting principal moments of inertia are

$$I_{MR} = 10^{-1} \text{diag}(0.33 \quad 0.33 \quad 0.66) \text{ m}^3 \text{ kg}$$

and

$$I_{TR} = 10^{-4} \text{diag}(0.15 \quad 0.15 \quad 0.3) \text{ m}^3 \text{ kg}.$$

According to Euler's law the following torques are required for the previously specified motions

$$T_{MR} = \begin{bmatrix} 15 & -15 & 0.20 \end{bmatrix}^T, \quad |T_{MR}| = 21.7 \text{ N m}$$

and

$$T_{TR} = \begin{bmatrix} 0.033 & -0.033 & 0.0001 \end{bmatrix}^T, \quad |T_{TR}| = 0.046 \text{ N m}.$$

Note, we assumed rotations about the principles axes of inertia for each of the three bodies. In reality we would have to deal with rotations about axes that go through the combined center of gravity C . In this case the moments of inertia need to be transformed into frame \mathcal{B} by exploiting the Huygens-Steiner theorem. Since C is closer to the fuselage's center of gravity F than it is to MR or TR ² the largest increase would be experienced by I_{MR} and I_{TR} . Thereby the torque demands to rotate the fuselage and the main rotor would differ even more.

² Due to the significantly higher mass of the fuselage.



Figure 7: Turbine powered Flettner helicopter with spray attachment

3.4.1 Conclusion

Interestingly, one can see, that the contribution of the tail rotor to the total torque requirements is negligible, since its several magnitudes lower.³ The inertial torque to rotate the fuselage about axis \mathbf{b}_1 and \mathbf{b}_2 is over one magnitude smaller than that for the main rotor. The inertial torque requirements for rotating the fuselage around axis \mathbf{b}_3 could be neglected since the aerodynamic drag of the main rotor, which is not taken into account in the calculations above, is at least one magnitude larger, [18].

Based on these rough estimations the following conclusions can be drawn:

- it is safe to reduce the tail rotor to a source of aerodynamic force
- the gyroscopic effects of the main rotor have by far the biggest impact on the rotational dynamics
- for model simplification the fuselage could be reduced to a point mass

These findings are consistent with the results from Kondak et al. [18] for a smaller sized helicopter (Logo 14). Generally, the relative influence of the main rotor on the rotational dynamics compared to the fuselage, increases with decreasing helicopter size. As preparations have already been made to expand the application of the MAPLE algorithm, developed in this thesis, to calculate Kane's equations for significantly larger Flettner helicopters, see fig. 7, the fuselage is modeled as rigid body.

3.5 EQUATIONS OF MOTION

By employing the procedure presented in section 3.3 we arrive at the following equations of motions for the HE-1 Helicopter. All calculations were

³ Even after applying Huygens-Steiner theorem.

carried out in the computer algebra system MAPLE. The corresponding code can be found in file: `Dynamics_Kane_Basis_Vectors.mw`.

Translational dynamics:

$$\dot{u}_1 = -qw + rv - g \sin(\theta) + F_x / m \quad (3.37)$$

$$\dot{u}_2 = pw - ru + g \cos(\theta) \sin(\phi) + F_y / m \quad (3.38)$$

$$\dot{u}_3 = pv + qu + g \cos(\phi) \cos(\theta) + F_z / m \quad (3.39)$$

Rotational dynamics:

$$(m_F z_F^2 + m_{mr} z_{mr}^2 + I_{mr_{xx}} + I_{F_{xx}}) \dot{u}_4 = (m_F z_F^2 + m_{mr} z_{mr}^2 + I_{mr_{yy}} + I_{F_{yy}} - I_{mr_{zz}} - I_{F_{zz}}) u_5 u_6 - I_{mr_{xx}} u_5 \dot{\alpha} + F_{tr} z_{tr} + T_X \quad (3.40)$$

$$(m_F z_F^2 + m_{mr} z_{mr}^2 + I_{mr_{yy}} + I_{F_{yy}}) \dot{u}_5 = (-m_F z_F^2 - m_{mr} z_{mr}^2 - I_{mr_{xx}} + I_{mr_{zz}} - I_{F_{xx}} + I_{F_{zz}}) u_4 u_6 + I_{mr_{yy}} u_4 \dot{\alpha} + F_{mr} x_{mr} + T_Y \quad (3.41)$$

$$(I_{mr_{zz}} + I_{F_{zz}}) \dot{u}_6 = (-I_{mr_{xx}} + I_{mr_{yy}} - I_{F_{xx}} + I_{F_{yy}}) u_4 u_5 + F_{tr} x_{tr} + I_{mr_{zz}} \ddot{\alpha} + F_{tr} x_{tr} + T_Z \quad (3.42)$$

Rotational dynamics (compact):

$$(I_S + I_{xx}) \dot{u}_4 = (I_S + I_{yy} - I_{zz}) u_5 u_6 - I_{mr_{xx}} u_5 \dot{\alpha} + F_{tr} z_{tr} + T_X \quad (3.43)$$

$$(I_S + I_{yy}) \dot{u}_5 = (-I_S - I_{xx} + I_{zz}) u_4 u_6 + I_{mr_{yy}} u_4 \dot{\alpha} + F_{mr} x_{mr} + T_Y \quad (3.44)$$

$$I_{zz} \dot{u}_6 = (-I_{xx} + I_{yy}) u_4 u_5 + I_{mr_{zz}} \ddot{\alpha} + F_{tr} x_{tr} + T_Z \quad (3.45)$$

with

$$m = m_f + m_m r \quad (3.46)$$

$$I_{xx} = I_{mr_{xx}} + I_{F_{xx}} \quad (3.47)$$

$$I_{yy} = I_{mr_{yy}} + I_{F_{yy}} \quad (3.48)$$

$$I_{zz} = I_{mr_{zz}} + I_{F_{zz}} \quad (3.49)$$

$$I_S = m_F z_F^2 + m_{mr} z_{mr}^2 \quad (3.50)$$

F_i are the resultant external forces acting on the center of gravity C in direction of axis i , where $i = X, Y, Z$. T_i is the resultant torque acting on the helicopter about axis i .

3.6 LINEARIZATION

Before we can proceed with the design of linear H_∞ optimization based controllers (see chapter 6) we need a linear model. The system of 6 nonlinear differential equations (3.37)-(3.42) that describe the helicopter dynamics and can be written in short form as

$$\dot{\mathbf{x}} = \mathbf{f}(\mathbf{x}, \mathbf{u}, \mathbf{d}, t), \quad (3.51)$$

with \mathbf{f} being a nonlinear function of the aircrafts states \mathbf{x} , control inputs \mathbf{u} , external disturbances \mathbf{d} and time t . The state vector is composed as follows

$$\mathbf{x} = \begin{bmatrix} u & v & w & p & q & r & x & y & z & \phi & \theta & \psi \end{bmatrix}^T. \quad (3.52)$$

Three characteristics – *trim*, *stability* and *reponse* – are essential when discussing the flight mechanics of a helicopter.

TRIM. Trim is an equilibrium flight state such that $\dot{\mathbf{x}} = \mathbf{0}$ and $\mathbf{u} = \text{const.}$, i.e.

$$\mathbf{f}(\mathbf{x}_e, \mathbf{u}_e, \mathbf{d}_e, t) = \mathbf{0} \quad (3.53)$$

Subscript e indicates a trim state. The most general trim would be a turning about the vertical axis, ascending or descending, sideslipping maneuver at constant speed. More basic flight conditions such as hover, cruise, sustained turns or autorotation are also trims, [25].

See Padfield [25, p. 192ff.] for more information about detailed trim analysis and the general trim problem.

STABILITY. Stability is concerned with the analysis whether a helicopter returns to its equilibrium point after being disturbed from its trim state. By determining the eigenvalues of the system matrix A , of the linearized system about a particular trim state \mathbf{x}_e , we can check for stability

$$\det \left(\lambda \left(\frac{\delta \mathbf{f}}{\delta \mathbf{x}} \Big|_{\mathbf{x}_e} \right) \right) = 0. \quad (3.54)$$

RESPONSE The systems response to a certain control input \mathbf{u} can be analyzed by evaluating the following equation

$$\mathbf{x}(t) = \mathbf{x}(0) + \int_0^t \mathbf{f}(\mathbf{x}(\tau), \mathbf{u}(\tau), \tau) d\tau. \quad (3.55)$$

3.6.1 Linearization about an arbitrary Trim State

From now on, in good approximation, the rotor speeds are assumed to be constant, i.e. $\ddot{\alpha} = \ddot{\beta} = 0$. Only gravitational forces, the thrust of the main and

tail rotor as well as the tilting moments induced by the main rotor are taken into account, Aerodynamic and other external forces are neglected, therefore

$$\begin{aligned} F_X &= 0 & F_Y &= F_{tr} & F_Z &= -F_{mr} \\ T_X &= T_{mr,1} & T_Y &= T_{mr,2} & T_Z &= T_{mr,3} \end{aligned}$$

Linearizing the EoM about an arbitrary trim state e yields the following state space system where the matrices A in eq. (3.57) and B in eq. (3.58) are, respectively, the system matrix and the control matrix

$$\dot{\mathbf{f}}(\mathbf{x}, \mathbf{u}, \mathbf{d}, t) \doteq \underbrace{\mathbf{f}(\mathbf{x}_e, \mathbf{u}_e, \mathbf{d}_e, t)}_{=0} + \underbrace{\left. \frac{\partial \mathbf{f}}{\partial \mathbf{x}} \right|_{\mathbf{x}_e}}_A \Delta \mathbf{x} + \underbrace{\left. \frac{\partial \mathbf{f}}{\partial \mathbf{u}} \right|_{\mathbf{u}_e}}_B \Delta \mathbf{u} + \underbrace{\left. \frac{\partial \mathbf{f}}{\partial \mathbf{d}} \right|_{\mathbf{d}_e}}_E \Delta \mathbf{d} \quad (3.56)$$

where the deviation variables are defined as

$$\Delta \mathbf{x} = \mathbf{x} - \mathbf{x}_e, \quad \Delta \mathbf{u} = \mathbf{u} - \mathbf{u}_e, \quad \Delta \mathbf{d} = \mathbf{d} - \mathbf{d}_e.$$

Subindex e indicates linearization about an arbitrary trim state e .

System Matrix A linearized about an arbitrary trim flight condition \mathbf{x}_e .

$$\begin{bmatrix}
 0 & r_e & -q_e & 0 & -w_e & v_e & 0 & -g \cos(\theta_e) & 0 & 0 & 0 & 0 \\
 -r_e & 0 & p_e & w_e & 0 & u_e & g \cos(\phi_e) \cos(\theta_e) & -g \sin(\phi_e) \sin(\theta_e) & 0 & 0 & 0 & 0 \\
 q_e & -p_e & 0 & -v_e & u_e & 0 & -g \sin(\phi_e) \cos(\theta_e) & -g \cos(\phi_e) \sin(\theta_e) & 0 & 0 & 0 & 0 \\
 0 & 0 & 0 & 0 & \frac{(I_S + I_{YY} - I_{ZZ})u_{6,e} - I_{MR_{XX}}\dot{\alpha}}{I_S + I_{XX}} & \frac{(I_S + I_{YY} - I_{ZZ})u_{5,e}}{I_S + I_{XX}} & 0 & 0 & 0 & 0 & 0 & 0 \\
 0 & 0 & 0 & \frac{(-I_S - I_{XX} + I_{ZZ})u_{6,e} + I_{MR_{YY}}\dot{\alpha}}{I_S + I_{YY}} & 0 & \frac{(-I_S + I_{XX} + I_{ZZ})u_{4,e}}{I_S + I_{YY}} & 0 & 0 & 0 & 0 & 0 & 0 \\
 0 & 0 & 0 & \frac{(-I_{XX} + I_{YY})u_{5,e}}{I_{ZZ}} & \frac{(I_{XX} - I_{YY})u_{4,e}}{I_{ZZ}} & 0 & 0 & 0 & 0 & 0 & 0 & 0 \\
 1 & 0 & 0 & 0 & 0 & 0 & 0 & 0 & 0 & 0 & 0 & 0 \\
 0 & 1 & 0 & 0 & 0 & 0 & 0 & 0 & 0 & 0 & 0 & 0 \\
 0 & 0 & 1 & 0 & 0 & 0 & 0 & 0 & 0 & 0 & 0 & 0 \\
 0 & 0 & 0 & K^{-1}(1,1) & K^{-1}(1,2) & K^{-1}(1,3) & 0 & 0 & 0 & 0 & 0 & 0 \\
 0 & 0 & 0 & K^{-1}(2,1) & K^{-1}(2,2) & K^{-1}(2,3) & 0 & 0 & 0 & 0 & 0 & 0 \\
 0 & 0 & 0 & K^{-1}(3,1) & K^{-1}(3,2) & K^{-1}(3,3) & 0 & 0 & 0 & 0 & 0 & 0
 \end{bmatrix} \quad (3.57)$$

$$B_e = \begin{bmatrix} 0 & 0 & 0 & 0 \\ 0 & 1/m & 0 & 0 \\ 1/m & 0 & 0 & 0 \\ 0 & \frac{z_{TR}}{I_S + I_{zz}} & \frac{1}{I_S + I_{zz}} & 0 \\ 0 & 0 & 0 & \frac{1}{I_S + I_{yy}} \\ 0 & \frac{x_{TR}}{I_S + I_{zz}} & 0 & 0 \\ 0 & 0 & 0 & 0 \\ 0 & 0 & 0 & 0 \\ 0 & 0 & 0 & 0 \\ 0 & 0 & 0 & 0 \\ 0 & 0 & 0 & 0 \\ 0 & 0 & 0 & 0 \end{bmatrix} \quad (3.58)$$

with the corresponding input vector

$$\mathbf{u} = \begin{bmatrix} F_{MR} & F_{TR} & T_{MR,1} & T_{MR,2} \end{bmatrix}^T \quad (3.59)$$

These are the four control inputs to the helicopter system. The main rotor lift force F_{MR} is controlled via the main rotor cyclic pitch angle θ_0 . Similarly, the side force of the tail rotor F_{TR} is controlled via the tail rotor cyclic pitch angle θ_{0T} . Whereas the tilting moments $T_{MR,1}$ and $T_{MR,2}$ are controlled via the lateral cyclic pitch θ_{1c} and longitudinal cyclic pitch θ_{1s} , respectively.

Linearization of the EoM about hovering trim state yields the following system and control matrices. The subindex 0 indicates linearization about hover trim state.

$$B_0 = B_e \quad (3.60)$$

System Matrix A linearized about hovering state \mathbf{x}_0 .

$$\begin{bmatrix} 0 & 0 & 0 & 0 & 0 & 0 & 0 & -g & 0 & 0 & 0 & 0 \\ 0 & 0 & 0 & 0 & 0 & 0 & g & 0 & 0 & 0 & 0 & 0 \\ 0 & 0 & 0 & 0 & 0 & 0 & 0 & 0 & 0 & 0 & 0 & 0 \\ 0 & 0 & 0 & 0 & -\frac{I_{MR_{XX}}\dot{\alpha}}{I_S + I_{XX}} & 0 & 0 & 0 & 0 & 0 & 0 & 0 \\ 0 & 0 & 0 & \frac{I_{MR_{YY}}\dot{\alpha}}{I_S + I_{YY}} & 0 & 0 & 0 & 0 & 0 & 0 & 0 & 0 \\ 0 & 0 & 0 & 0 & 0 & 0 & 0 & 0 & 0 & 0 & 0 & 0 \\ 1 & 0 & 0 & 0 & 0 & 0 & 0 & 0 & 0 & 0 & 0 & 0 \\ 0 & 1 & 0 & 0 & 0 & 0 & 0 & 0 & 0 & 0 & 0 & 0 \\ 0 & 0 & 1 & 0 & 0 & 0 & 0 & 0 & 0 & 0 & 0 & 0 \\ 0 & 0 & 0 & 1 & 0 & 0 & 0 & 0 & 0 & 0 & 0 & 0 \\ 0 & 0 & 0 & 0 & 1 & 0 & 0 & 0 & 0 & 0 & 0 & 0 \\ 0 & 0 & 0 & 0 & 0 & 1 & 0 & 0 & 0 & 0 & 0 & 0 \end{bmatrix} \quad (3.61)$$

3.7 HEAVE DYNAMICS

The vertical dynamics of the multi-rigid-bodies model are governed by equation (3.39)

$$\dot{u}_3 = pv + qu - g \cos(\phi) \cos(\theta) + \frac{F_z}{m} \quad (3.62)$$

with F_z being the sum of all external forces referred to the combined center of gravity C . All external forces are assumed to be continuous functions of the vehicles states and control variables. Hence, their perturbations can be expressed using a Taylor series expansion about a trim state \mathbf{x}_e . For small changes in the states x_i (i.e. Δx_i small) we can drop the higher order terms. The external force F_z written in its linear, approximate form equals

$$F_z = F_{z,e} + \frac{\partial F_z}{\partial u} \Big|_e \Delta u + \dots + \underbrace{\frac{\partial F_z}{\partial p} \Big|_e}_{Z_p} \Delta w + \dots + \frac{\partial F_z}{\partial \psi} \Big|_e \Delta \psi + \underbrace{\frac{\partial F_z}{\partial \theta_0} \Big|_e}_{Z_\theta} \Delta \theta_0 + \dots + \frac{\partial F_z}{\partial \theta_{1c}} \Big|_e \Delta \theta_{1c} \quad (3.63)$$

Where θ_0 is the collective pitch angle of the main rotor. In literature the total vertical force F_z is often labeled Z . For better flow of reading we will adopt this notation and abbreviate perturbed states $\Delta x_i \equiv x_i$. With that in mind approximation (3.63) can be written in the following form

$$Z = Z_e + Z_u u + \dots + Z_p p + \dots + Z_\phi \phi + \dots + Z_x x + \dots + Z_{\theta_0} \theta_0 + \dots + Z_{\theta_{1c}} \theta_{1c}. \quad (3.64)$$

Since we are primarily interested in the helicopter dynamics along the vertical axis, and especially in the dynamics in hovering⁴ condition, we assume Z to be a function of θ_0 , w and z only, therefore parameters Z_e , Z_w and Z_z need to be determined. Z_w is called *heave dampening derivative* and Z_{θ_0} *control sensitivity derivative*. For the controller designs the helicopter is assumed to operate out of ground effect. Therefore the effect of the flight altitude on Z is negligible and Z_z can be neglected. The range of operation is too small for having the variation of air density with altitude to have any effect. In the end the helicopter will indeed be operated in ground effect, but the controller shall be robust enough to be able to cope with that situation.

Under these assumptions, the vertical dynamics of the helicopter, while hovering, simplifies to

$$\begin{aligned}\dot{w} &= -g + \frac{Z_0}{m} + Z_w w + Z_{\theta_0} \theta_0 = Z_w w + Z_{\theta_0} \theta_0, \\ \dot{w} &= -g + Z_w w + \frac{F_{MR}}{m},\end{aligned}\tag{3.65}$$

reducing the number of unknown parameters to two. F_0 is the vertical lift required to keep the helicopter in hovering state. The total helicopter mass m is subsumed within the heave dampening derivative Z_w and the control sensitivity derivative Z_{θ_0} , i.e.

$$Z_w = Z_w/m, \quad Z_{\theta_0} = Z_{\theta_0}/m,\tag{3.66}$$

which is common practice in helicopter flight dynamics [25]. Z_e is the vertical lift required to stay in hovering condition. The total vertical thrust of the main rotor in positive z direction would be $Z_e + Z_{\theta_0} \theta_0$. The vertical stability of the helicopter is described by the solution of the homogeneous differential equation

$$\dot{w} = Z_w w.$$

Obviously, eq. (3.66) has stable solutions if and only if Z_w has negative values.

Transformation of the inhomogeneous differential equation into the frequency domain yields the following transfer function between main rotor collective pitch angle θ_0 and \dot{w}

$$G_{w,\delta_{coll}} = \frac{w(s)}{\theta_0(s)} = \frac{Z_{\theta_0}}{s + Z_w},\tag{3.67}$$

where $Z_w > 0$ and $Z_{\theta_0} < 0$. Typical values for Z_w for manned helicopter lie in the range of -0.25 to -0.40 . For unmanned, small-scaled helicopters Z_w varies a lot.

To get a feeling how complex even the heave dynamics of a helicopter are, two physical phenomena that affect the low-frequency heave dynamics primarily are introduced:

⁴ When speaking of hover, we assume the helicopter to be in horizontal orientation with Euler angles $\phi = \theta = 0$. ψ can have arbitrary values, since the vertical dynamics are assumed to be independent of the helicopter's orientation about the b_3 axis.

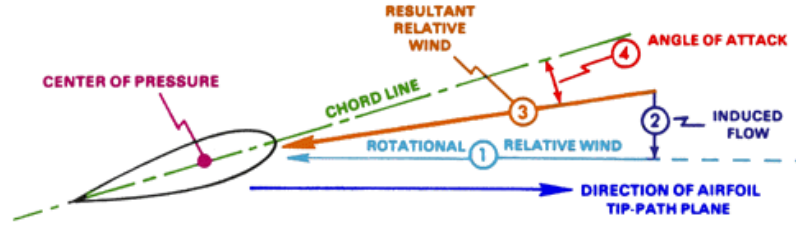


Figure 8: Angle of attack, rotational and resultant relative wind, induced flow, [5]

- Change in angle of attack due to Induced Inflow v_i and relative motion
- Ground effect

Rotor dynamics effects such as rotor coning, flapping and lead-lag that are crucial for the high-frequency dynamics of the helicopter are not introduced here due to the complexity of these effects. Padfield [25] and Leishman [20] explain these effects in great detail and present methods how to model them.

Remark. It has to be stressed that these higher frequency rotor dynamics are not covered by our simplified approximation of the heave dynamics in eq. (3.65). Neither are any unsteady aerodynamics or aerodynamic cross couplings governed. This

LIFT. The main rotor is composed of two symmetrical airfoils that provide the vertical thrust enabling the helicopter to lift off. The lift force L , generated by an airfoil for a specific flow condition, can be calculated by the following lift equation

$$L = \frac{1}{2} c_L \rho V^2 A. \quad (3.68)$$

where c_L is the *lift coefficient*, ρ the density of the surrounding fluid, v the *true airspeed* and A the projected area of the air foil (*planform area*).

For low *angle of attack* values α the lift coefficient can be approximated as a linear function of α . For higher angles, especially past the stall angle, the dependency becomes highly non-linear. The main and tail rotor of HE-1 and HE-2 feature symmetrical airfoils⁵, i.e. $c_L(\alpha=0) = 0$.

3.7.1 Change in Angle of Attack due to Induced Inflow v_i

The lift and drag of the main rotor depends primarily on the *angle of attack*, which is defined as the angle between the *resultant relative wind* and the airfoils *chord line*, see fig. 8. By altering the angle of attacking we vary the lift force and therefore the acceleration of the helicopter.

Resultant rel. wind

The resultant relative wind depends how the airfoil moves through the air and is defined as the airflow relative to an airfoil. Mathematically, it can be

⁵ Symmetrical airfoil provide higher stability while asymmetrical airfoils are more (lift) efficient on the cost of stability. Also stall characteristics and lift to drag ratios are advantageous. With changing angle of attack the center of pressure moves up and down the cord line, which induces torques and twisting loads on the airfoil.

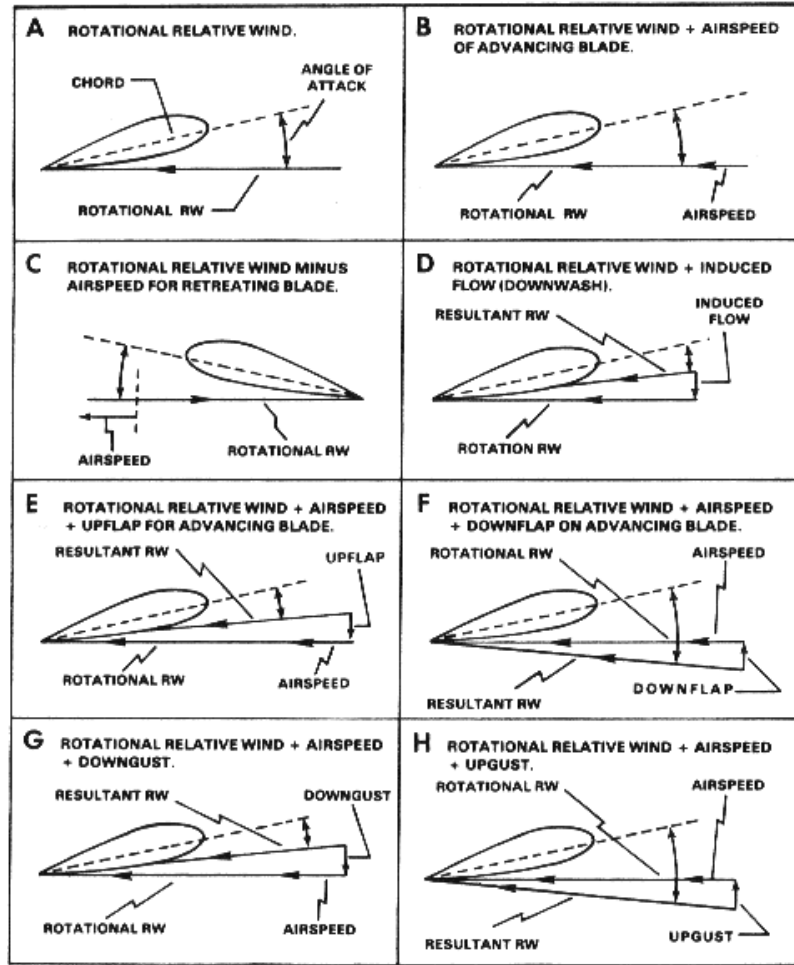


Figure 9: Components of relative wind and how they affect the angle of attack [5]

calculated by vector addition of the *rotational relative speed* and the *induced flow*.

For a helicopter in hovering state under no-wind conditions, the *rotational relative speed* lies in the rotor plane and solely depends on the rpm of the rotor, see teal vector in figure 8. Wind gusts and lateral motions of the helicopter alter the rotational relative speed, whereby it affects the advancing and retreating blade in opposite fashion.

From a Newtonian perspective, lift is generated by turning a flow of air [36]. This flow turning is also known as *induced flow* v_i or *downwash*. It reduces the angle of attack and thereby lowers the rotor's lift.

So we can summarize that generally, blade advancement, descent, forward helicopter airspeed for the advancing blade, downflap and upgust increase the angle of attack, while blade re-treatment, climbing, forward helicopter airspeed for the retreating blade, upflap and downgust have a negative effects. Figure 9 from Ean and Army [5] summarizes these relations. How the lift forces changes while climbing or descending is described by Z_w .

Remark. The lift force L which is a component of the total aerodynamic forces always points in a direction perpendicular to the flow direction.

Rotational relative speed

Induced flow

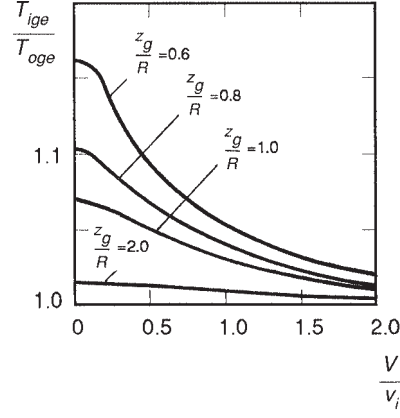


Figure 10: Ground effect, [25]

3.7.2 Ground Effect

Operating the helicopter in close range to the ground alters some of its flight characteristics. The most significant effect is the variation of the induced velocity v_i at the main rotor with its distance from the ground z_g , which eventually alters the rotor thrust and the power required for a certain flight condition. Figure 10 illustrates the variation of the ratio of rotor thrust in-ground effect T_{ige} to rotor thrust out-of ground effect T_{oge} with distance from the ground. As a rule of thumb, the ground effects significantly affects the lift below heights in the order of the rotor radius R . The higher the forwards speed V the less significant the effect becomes, as the rotor "escapes" its own wake.

3.7.3 Analytical Determination of Z_w

Padfield [25] and Leishman [20] show ways to derive the heave dampening parameter analytically. Results of these calculations are to be treated with caution, but the formulas help to understand what parameters influence Z_w . For deriving Z_w the induced downwash λ_i is assumed to be uniform and constant over the rotor disc. „The induced rotor downwash is one of the most important components of helicopter flight dynamics; it can also be the most complex. The downwash, representing the discharged energy from the lifting rotor, actually takes the form of a spiraling vortex wake with velocities that vary in this introduction to the topic we make some major simplifications“ [25]. In hovering state the downwash can be written as

$$v_{i_{hover}} = \sqrt{\frac{T}{2\rho A_d}} \quad (3.69)$$

or, in normalized form as

$$\lambda_i = \frac{v_i}{R\omega} = \sqrt{\frac{C_T}{2}} \quad (3.70)$$

where C_T is the thrust coefficient in hover and vertical flight conditions

$$C_T = \frac{\alpha_0 s}{2} \left(\frac{\theta_0}{3} + \frac{\mu_z - \lambda_i}{2} \right). \quad (3.71)$$

and μ_z is the normal velocity of the rotor, positive downwards and is about equal to the aircraft's vertical velocity component w , which is especially true for hovering trim state. Padfield [25, p. 220] uses the thrust coefficient derivative $\frac{\partial C_T}{\partial \mu_z}$ to derive Z_w

$$\begin{aligned} Z_w &= -\frac{\rho(\omega R)\pi R^2}{M} \frac{\partial C_T}{\partial \mu_z} \\ &= -\frac{2\alpha_0 A_b \rho(\omega R)\lambda_i}{(16\lambda_i + \alpha_0 s)M} \end{aligned} \quad (3.72)$$

where

- A_b blade area [m²]
- A_d disc area [m²]
- s blade solidity; ratio of blade area to disc area
- ρ air density [kg/m³]
- ω rpm of main rotor
- C_T lift coefficient
- λ_i induced hover downwash
- α_0 lift curve slope
- M mass of helicopter [kg]

One key parameter is the blade loading A_b/M . The analytically determined Z_w value for helicopter HE-1 and HE-2 is -1.96 , being equivalent to a time constant of the helicopter's vertical motion of 0.51 s, see section 3.7.4.

Remark. Relation 3.72 is only valid in hovering state. Approximations for Z_w in forward flight are found in Padfield [25, p. 220].

3.7.4 Interpretation of the Heave Dampening Derivative Z_w

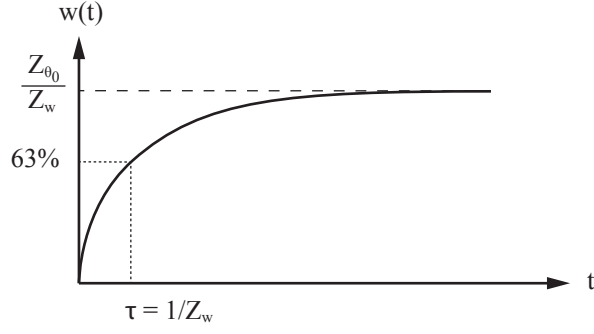
To get a feeling for the influence of the heave dampening derivative Z_w on the vertical dynamics it is helpful to consider a step response of $G_{w,\delta_{coll}}(s)$.

$$w(s) = G_{w,\delta_{coll}}(s)\sigma(s) = \frac{Z_{\theta_0}}{s + Z_w} \frac{1}{s} \quad (3.73)$$

$$w(t) = \mathcal{L}^{-1} \left\{ \frac{Z_{\theta_0}}{s + Z_w} \frac{1}{s} \right\} = \frac{Z_{\theta_0}}{Z_w} (1 - e^{-Z_w t}). \quad (3.74)$$

By looking at the term in parentheses in eq. (3.74) it becomes obvious that Z_w determines the time constant τ of the system

$$\tau = \frac{1}{Z_w}, \quad (3.75)$$

Figure 11: Step response of $G_{w,\delta_{coll}}(s)$

which means after a (unit) step input $\sigma(s)$, $w(t)$ reaches 63% of its final value $\frac{Z_{\theta_0}}{Z_w}$ after $\frac{1}{Z_w}$ seconds, see also fig. 11.

Step response analysis of the transfer function

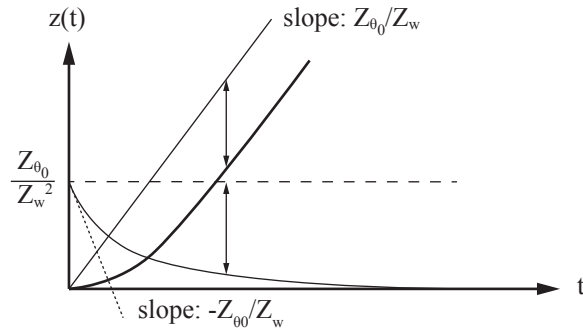
$$G_{z,\delta_{coll}} = \frac{1}{s} G_{w,\delta_{coll}} = \frac{z(s)}{\theta_0(s)} = \frac{1}{s} \frac{Z_{\theta_0}}{s + Z_w} \quad (3.76)$$

between height and collective pitch deviation angle θ_0 and the vertical height yields

$$\begin{aligned} z(s) &= G_{z,\delta_{coll}}(s) \sigma(s) = \frac{Z_{\theta_0}}{s + Z_w} \frac{1}{s^2} \\ &= \frac{Z_{\theta_0}}{Z_w} \left(-\frac{1}{Z_w s} + \frac{1}{s^2} + \frac{1}{Z_w} \frac{1}{s + Z_w} \right) \end{aligned} \quad (3.77)$$

$$\begin{aligned} z(t) &= \mathcal{L}^{-1} \left\{ \frac{Z_{\theta_0}}{s + Z_w} \frac{1}{s^2} \right\} \\ &= \frac{Z_{\theta_0}}{Z_w} \left(-\frac{\sigma(t)}{Z_w} + t + \frac{1}{Z_w} e^{-Z_w t} \right) \\ &\stackrel{t \geq 0}{=} \frac{Z_{\theta_0}}{Z_w} \left(-\frac{1}{Z_w} + t + \frac{1}{Z_w} e^{-Z_w t} \right) \end{aligned} \quad (3.78)$$

giving the following time behavior shown in fig. 12.

Figure 12: Step response of $G_{z,\delta_{coll}}(s)$

3.7.5 Z_w and its Relation to Vertical Gust Response in hover

The acceleration of the helicopter due to vertical gusts can be derived from the linear approximation of the heave dynamics (3.65)

$$\dot{w} = Z_w(w + w_g) \stackrel{\text{hover}}{=} Z_w w_g \quad (3.79)$$

where w_g is the vertical gust velocity. Thus the initial acceleration due to a step-like vertical gusts can be written as

$$\left. \frac{dw}{dt} \right|_{t=0} = Z_w w_g, \quad (3.80)$$

which can be regarded as a quantitative measure of ride quality, in terms of vertical bumpiness, [25]. Increasing values of Z_w increase the helicopter's susceptibility to vertical gusts. According to eq. (3.80), vertical gusts of magnitude 5m/s result in an initial acceleration of about $2.5 \text{ m/s}^2 \approx 0.25g$ for HE-1 and HE-2.⁶ This should be regarded as a rough estimation. Close to the ground vertical gusts of this magnitude are rare and, due to the low Z_w values, they generally have a rather low influence on the helicopter dynamics. But in situations where the helicopter is operated close to obstacles (e.g. aerial manipulation of large objects) the power margin and the heave sensitivity play a critical role when concerning vertical performance and handling qualities.

3.7.6 Vertical Gust Response in Forward Flight

According to Padfield [25] the following set of equations describe the induced downwash $v_{i\mu}$ and heave dampening Z_w in forward flight. V is the aircraft's forward velocity and V' is the forward component of the total velocity at the rotor disc

$$v_{i\mu} = \frac{T}{2\rho A_d V'} \quad (3.81)$$

$$\frac{\partial C_T}{\partial \mu_z} = \frac{2\alpha_0 s \mu}{8\mu + \alpha_0 s} \quad (3.82)$$

$$\mu = \frac{V}{\omega R} \quad (3.83)$$

$$Z_w = - \underbrace{\frac{\rho \alpha_0 V A_b}{2M_a}}_{Z_{wFW}} \left(\frac{4}{8\mu + \alpha_0 s} \right). \quad (3.84)$$

Z_{wFW} is the corresponding heave dampening parameter for a fixed-wing aircraft with wing area A_b . From equations (3.83)-(3.84) follows that helicopter heave dampening parameters converge against fixed values with increasing forward velocity, whereas those for fixed-wing aircrafts increase linearly. Typically lift curve values for helicopter blades are higher than for fixed-wing airplanes, but blade loadings for helicopters are significantly higher than wing

⁶ With an assumed Z_w value of 0.5 s^{-1} , which was derived with PEM system identification, see chapter 4.

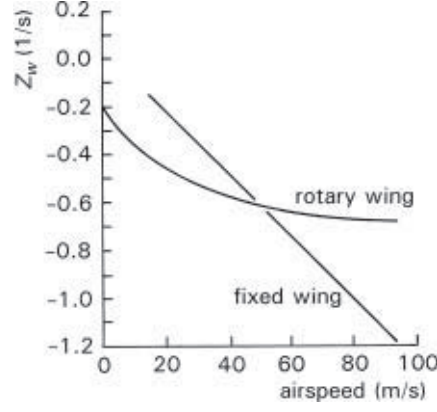


Figure 13: Heave damping derivative in forward flight, [25]

loadings for airplanes of the similar weight class, resulting in higher (absolute) Z_w for low velocities, see fig. 13.

3.7.7 Modeling Vertical Wind Disturbance

As suggested by Skogestad and Postlethwaite [32] the atmospheric disturbance are modeled as gust velocity components that perturb the helicopter's velocity states u, v, w by d_u, d_v, d_w yielding the following disturbed system description

$$\dot{\mathbf{x}} = \mathbf{A}\mathbf{x} + \mathbf{A} \begin{bmatrix} d_u \\ d_v \\ d_w \\ 0 \\ \vdots \\ 0 \end{bmatrix} + \mathbf{B}\mathbf{u}. \quad (3.85)$$

Which means, when considering the heave dynamics only, we can set

$$G_d = G_w \delta_{coll}. \quad (3.86)$$

See [32, p. 496] for a more detailed argumentation.

3.8 SCALING

Note, that prior to controller design the model was scaled. Figure 14 illustrates the scaling of the input variable u . The value of u represents the width in ms of the pulse width modulated (PWM) input signal u . \hat{u}_{max} represents the trim value for the hovering state (1052 ms). The actual input value is allowed to vary by ± 300 ms about the trim value, i.e. $\hat{u} \in [\hat{u}_{trim} - \hat{u}_{max}, \hat{u}_{trim} + \hat{u}_{max}]$. Remember, that for the linearized system $\theta_0 = u - u_{trim}$.

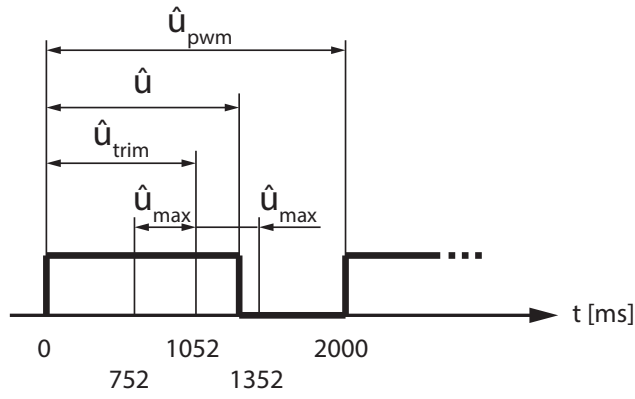


Figure 14: Pulse width modulated input signal

\hat{u}_{max}	$= 300 \text{ m s}$	$\equiv D_u$	largest allowed input change
\hat{y}_{max}	$= 10 \text{ m}$		largest allowed change of output value
\hat{d}_{max}	$= 10 \text{ m/s}$	$\equiv D_d$	largest allowed change of disturbance value
\hat{e}_{max}	$= 1 \text{ m}$	$\equiv D_e$	largest allowed control error
\hat{r}_{max}	$= 10 \text{ m}$	$\equiv D_r$	largest expected change of reference value

SYSTEM IDENTIFICATION

Since analytical calculations of Z_w are all but reliable, system identification tools of MATLAB were used to determine its value. The second parameter of $G_{w,\delta coll}$, see eq. (3.67), which is characteristic for the heave dynamics, the control sensitive derivative $Z_{\theta 0}$, was also determined via system identification. The data of two flight sessions, one at Grob airfield and one at the DLR, Oberpfaffenhofen area, was used. During those flights vertical steps of varying heights were flown. The recorded vertical velocity and acceleration data was then used to identify the above mentioned parameters. To estimate these unknown parameters the *Prediction Error Minimization (PEM)* Method of the MATLAB System Identification Toolbox was employed. Two slightly different sets of parameters (Grob and DLR) were estimated from the flight data. During re-evaluation of the recorded data it became apparent that the data logger didn't function perfectly as intended during the flights at Grob. Prior to the second round of test flights (DLR) some adjustments in the logging procedure were made to resolve the issue. Therefore more trust was put into the system identification results based on the flight data at DLR. Nevertheless the results derived from the erroneous data record are shown below (Grob).

The results of the system identification process can be seen in figure on page 43. The upper plot shows the recorded velocity data of the flight at the DLR area in yellow. The yellow line in the lower plot represents the corresponding accelerations during that flight. The green lines show the predictions of the identified models based on the recorded servo input data (PWM), shown in figure .

$G_{w,\delta coll}(DLR, modified)$ represents an intermediary model between $G_{w,\delta coll}(Grob)$ and $G_{w,\delta coll}(DLR)$ and was chosen by hand. $G_{w,\delta coll}(DLR, modified)$ was extended by a 2nd order transfer function approximation of the servo dynamics, its predictions are shown by the red lines; $G_{w,\delta coll}(DLR, modified, servo dynamics)$. The predictions improved only slightly by including servo dynamics. The improvements were deemed non worthy the increase in model order, thereby model $G_{w,\delta coll}(DLR, modified)$ was used for controller design in chapter 6.

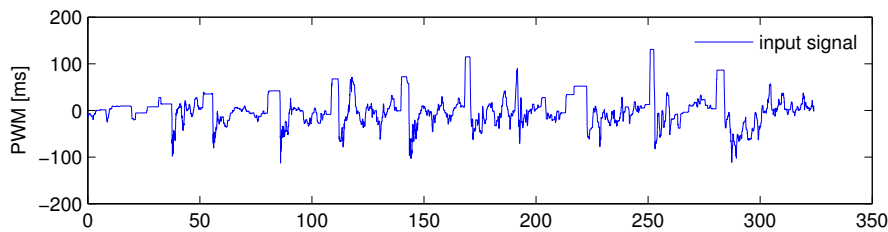


Figure 15

Figures 17-19 visualize the effect of parameter uncertainty on the heavy dynamics. Figure 17 shows the effect of varying Z_w by $\pm 20\%$ of its nominal value of 0.5 s^{-1} in equidistant intervals. In analog fashion, figure 18 shows the effect of varying Z_{θ_0} by $\pm 20\%$ of its nominal values of -0.0230 m/s^2 in equidistant intervals. To show the combined effect of uncertain Z_w and Z_{θ_0} , both variables were randomly varied by $\pm 20\%$ of their respective nominal values.

In cooperation with Aaron Barth from the Institute of Helicopter Technology of the Technical University of Munich (TUM) state-space matrices for the helicopter in hovering trim were derived with CAMRAD II.¹ The result for the heave dampening derivative of 0.7 matched that of the system identification process of surprisingly well. There is definitely a lot of potential in using CAMRAD II to derive the linearized helicopter dynamics for any desired number of flight states – thereby providing a basis to realize MIMO control concepts with optional gain scheduling.

4.1 FREQUENCY-DOMAIN SYSTEM IDENTIFICATION

Originally, it was planned to record frequency sweep flight data and perform frequency-domain system identification with the software CIPHER[®], but due to time constraints it had to be postponed. This method is especially well-suited for system identification of aircraft and rotorcraft dynamics models from flight data, and nice summarization of the differences between time-response and frequency-response methods can be found in table 1.4 in Tischler and Remple [34]. CIPHER is an advanced modeling tool that has been developed by NASA's Ames Research Center which has been successfully used to analyze the dynamics of a wide range of rotary-wing and fixed-wing aircrafts including: XV-15, Bell-214ST, BO-105, AH-64, UH-60, V-22, AV-8B Harrier, and OH-58D. An in-depth introduction to aircraft and rotorcraft system identification using frequency-domain-based methods is given in Tischler and Remple [34] and in Mettler [23] with special focus on small-sized RUAV. Author of the former book, Mark B. Tischler has led development of CIPHER.

¹ CAMRAD II is an aeromechanical analysis of helicopters and rotorcraft that incorporates a combination of advanced technology, including multibody dynamics, nonlinear finite elements, structural dynamics, and rotorcraft aerodynamics.

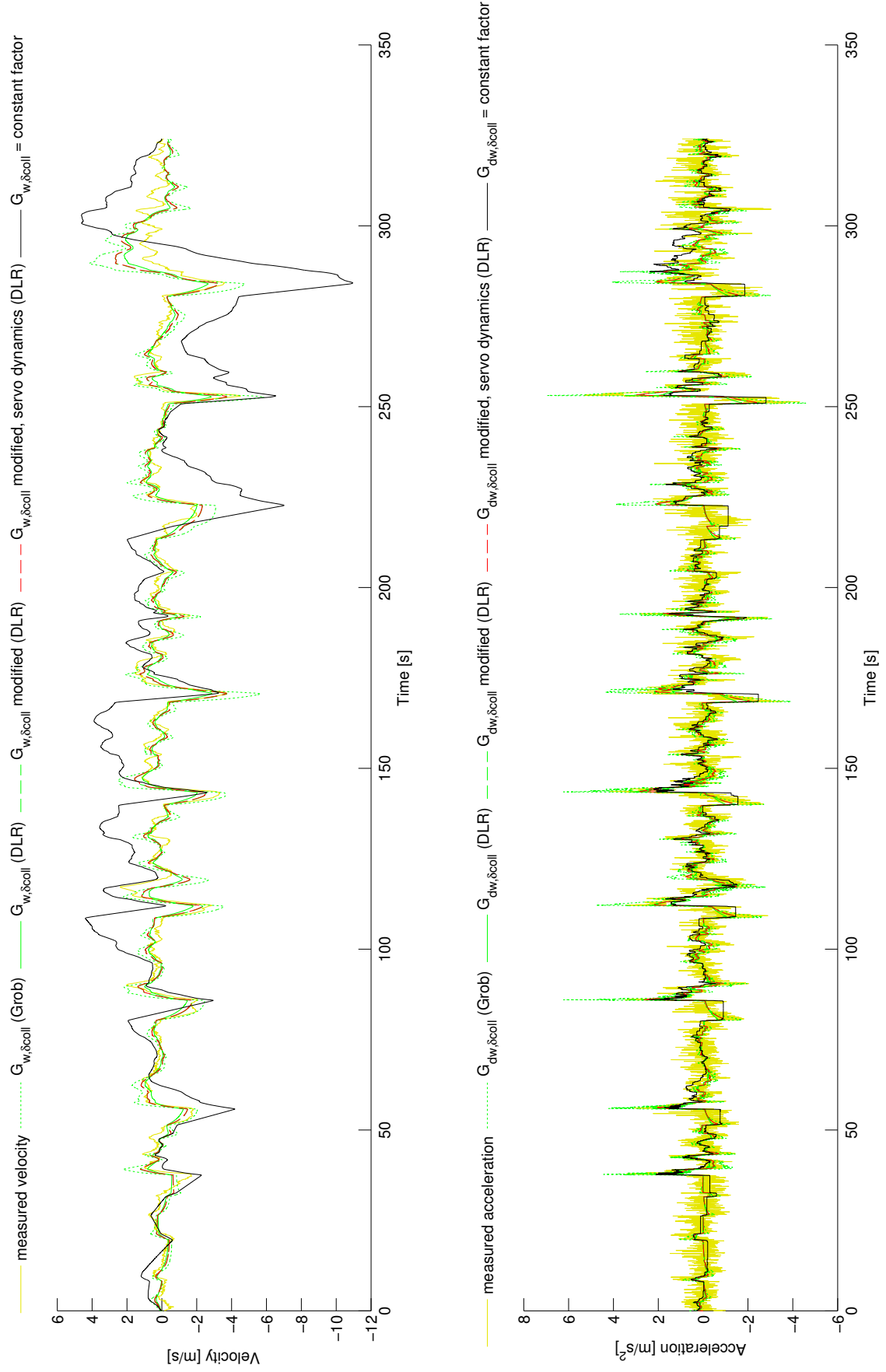


Figure 16: System Identification Results

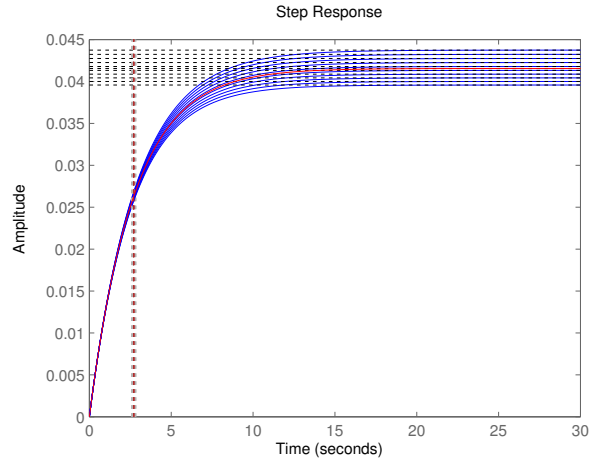


Figure 17: Variation of Z_w about plus minus $\pm 20\%$ of its nominal value of 0.5 s^{-1} in equidistant intervals

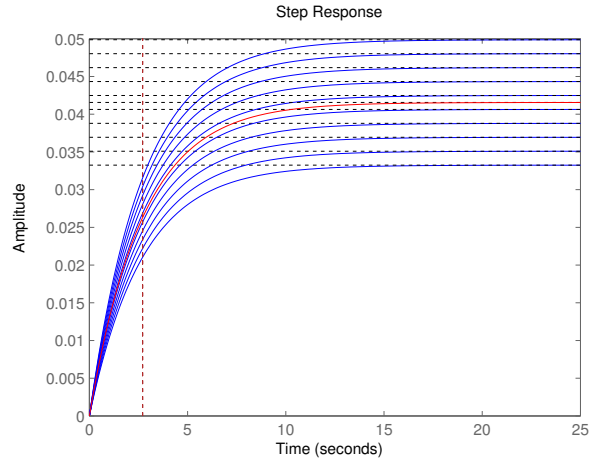


Figure 18: Variation of Z_{θ_0} about plus minus $\pm 20\%$ of its nominal value of $-0.0230 \text{ m/s}^2/\text{ms}$ in equidistant intervals

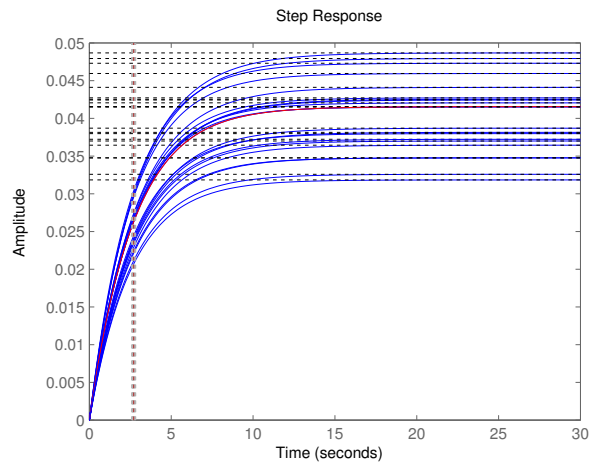


Figure 19: Random variation of Z_w and Z_{θ_0} about plus minus $\pm 20\%$; of their nominal values

Part II

CONTROL

"In the application of automatic controller, it is important to realize that controller and process form a unit; credit or discredit for results obtained are attributable to one as much as the other.

A poor controller is often able to perform acceptably on a process which is easily controlled. The finest controller made, when applied to a miserably designed process, may not deliver the desired performance. True, on badly designed processes, advanced controllers are able to eke out better results than older models, but on these processes, there is a definite end point which can be approached by instrumentation and it falls short of perfection."

— Ziegler-Nichols [41]

MATHEMATICAL PRELIMINARIES

This chapter gives a short overview of mathematical concepts crucial for designing H_∞ controller. [Li et al. \[21\]](#) gives a nice summary about the physical interpretation of the H_∞ norm and explains how to formulate the H_∞ optimization problems and how to derive the respective generalized plant in state-space realization. A nice tutorial about loop shaping design is given by [Glover et al. \[9\]](#), K. Glover and D.C. McFarlane both played decisive roles in advancing and developing H_∞ design techniques.

5.1 GAIN OF A SYSTEM $G(s)$

For the SISO case the *gain* of a system $y = Gd$ at a given frequency ω is given by

$$|G(j\omega)| = \frac{|y(\omega)|}{|u(\omega)|} = \frac{|G(j\omega)u(\omega)|}{|u(\omega)|}, \quad G \in \mathbb{C}. \quad (5.1)$$

For a MIMO System $\mathbf{y} = G\mathbf{u}$ the *gain* at a given frequency ω is given by

$$|G(j\omega)| = \frac{\|\mathbf{y}(\omega)\|_2}{\|\mathbf{u}(\omega)\|_2} = \frac{\|G(j\omega)\mathbf{u}(\omega)\|_2}{\|\mathbf{u}(\omega)\|_2}, \quad G \in \mathbb{C}^{m \times n}. \quad (5.2)$$

REMARK. In the SISO case, the gain depends on the frequency and is independent of the input magnitude $|u|$. The same is true for MIMO systems, but the gain is additionally dependent on the *direction* of the input \mathbf{u} .

5.1.1 Measuring the Gain of MIMO Systems

The magnitudes of the eigenvalues of a transfer matrix $|\lambda_i(G(j\omega))|$ provide no tool to generalize the SISO gain $|G(j\omega)|$. This becomes most apparent for matrices whose eigenvalues are zero but still there exist input vectors whose corresponding output vector are non zero, see [Skogestad and Postlethwaite \[32, p. 77\]](#). Eigenvalues only provide a measure of the gain when the input and output vectors point into the same direction, i.e. the direction of the eigenvectors \mathbf{v}_i

$$y = G\mathbf{v}_i = \lambda_i \mathbf{v}_i. \quad (5.3)$$

The spectral norm $\sigma(A)$ of a matrix A

$$\rho(A) = \max_i |\lambda_i(A)| \quad (5.4)$$

does not fulfill the properties of a matrix norm since the triangular property and multiplicative property are violated. See appendix [A.4](#) for more informa-

tion about matrix norms. But the spectral radius is valuable in that regard, that it provides a lower bound on any matrix norm

$$\rho(A) \leq \|A\|. \quad (5.5)$$

5.2 SINGULAR VALUES

A measure of gain for MIMO systems that, opposed to EV, takes into account the direction of the input \mathbf{u} are the *singular values* of G . The maximum value of the gain in (5.2) for a given frequency ω , for all possible input directions, is the maximum singular value of G

$$\bar{\sigma} = \max_{\mathbf{u} \neq \mathbf{0}} \frac{\|G\mathbf{u}\|_2}{\|\mathbf{u}\|_2} = \max_{\|\mathbf{u}\|_2=1} \|G\mathbf{u}\|_2 \quad (5.6)$$

The largest singular value of a matrix, sometimes called spectral norm, is equal to its induced 2 norm. All induced norms are matrix norms, therefore relation (5.5) holds true. A simple interpretation is that matrix norms search for the maximum gain in all directions whereas the eigenvalues measure the gain of the matrix only in certain directions – that of the eigenvectors. Therefore, the singular values actually bound the magnitude of the eigenvalues

$$\underline{\sigma} \leq |\lambda_i(A)| \leq \bar{\sigma}, \quad (5.7)$$

where $\underline{\sigma}(G)$ is the minimum singular value of G

$$\underline{\sigma} = \min_{\mathbf{u} \neq \mathbf{0}} \frac{\|G\mathbf{u}\|_2}{\|\mathbf{u}\|_2} = \min_{\|\mathbf{u}\|_2=1} \|G\mathbf{u}\|_2. \quad (5.8)$$

An interesting relationship between the largest singular value and the largest element $\|A\|_{\max}$ of a $m \times n$ matrix A is given in [Skogestad and Postlethwaite \[32\]](#)

$$\|A\|_{\max} \leq \bar{\sigma}(A) \leq \sqrt{mn} \|A\|_{\max}. \quad (5.9)$$

5.2.1 Singular Value Decomposition

Theorem 5.1 (Singular Value Decomposition, [40]). *Let $G \in \mathbb{F}^{n \times m}$. There exist unitary matrices*

$$\begin{aligned} U &= [u_1, u_2, \dots, u_m] \in \mathbb{F}^{m \times m} \\ V &= [v_1, v_2, \dots, v_n] \in \mathbb{F}^{n \times n} \\ \Sigma &= \begin{bmatrix} \Sigma_1 & 0 \\ 0 & 0 \end{bmatrix} \in \mathbb{F}^{m \times n} \end{aligned}$$

such that

$$G = U \Sigma V^*, \quad (5.10)$$

where $(\cdot)^*$ denotes the conjugate transpose, or adjoint matrix and

$$\Sigma_1 = \begin{bmatrix} \sigma_1 & 0 & \cdots & 0 \\ 0 & \sigma_2 & \cdots & 0 \\ \vdots & \vdots & \ddots & \vdots \\ 0 & 0 & \cdots & \sigma_p \end{bmatrix} \quad (5.11)$$

and

$$\sigma_1 \geq \sigma_2 \geq \cdots \geq \sigma_p \geq 0, p = \min\{m, n\}. \quad (5.12)$$

A proof of theorem 5.1 can be found in Zhou [40]. The diagonal elements of Σ are called singular values of G , the m columns of U are called the *left singular vectors* and the n columns of V are called the *right singular vector*, respectively. From the unitarity of V , i.e. $V^*V = I$, follows directly $GV = U\Sigma$, evaluated for the i -th columns yields

$$G\mathbf{v}_i = \sigma_i \mathbf{u}_i \quad (5.13)$$

and

$$G^* \mathbf{u}_i = \sigma_i \mathbf{v}_i, \quad (5.14)$$

respectively. Which can be rewritten as

$$\begin{aligned} G^* G \mathbf{v}_i &= \sigma_i^2 \mathbf{v}_i \\ G G^* \mathbf{u}_i &= \sigma_i^2 \mathbf{u}_i. \end{aligned}$$

It becomes obvious that the singular values are the square roots of the eigenvalues of G^*G ,

$$\sigma_i(G) = \sqrt{\lambda_i(G^*G)}. \quad (5.15)$$

5.2.2 Role of Singular Values in Control Theory

The orthonormal column vectors \mathbf{u}_i and \mathbf{v}_i represent, respectively, the *output* and *input directions* of the plant G . Note, the input and output directions are related via the singular values as stated in eq. (5.13). That is, an input \mathbf{v}_i into plant G yields an output signal in direction \mathbf{u}_i of the magnitude $\sigma_i(G)$. The relation between the magnitude of the output signal and the corresponding singular value stems from the fact that $\|\mathbf{u}_i\|_2 = 1$, which can be written as

$$\|\sigma_i(G)\mathbf{u}_i\| = \sigma_i(G) = \|G\mathbf{v}_i\|_2 = \frac{\|G\mathbf{v}_i\|_2}{\|\mathbf{v}_i\|_2} \quad (5.16)$$

$$G = \underbrace{\begin{bmatrix} \underbrace{\mathbf{u}_1}_{\text{'highest gain'}} & \dots & \underbrace{\mathbf{u}_m}_{\text{'lowest gain'}} \\ \text{output directions} \end{bmatrix}}_U \underbrace{\begin{bmatrix} \sigma_1 & 0 & \dots & 0 & & \\ 0 & \sigma_2 & \ddots & \vdots & & \\ \vdots & \ddots & \ddots & 0 & & \\ 0 & \dots & 0 & \sigma_p & & \\ & & & & \mathbf{0} & \\ & & & & & \mathbf{0} \end{bmatrix}}_{\Sigma} \underbrace{\begin{bmatrix} \underbrace{\mathbf{v}_1}_{\text{'highest gain'}} & \dots & \underbrace{\mathbf{v}_n}_{\text{'lowest gain'}} \\ \text{input directions} \end{bmatrix}^*}_{V^*} \quad (5.17)$$

Since the magnitude of the singular values are descending from σ_1 to σ_p , \mathbf{u}_1 (\mathbf{u}_m) represent the *highest (lowest) gain output direction*, while \mathbf{v}_1 (\mathbf{v}_n) represent the *highest (lowest) gain input direction*. In other words, for any input direction \mathbf{u} , excluding the null space of G , we have that

$$\underline{\sigma}(G(j\omega)) \leq \frac{\|G\mathbf{u}(\omega)\|_2}{\|\mathbf{u}(\omega)\|_2} \leq \overline{\sigma}(G(j\omega)) \quad (5.18)$$

and

$$G\mathbf{v}_1 = \overline{\sigma}\mathbf{u}_1, \quad G\mathbf{v}_n = \underline{\sigma}\mathbf{u}_m. \quad (5.19)$$

CONDITION NUMBER. Systems are *ill-conditioned* if some combinations of inputs have strong effects on the output while others have weak effects. One way to quantify this is the *condition number* – the ratio between the gains in the high gain and low gain directions. Ill-conditioned systems with input uncertainty may become hard to control.

MINIMUM SINGULAR VALUE. Generally $\underline{\sigma}(G)$ is desired to be as large as possible. To avoid input saturation $\underline{\sigma}$ must be larger than about 1 in all frequency regions where control is required, see [Skogestad and Postlethwaite \[32\]](#).

5.2.3 Singular Values as a Measure for Performance

Evaluating the sensitivity function S (see section 6.1.1) as function of frequency allows a valuable estimation of the feedback error. Let $r(\omega)$ be the vector of reference inputs and $e(\omega)$ the vector of control errors then bounds for the relative control error $\|e(\omega)\|_2/\|r(\omega)\|_2$ can be given by exploiting inequality (5.18)

$$\underline{\sigma}(S(j\omega)) \leq \frac{\|e(\omega)\|_2}{\|r(\omega)\|_2} \leq \overline{\sigma}(S(j\omega)). \quad (5.20)$$

Therefore, in the worst-case direction the relative control error is bounded by the maximum singular value of S .

If we now define an upper limit for $\bar{\sigma}(j\omega)$ we can limit the maximum allowed magnitude of the relative control error. Since the maximum singular value of S is a function of frequency ω we can define frequency dependent bounds for the relative control error. Let $1/w_P(j\omega)$, the so called *performance weight*, be such an upper bound which results in the following performance requirement

$$\bar{\sigma}(S(j\omega)) < 1/|w_P(j\omega)| \quad \forall \omega \quad \Leftrightarrow \quad \bar{\sigma}(w_P S) < 1 \quad \forall \omega \quad (5.21)$$

$$\Leftrightarrow \quad \|w_P S\|_\infty < 1 \quad \forall \omega \quad (5.22)$$

therefore

$$\frac{\|e(\omega)\|_2}{\|r(\omega)\|_2} < 1/|w_P(j\omega)| \quad \Leftrightarrow \quad \|w_P S\|_\infty < 1 \quad \forall \omega. \quad (5.23)$$

Typical performance weights are given in section 6.5.

5.3 \mathcal{H}_∞ NORM

5.3.1 Definition

Consider a stable, linear SISO system with transfer function $G(s)$. The H_∞ norm is defined as

$$\|G\|_\infty = \sup_{\omega} |G(j\omega)|. \quad (5.24)$$

Whereby $|G(j\omega)|$ is the amplification factor by which the system amplifies a sinusoidal input signal u with angular frequency ω . Toivonen [35] shows that the H_∞ norm can be characterized as

$$\|G\|_\infty = \sup \left\{ \frac{\|Gu\|_2}{\|u\|_2} : u \neq \vec{0} \right\}. \quad (5.25)$$

In this form it becomes apparent that the H_∞ is the maximal factor by which the system – described by $G(s)$ – amplifies the L_2 norm of any input u . In operator theory, the H_∞ norm would be called a L_2 norm induced operator norm.

In an analogous fashion, the H_∞ norm can be defined for MIMO systems. Toivonen [35] shows a natural way to extend the definition (5.25) to the MIMO case. First, the concept of the gain $|G(j\omega)|$ of a SISO system at a certain frequency ω is generalized to the multi-variable case. Let $\mathbf{u} = [u_1, \dots, u_m]^T \in \mathbb{C}^m$ be a complex valued input vector, with

$$\|\mathbf{u}\| = (|u_1|^2 + \dots + |u_m|^2)^{1/2} \quad (5.26)$$

being its *Euclidean norm*. Then the maximum gain of the transfer function matrix $G(s)$ at a given frequency ω is given by

$$\|G\| = \max_{\mathbf{u}} \left\{ \frac{\|G(j\omega)\mathbf{u}\|}{\|\mathbf{u}\|} : \mathbf{u} \neq 0, \mathbf{u} \in \mathbb{C}^m \right\}. \quad (5.27)$$

In analogy to (5.25) the H_∞ norm can be defined as the supremum of the maximum gain of $G(j\omega)$ over all frequencies ω , which is, as shown above, equal to its maximum singular value $\overline{\sigma}(G(j\omega))$

$$\|G\|_\infty := \sup_{\omega} \|G(j\omega)\| \quad (5.28)$$

5.3.2 Interpretation

Assuming $G(s)$ is a stable matrix transfer function, then its \mathcal{H}_∞ norm can be interpreted in the following way.

SISO In case of a SISO system the \mathcal{H}_∞ norm of its transfer function $G(s)$ can be regarded as the largest possible amplification factor of the system's steady state response to a sinusoidal, [40]. The steady-state response of the system with respect to a sinusoidal input

$$u(t) = U \sin(\omega t + \phi) \quad (5.29)$$

is given by

$$y(t) = U|G(j\omega)| \sin(\omega t + \phi + \arg(G(j\omega))). \quad (5.30)$$

Thus, the maximal possible amplification factor is $\sup_{\omega} |G(j\omega)| =: \mathcal{H}_\infty$.

MIMO In analogy with the SISO case, (5.28) can be interpreted in terms of how a plant G effects vector-valued sinusoidal inputs of the form

$$\mathbf{u}(t) = [a_1 \sin(\omega t + \phi_1), \dots, a_n \sin(\omega t + \phi_n)]^T. \quad (5.31)$$

Now, we look for the maximum possible steady-state response of G to the above defined sinusoidal input signal. The output $\mathbf{y} = G\mathbf{u}$ is another vector-valued sinusoid signal of the same frequency ω , but of different phase and magnitudes of its components

$$\mathbf{y}(t) = [b_1 \sin(\omega t + \psi_1), \dots, b_n \sin(\omega t + \psi_n)]^T. \quad (5.32)$$

In that case, it can be shown that (5.28) is equal to

$$\|G\|_\infty = \sup_{\omega} \max_{\{a_i\}, \{\phi_i\}} \left\{ \frac{\|\mathbf{y}\|_2}{\|\mathbf{u}\|_2} : \mathbf{y} = G\mathbf{u}, \mathbf{u} \in \mathbb{C}^m \right\}, \quad (5.33)$$

with the respective euclidean norms

$$\|\mathbf{u}\| = (a_1^2 + \dots + a_n^2)^{1/2} \quad (5.34)$$

$$\|\mathbf{y}\| = (b_1^2 + \dots + b_n^2)^{1/2}, \quad (5.35)$$

see Zhou [40, p. 58] and Toivonen [35, p. 18]. Thereby the H_∞ norm can be interpreted as the maximal factor by which the magnitude of a vector-valued sinusoidal input signal, as defined in (5.31), gets amplified by the system G .

Li et al. [21, p. 945] and Desoer and Vidyasagar [1] give physical interpretations of the H_∞ norm of MIMO systems from the energy and power point of view of the input and output signals.

H INFINITY CONTROL

This chapter presents the various H_∞ norm optimization based controllers that were designed for controlling the heave dynamics of helicopter HE1. Introductions to the respective underlying mathematical concepts are given as well. For all the theory that follows the model is assumed to be scaled. Simulink models that were used to simulate the closed loop behavior are introduced at the end.

6.1 DESIGN GOALS AND TRADE-OFFS IN MIMO FEEDBACK DESIGN

Most methodologies are based on shaping the singular values of specified transfer functions such as the loop transfer function L or one or more of the closed loop transfer functions such as the sensitivity function S , the complementary sensitivity function T or KS .

6.1.1 Closed Loop Transfer Functions

Figure 20 shows a block diagram of a standard one degree-of-freedom negative feedback control system with the plant model G and the disturbance transfer function G_d . r is the reference value, d the disturbance signal, n the measurement noise on the output signal y and the input signal to the plant is given by

$$u = K(s)(r - y - n). \quad (6.1)$$

The control error will from now on be defined as

$$e = y - r. \quad (6.2)$$

The goal of control is to minimize the control error while the system is affected by disturbances d and measurement noise n . In accordance with figure 20 the output equation can be written as

$$y = G(s)u + G_d(s)d. \quad (6.3)$$

Substitution of (6.1) into (6.3) yields

$$y = G(s)K(s)(r - y - n) + G_d d, \quad (6.4)$$

rearranging above equation yields a relation for the closed-loop response

$$y = \underbrace{(I + GK)^{-1}GK}_{T} r + \underbrace{(I + GK)^{-1}G_d}_{S} d - \underbrace{(I + GK)^{-1}GK}_{T} n. \quad (6.5)$$

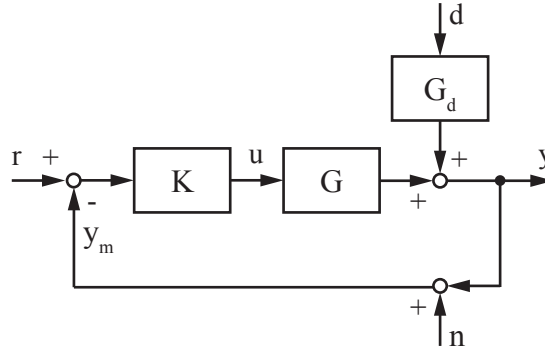


Figure 20: Standard 1 DoF feedback control system

With the following abbreviations

$$\begin{aligned}
 L &= GK && \text{loop transfer function} \\
 S &= (I + GK)^{-1} = (1 + L)^{-1} && \text{sensitivity function} \\
 T &= GK(I + GK)^{-1} = L(I + L)^{-1} && \text{complementary sensitivity function}
 \end{aligned}$$

equation (6.3) simplifies to

$$y = Tr + SG_d d - Tn \quad (6.6)$$

By exploiting that $S + T = I$ we obtain the following relation for the control error e

$$e = y - r = -Sr + SG_d d - Tn \quad (6.7)$$

with the corresponding control input signal u given by

$$u = KSr - KSG_d d - KSn \quad (6.8)$$

The name „complementary“ sensitivity function originates from the important identity

$$S + T = I. \quad (6.9)$$

6.2 CLOSED LOOP STABILITY

The following three methods are commonly used to analyze closed loop stability behavior.

- Pole Analysis
- Nyquist's Stability Criterion
- Bode's Stability Criterion

6.3 PERFORMANCE CRITERIONS

For evaluating the closed loop performance of the controller, quantitative performance measures are needed.

6.3.1 Time Domain Performance

The following list gives common specifications for time-domain behavior of control systems and typical values suggested by [32] Skogestad and Postlethwaite.

RISE TIME (t_r): the time it takes the system to reach 90% of its final value.

RISE TIME (t_p): the time required to reach the maximum peak.

ε -SETTLING TIME: the time after which $y(t)$ stays within ε of y_f .

$$t_{s,\varepsilon} := \inf_{\tau} \{ \tau \mid ||y(t) - y_f|| < \varepsilon \forall t \in [\tau, \infty) \} \quad (6.10)$$

MAXIMUM OVERSHOOT (y_{os}): is defined as

$$y_{os} := \sup_t \{ y(t) / y_f \} \quad (6.11)$$

DECAY RATIO (r_d): the ratio of the second and first peak

$$r_d := A / B \quad (6.12)$$

STEADY-STATE OFFSET: the difference between the final value and the desired final value.

$$e_{SSE} := \lim_{t \rightarrow \infty} \{ y(t) - y_{des} \} \quad (6.13)$$

MEAN SQUARED ERROR (e_{MSE}):

$$e_{MSE} := ||e(t)||_2 = \sqrt{\int_0^{\infty} |e(\tau)| d\tau} \quad (6.14)$$

6.3.1.1 Design Goals

Design goals for the heave dynamics controller are zero steady-state offset, minimal possible overshoot and minimization of the mean squared error in hovering condition. These requirements primarily determine the helicopter's aerial manipulation capabilities. Throughout all flight missions the steepness of the height reference trajectory will be limited by a rate limiter¹; maximal heave velocity is limited to 1.5 m/s. Therefore rise time t_r has to be just as little as is required to reach the maximal allowed heave velocity.

¹ In addition, the reference signal is also filtered in standard missions, see fig. 39-41

6.3.2 Frequency Domain Performance

Time-domain performance specifications are the easiest to get a feeling for. However, frequency-domain performance specifications offer several advantages. A lot of modern controller design methods rely on frequency domain specifications. Compared to step response analysis a wider spectrum of input signals can be considered – usually sinusoids of any frequency. Since „any“ signal can be described as a superposition of harmonic functions like sinusoids a broad spectrum of input signals can be covered.

6.3.2.1 Gain Margin

The *gain margin* is the factor by which the loop gain $|L(j\omega_{180})|$ can be increased before the closed-loop system becomes unstable. It is defined as

$$GM = \frac{1}{|L(j\omega_{180})|} \quad (6.15)$$

where ω_{180} is the *phase crossover frequency*. It's defined as the frequency where the Nyquist curve of loop transfer function $L(j\omega)$ crosses the negative real axis between 0 and -1 , i.e.

$$\angle L(j\omega) = -180^\circ \quad (6.16)$$

In case L crosses the real axis multiple times between 0 and -1 , the closest crossing to -1 is regarded. Generally $GM > 2$ is required, [32].

6.3.2.2 Phase Margin

The *phase margin* describes how much more negative phase (phase lag) can be added to the loop transfer function until $L(j\omega_c)$ equals -1 which means closed-loop instability. It is defined as

$$PM = \angle L(j\omega_c) + 180^\circ \quad (6.17)$$

where ω_c is the *gain crossover frequency*, i.e.

$$|L(j\omega_c)| = 1. \quad (6.18)$$

[32] Skogestad and Postlethwaite suggests the PM to be larger than 30° . The higher the time delay uncertainty the higher the recommended PM, which becomes obvious by the following relation [32, p. 32]

$$\theta_{max} = PM / \omega_c, \quad (6.19)$$

where θ_{max} is the maximum time delay that can be added until the closed-loop system becomes unstable. Interestingly, the lower ω_c the higher time delays the system can tolerate.

Design goals	Dependencies	Requirem.	at freq. where
<i>Disturbance rejection</i>	$e = (1 + L)^{-1} G_d d$	large $\underline{\sigma}(L)$	$\underline{\sigma}(L) \gg 1$
<i>Reference tracking</i>	$e = (1 + L)^{-1} r$	large $\underline{\sigma}(L)$	$\underline{\sigma}(L) \gg 1$
<i>Noise attenuation</i>	$e = L(1 + L)^{-1} n$	small $\overline{\sigma}(L)$	$\overline{\sigma}(L) \ll 1$
<i>Input usage reduction</i>	$u = K(r - y - n)$	small $\overline{\sigma}(K)$	$\overline{\sigma}(GK) \ll 1$
<i>Input usage disturbance</i>	$u = K(1 + L)^{-1} G_d d$	small $\overline{\sigma}(K)$	$\overline{\sigma}(L) \ll 1$
<i>Physical system must be strictly proper</i>		$\lim_{\omega \rightarrow \infty} L = 0$	
<i>Robust stability (multipl. output uncert.)</i>		small $\overline{\sigma}(GK)$	$\overline{\sigma}(GK) \ll 1$
<i>Robust stability (additive output uncert.)</i>		small $\overline{\sigma}(K)$	$\overline{\sigma}(GK) \ll 1$

Table 2: Trade-offs in feedback control in terms of open-loop objectives L and K .

6.3.3 Maximum Peak Performance Criteria

The maximum peaks of the sensitivity function

$$M_S := \|S\|_\infty \quad (6.20)$$

and complementary sensitivity function

$$M_T := \|T\|_\infty \quad (6.21)$$

can be used as performance and robustness indicators. Typically, it is required that M_S is less than 2 and M_T is less than 1.25, [32, p. 36]. These recommendations stem from the close relations between the peak values of S and T and the GM and PM

$$GM \geq \frac{M_S}{M_S - 1}; \quad PM \geq \frac{1}{M_S} [\text{rad}] \quad (6.22)$$

$$GM \geq 1 + \frac{1}{M_T}; \quad PM \geq \frac{1}{M_T} [\text{rad}]. \quad (6.23)$$

6.3.4 Trade-offs of Loop-shaping in terms of L

To achieve „perfect“ control, i.e. $e = 0$, we require $S \rightarrow 0$ (disturbance rejection and command tracking) and $T \rightarrow 0$ (noise attenuation), compare eq. (6.7). Small S implies large L since $S = (1 + L)^{-1}$, whereas small T implies small L since $T = L/(1 + L)^{-1}$. This illustrates that trade-offs have to be made when designing feedback controllers.

Usually we want the control input u to be constrained within specified borders. Since $u = K(s)(r - y - n)$, see eq. (6.8), small magnitudes of u correspond to small controller gains K and therefore small $L = GK$. Since design goals usually have to be met in different frequency ranges, most design goals can be fulfilled simultaneously by choosing large loop gains at low frequencies and small loop gains at high frequencies. The frequency ω_c at which $\overline{\sigma}(L)$ drops below 1 is called *gain crossover frequency*. Generally we want $\underline{\sigma}(L)$ to be as large as possible below ω_c and L to fall as sharply as possible

Design goals	Dependencies	Requirements
<i>Disturbance rejection</i>	$e = SG_d d$	minimize $\ S\ _\infty$
<i>Reference tracking</i>	$e = Sr$	minimize $\ S\ _\infty$
<i>Noise attenuation</i>	$e = Tn$	minimize $\ T\ _\infty$
<i>Input usage reduction</i>	$u = KS(r - n)$	minimize $\ KS\ _\infty$
<i>Input usage disturbance</i>	$u = KSG_d d$	minimize $\ KSG_d\ _\infty$

Table 3: Trade-offs in feedback control in terms of closed-loop transfer functions

above ω_c (high *roll-off*) rate. Under the aspect of achieving sufficient GM and PM these design goals are contradictory. For $|L(j\omega)|$ typically a slope of -1 at ω_c and a slope of at least -2 above crossover is desirable.

To achieve desirable low-frequency performance and offset-free reference tracking, $L(s)$ must contain at least one integrator for each integrator in $r(s)$, see [32, p. 44] Skogestad and Postlethwaite.

6.3.5 Trade-offs of Loop-shaping in Terms of Closed-Loop Transfer Functions

Equation (6.7) shows how to design the closed-loop transfer function S and T to achieve „perfect“ control, i.e. $e = 0$. Generally we want $S \rightarrow 0$ to achieve optimal disturbance rejection and command tracking, and we want $T \rightarrow 0$ for optimal noise attenuation. Since $S + T = I$, trade-offs have to be made. Table 3 summarizes design goals in terms of closed-loop transfer functions.

Again, the contradicting design objectives have to be met at different frequencies. Generally we want $\|S\|_\infty$ to be small in the low frequency area and $\|T\|_\infty$ to be small in the high frequency area.

Remark. In the open-loop case with no control, i.e. $K = 0$, the control error equals

$$e = y - r = G_d d + 0 \cdot n - r, \quad (6.24)$$

whereas in the closed-loop case it equals

$$e = S(-r + G_d d - Ln). \quad (6.25)$$

Imagine a SISO system, then it becomes obvious that feedback improves performance in frequency areas where $|S| < 1$.

Remark. Probably the biggest advantage of shaping S and T is the fact that only their magnitudes have to be taken into consideration, as opposed to when shaping L , their phases can be neglected. As mentioned above, we generally desire $S \approx 0$ and $T \approx 0$ for certain frequency areas, which will be the case if $|S| \approx 0$ and $|T| \approx 0$, respectively, independent of their respective phases.

6.4 GENERAL CONTROL CONFIGURATION

Doyle [2], [3] proposed a general method of formulating control problems which is based on casting the problem into the so called *general control configuration* which is shown in figure 21. The main advantage of that standard formulation is that any problem may be arranged into that form. Once the

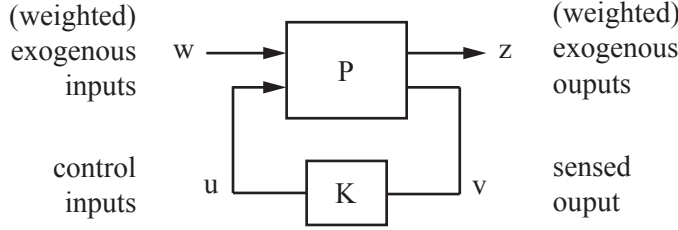


Figure 21: General Control Configuration

problem is casted into the general control configuration the design goal of H_∞ control becomes to determine a stabilizing controller that minimizes the H_∞ -norm of the closed loop transfer function N from w to z

$$z = Nw. \quad (6.26)$$

In other words, the controller K generates a control signal u , which depends on the measured output v , to counteract the influence of the external inputs w on the external outputs z . To define P one has to identify the signals w, z, u and v which then allows setting up the transfer function matrix. This can either be done by writing down the outputs z and v as functions of the inputs w and u

$$z = P_{11}(s)w + P_{12}(s)u \quad (6.27)$$

$$v = P_{21}(s)w + P_{22}(s)u \quad (6.28)$$

and subsequently combining the elements of P

$$P = \begin{bmatrix} P_{11} & P_{12} \\ P_{21} & P_{22} \end{bmatrix}, \quad (6.29)$$

or by directly inspecting the block diagram representation of the control problem. Often it is useful to have a state space representation of P

$$P = \left[\begin{array}{c|cc} A & B_1 & B_2 \\ \hline C_1 & D_{11} & D_{12} \\ C_2 & D_{21} & D_{22} \end{array} \right]. \quad (6.30)$$

6.4.1 Closed Loop Transfer Function N

Once P is setup the closed-loop transfer function N can be derived by *lower linear fractional transformation (LFT)* of P with K as the parameter.

$$N = F_l(P, K) = P_{11} + P_{12}K(I - P_{22}K)^{-1}P_{21} \quad (6.31)$$

N can be numerically derived from P by employing MATLAB command `lft`.

A stabilizing, H_∞ optimal controller that minimizes

$$\|F_l(P, K)\|_\infty = \max_{\omega} \overline{\sigma}((F_l(P, K)(j\omega)) \quad (6.32)$$

can then be determined with the general H_∞ algorithm introduced in the appendix, see theorem A.1.

Remark. Sometimes N can be directly derived manually from the block diagram of the corresponding design problem.

6.5 $S/KS/T$ MIXED SENSITIVITY OPTIMIZATION

$S/KS/T$ mixed sensitivity optimization is one of the most popular H_∞ controller design concepts, mainly due the fact that it can be quickly implemented and is more intuitive to the control engineer than to other design methods. $S/KS/T$ mixed sensitivity optimization is based on shaping one or more of the closed-loop transfer functions S , T and KS . In addition to the requirement that K stabilizes G , trade-offs have to be made when defining design objectives, which are summarized in table 3. Design specifications, such as the level of model uncertainty that can be tolerated, disturbance rejection, noise attenuation and desired bandwidth of the closed loop can be embedded in the design stage in the form of frequency dependent performance weights, see figure 22. The effects of the aforementioned closed-loop transfer func-

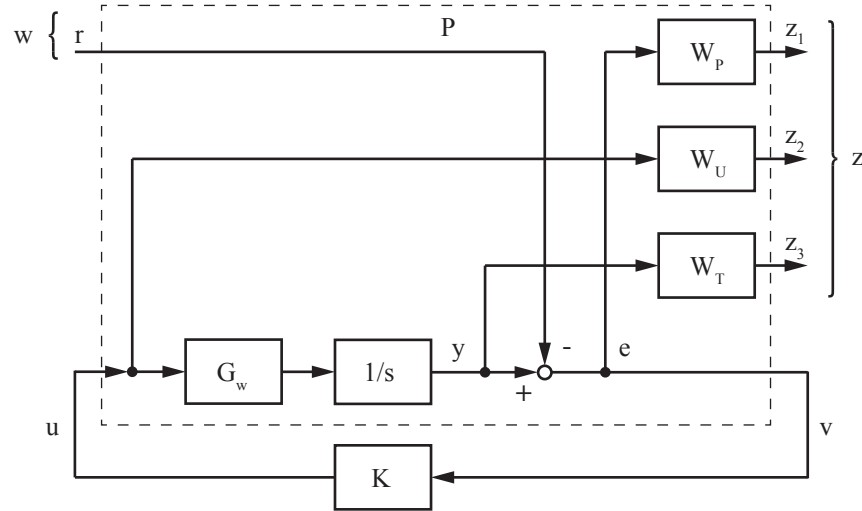


Figure 22: $S/KS/T$ mixed-sensitivity optimization

tions on design goals such as disturbance rejection, command tracking etc. can be seen by recalling equations (6.6)-(6.8). E.g. the sensitivity function S is the transfer function between the disturbance d and the output y . Therefore, feedback improves disturbance rejection performance in frequency areas where $\overline{\sigma}(S(j\omega)) < 1$. Since disturbances like wind gusts are usually of low frequency it is sufficient to minimize the maximum singular values of S over that same low frequencies. In this case we could choose a low-pass filter as

performance weight W_p whose bandwidth matches that of the disturbance signal and we would define $|1/W_p(j\omega)|$ as an upper bound for S

$$\|S(j\omega)\|_\infty \leq |W_p^{-1}(j\omega)| \quad \forall \omega. \quad (6.33)$$

One of the goals of the optimization algorithm would then be to minimize $\|W_p S\|_\infty$. By making these kind of considerations and having relations (6.6) - (6.8) in mind, weighting functions for the other closed loop transfer functions can be chosen to meet design requirements, yielding singular value inequalities of analog form

$$\|KS(j\omega)\|_\infty \leq |W_U^{-1}(j\omega)| \quad \forall \omega, \quad (6.34)$$

$$\|T(j\omega)\|_\infty \leq |W_T^{-1}(j\omega)| \quad \forall \omega. \quad (6.35)$$

To combine these design specification a mixed approach is applied, yielding the following overall specification

$$\|N\|_\infty < 1, \text{ where } N = \begin{bmatrix} W_p S \\ W_U KS \\ W_T T \end{bmatrix}. \quad (6.36)$$

The reason behind this stacked approach is purely mathematical convenience. One inherent disadvantage is, that this results in more conservative design specifications than originally defined, but since the selection of weights is an iterative process and the design specifications are generally rather rough, the advantages of this approach outweigh the disadvantages.

Figure 22 shows how the mixed-sensitivity approach can be casted into the general problem formulation. From figure 22 one can directly see that

$$z_1 = W_p e = W_p(Gu - r) = -W_p \frac{I}{I + GK} r = -W_p S r \quad (6.37)$$

$$z_2 = W_U u = W_U K v = W_U \frac{K}{I + GK} r = W_U K S u \quad (6.38)$$

$$z_3 = W_T y = W_T G u = W_T \frac{GK}{I + GK} r = W_T T r \quad (6.39)$$

and from these relations the generalized plant

$$P : \begin{bmatrix} w & u \end{bmatrix}^T \longrightarrow \begin{bmatrix} z & v \end{bmatrix}^T \quad (6.40)$$

can be derived

$$\begin{bmatrix} z \\ v \end{bmatrix} = \begin{bmatrix} z_1 \\ z_2 \\ z_3 \\ v \end{bmatrix} = \underbrace{\begin{bmatrix} -W_p & W_p G \\ 0 & W_U \\ 0 & W_T G \\ I & -G \end{bmatrix}}_P \begin{bmatrix} r \\ u \end{bmatrix} = P(s) \begin{bmatrix} w \\ u \end{bmatrix}. \quad (6.41)$$

With lower linear fractional transformation of P with parameter K the closed loop transfer function from w to z can be derived

$$N = \begin{bmatrix} -W_P S \\ W_T T \\ W_U K S \end{bmatrix}. \quad (6.42)$$

Alternatively N can be directly obtained by rearranging relations (6.37)-(6.39) that can be read out from figure 22. By comparing eq. (6.42) with eq. (6.36) it becomes clear that we gained N of the stacked approach. Since we are only interested in its H_∞ -norm the different sign does not matter.

6.5.1 Weight Selection

As a starting point, the weights were chosen to be similar to those used by Postlethwaite and Yue [28] and then iteratively adapted in simulation runs until desirable flight performance was achieved.

6.5.1.1 Selection of $W_P(s)$

In SISO case performance weights are typically in the form of

$$W_P = \frac{s/M + \omega_B^*}{s + \omega_B^* A} \quad (6.43)$$

where M , the *sensitivity peak*, defines the maximum peak magnitude of S , i.e. $\|S\|_\infty \leq M$. M has to be larger than 1 for robustness reasons, a typical value would be 2.

A is equal to the *maximum steady-state tracking error*. A value of $A = 0$ means no steady-state error and thereby demands a controller with integral action. MATLAB is used to synthesize the H_∞ controller. The command in use is `mixsyn`, its underlying algorithm asks for stable weights to avoid numerical problems. By shifting integrators slightly into the left half plane numerical issues can be circumvented. This doesn't affect the controllers practical performance.

The *bandwidth frequency* ω_B^* defines where W_P reaches $1/\sqrt{2}$ from below for the first time and where its asymptote crosses 1 at ω_B^* , respectively. The following helpful approximations of $1/|W_P|$, the upper bound of $\|S\|_\infty$, can be made

$$\lim_{\omega \rightarrow 0} 1/|W_P| = A \quad (6.44)$$

and

$$\lim_{\omega \rightarrow \infty} 1/|W_P| = M. \quad (6.45)$$

To improve performance a steeper slope for S for $\omega < \omega_B^*$ might be desirable, according weights are typically of the form

$$W_P = \frac{(s/M^{1/n} + \omega_B^*)^n}{(s + \omega_B^* A^{1/n})^n} \quad n \in \mathbb{N}, \quad (6.46)$$

where n determines the slope. In MIMO cases W_P usually are diagonal matrices with entries of the form given in equation (6.43) and (6.46), respectively.

The final weight W_P was chosen as follows

$$W_P(s) = 500 \frac{1 + s/6}{1 + s/0.006}, \quad (6.47)$$

which equals to $M = 2$, $\omega_B^* = 3 \text{ rad/s}$ and $A = 2 \times 10^{-3}$. There is no point in increasing the bandwidth ω_B^* beyond approximately 1 Hz since the high frequency helicopter dynamics, especially the rotor dynamics (flapping, coning, lead-lag etc.), are not modeled. In our case a bandwidth of approximately 0.5 Hz was chosen since higher bandwidths would increase overshooting to undesirable magnitudes.²

6.5.2 Selection of W_U

For W_U a first order high-pass filter was chosen as follows

$$W_U(s) = 0.5 \frac{1 + 50s}{1 + 0.05s}. \quad (6.48)$$

Figure 23 shows the frequency-domain characteristics of the selected weights W_P , W_U and their inverses.

Remark. In hindsight to the digital implementation of the controller, high frequency controller action should be avoided, which is realized with an actuator action punishing weight W_U that increases with frequency. This prevents very fast controller poles in the far left half-plane which would require the actuator to operate in a broad dynamic range, which of course, should be prevented as argued by Postlethwaite and Yue [28].

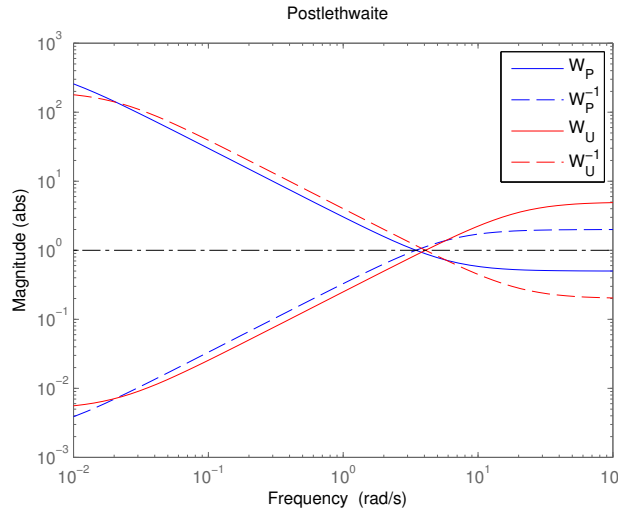


Figure 23: Bode plots of weights for mixed sensitivity optimization

² 0.5 Hz \approx 3 rad/s

$\gamma_{min} = \ N\ _\infty$	ω_c	M_S	M_T	GM	PM	$\omega_{GM}[\text{rad/s}]$	ω_{PM}	delay margin
1.88	1	1.44	1	6.60	66.33°	5.63	1.55	0.72

Table 4: Performance parameters of the H_∞ mixed sensitivity design

Remark. It's important to choose stable weights for mixed sensitivity H_∞ based optimization control, otherwise the general H_∞ algorithm A.1 is not applicable since the necessary assumption that (A, B_2, C_2) is stabilizable and detectable would be violated.

6.5.2.1 Selection of W_T

In the current controller design no W_T weights was used.³ T cannot be shaped independently from S , see eq. (6.9), therefore W_T weights can often times be neglected.

6.5.3 Analysis of the Controller

The number of states of the resulting controller is equal to that of the generalized plant P (4): plant G_z (2), performance weights W_U, W_P (2).

Figure 24 shows singular value plots of the transfer functions KS, S, T and weights W_P, W_U . As desired the singular value of S is small at low frequencies where feedback is effective. At high frequencies S approaches 1 like any strictly proper system

$$\omega \rightarrow \infty : L(j\omega) \rightarrow 0 \Rightarrow S(j\omega) \rightarrow I.$$

As with any real system $\overline{\sigma}(S(j\omega))$ has a peak greater 1. For any real system there exists a frequency ω_{180} where $L(j\omega)$ reaches a phase lag of -180° . From the definition of the GM (6.15) for SISO systems and relation (6.22) which states $GM > 1$, follows directly that $|S(j\omega)|$ must exceed 1 at frequency ω_{180} .

$$GM = \frac{1}{|L(j\omega_{180})|} \Leftrightarrow L(j\omega_{180}) = -\frac{1}{GM} \Leftrightarrow S(j\omega_{180}) = \frac{1}{1 - \frac{1}{GM}}.$$

We originally required $M_S < 2$, so a peak value of 1.31, at a frequency of 2.15 rad/s, is perfectly fine. The bandwidth frequency ω_B of 1.2 rad/s lies close to the desired bandwidth of 1 rad/s. For this design problem we achieved an H_∞ norm of $\gamma = 1.88$, so the design requirements (6.48)-(6.55) are not perfectly satisfied. The final design is proven to be successful in simulation, see chapter 7. Which is also backed up by the according performance parameters summarized in table 7.

Remark. When employing weights w_P and w_T is it necessary to ensure that the crossover frequency at which w_P passes 1 lies below the crossover frequency of w_T . This ensures a gap between the performance bound w_P and the robustness bound w_T^{-1} where open-loop transfer passes L can pass through.

³ No significant performance increases could be achieved by including one.

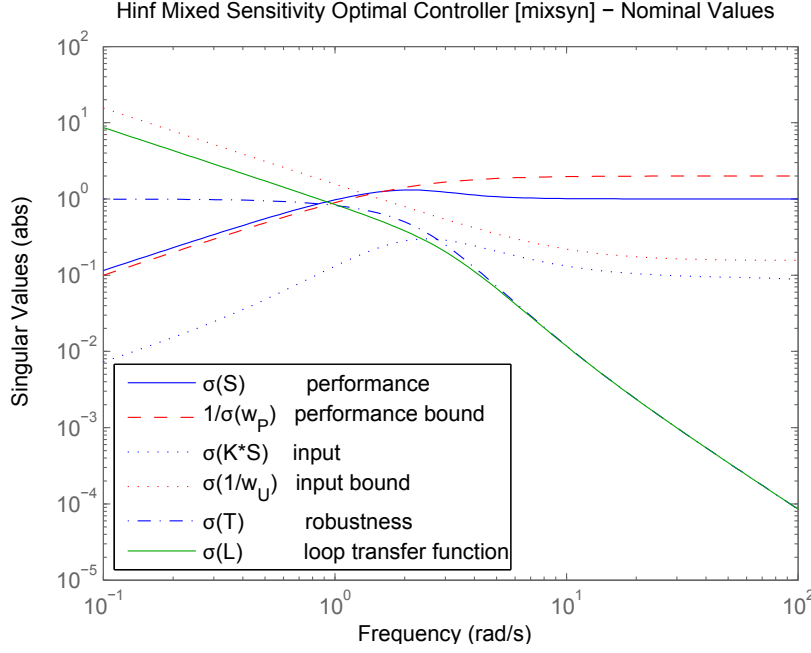


Figure 24: Singular value plot showing the results of the H_∞ mixed sensitivity controller design

6.6 SIGNAL-BASED H_∞ CONTROL

One major advantage of the signal based approach of H_∞ controller design is its generality. The engineer has a lot of freedom when defining the design objectives and multiple objectives can be considered at once. At first all exogenous inputs affecting the system and the *error signals*, whose H_∞ norm should be kept minimal, have to be defined. Weights W_d , W_i and W_n can be used to describe the frequency content of the exogenous signals d , r and n , as shown in fig. 25. Weights W_p and W_U are used to shape the frequency content of the error signal e and the control signal u . Transfer function G_d describes the disturbance (wind disturbances in our case). By adjusting the weight W_d the relative importance of disturbance rejection can be set. Sometimes an additional weight W_{ref} is implemented to force the closed-loop transfer function from the weighted reference value r_s to y to approximate the desired closed-loop transfer function given by W_{ref} .

The problem can then be casted into the general control configuration with the following exogenous inputs and outputs

$$\begin{aligned} w &= \begin{bmatrix} d \\ r \\ n \end{bmatrix} & z &= \begin{bmatrix} z_1 \\ z_2 \end{bmatrix} \\ v &= \begin{bmatrix} r_s \\ y_m \end{bmatrix} & u &= u, \end{aligned} \quad (6.49)$$

and generalized plant

$$\begin{bmatrix} z \\ v \end{bmatrix} = \begin{bmatrix} z_1 \\ z_2 \\ z_3 \\ v \end{bmatrix} = \begin{bmatrix} W_P G_d W_d & -W_P W_r & 0 & W_P G \\ 0 & 0 & 0 & W_U \\ W_T G_d W_d & 0 & 0 & W_T G \\ -G_d W_d & W_r & -W_n & -G \end{bmatrix} \begin{bmatrix} d \\ r \\ n \\ u \end{bmatrix} = P(s) \begin{bmatrix} w \\ u \end{bmatrix}. \quad (6.50)$$

Next, the standard H_∞ optimal control problem can be solved (see general H_∞ algorithm A.1).

6.6.0.1 Weight Selection

Weights W_U and W_P are chosen similar to those in the mixed sensitivity approach. A W_{ref} reference weight is not used. The weights for the exogenous input signals were chosen in an iterative process as follows:

$$W_r = 1 \quad W_d = 0.1 \quad W_n = 0. \quad (6.51)$$

Disturbance by noise wasn't taken into account when formulating the design problem, since simulation results suggested that no significant noise rejection improvements could be achieved by integrating an additional weight W_n for n without sacrificing tracking and wind disturbance rejection.

Remark. Compared to mixed sensitivity control the weights used in signal-based H_∞ control have not only to be stable but also proper, otherwise the general H_∞ algorithm would not be applicable.

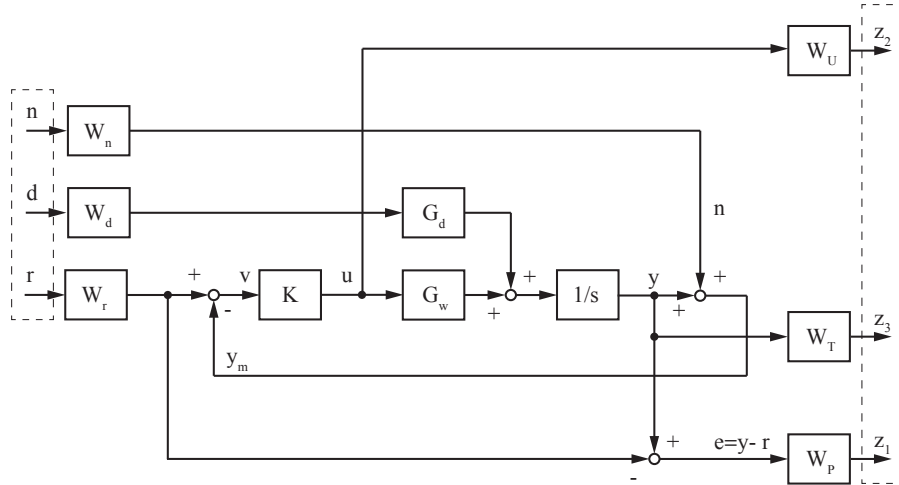


Figure 25: Signal-based H_∞ control problem

6.7 H_∞ LOOP-SHAPING DESIGN (1 DOF)

The following looping-shaping design procedures were first published by **McFarlan and Glover** [22]. It's a three-staged procedure:

1. Augment the nominal open-loop plant G by pre- and post-compensators W_1 and W_2 . The compensators allow to shape the singular values of the open-loop frequency response. The nominal system G and the weighting functions W_1 and W_2 are combined to form the *shaped plant* $G_s = W_2 G W_1$.
2. The normalized left coprime factorization of G_s is robustly stabilized, with stability margin ϵ , by a feedback controller K_∞ which is synthesized with the *Normalized LCF Stabilization Procedure*.
3. The final feedback controller is then formed as follows

$$K = W_1 K_s W_2. \quad (6.52)$$

See figure 26 for a block diagram representation of the design problem.

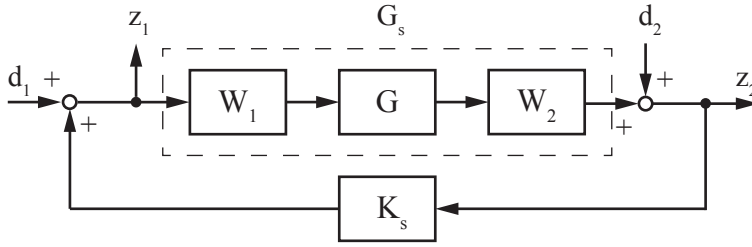


Figure 26: 1 DoF H_∞ loop-shaping setup

6.7.1 Shaped System G_s

The robust stabilization procedure presented below (6.7.2) could be directly applied to the original plant G , but this would leave the designer with little tuning options to influence the performance of the system. Therefore Glover and McFarlan [8] proposed shaping the nominal plants open-loop singular values with *pre-* and *post-compensators* W_1 and W_2 (*dynamic weighting matrices*) to achieve desirable open-loop properties in the frequency domain and thereafter robustly stabilizing the shaped plant $G_s = W_2 G W_1$. In our case we apply the normalised left coprime factor robust stabilization procedure presented in 6.7.2.

6.7.2 Robust Stabilization

Let G be a plant with a normalized left coprime factorization

$$G = M_l^{-1} N_l. \quad (6.53)$$

Once this factorization is known we can use so called coprime factor uncertainty description to describe a perturbed plant. Its sets of plants can be written as

$$G_p = (M_l + \Delta_M)^{-1} (N_l + \Delta_N), \quad \|[\Delta_N \quad \Delta_M]\|_\infty \leq \epsilon \quad (6.54)$$

where $\varepsilon > 0$ is the ∞ -norm bound of the stacked uncertainty and Δ_N, Δ_M are stable, unknown transfer functions which describe the uncertainty of the nominal plant model G , see figure 27 for a block diagram representation. The

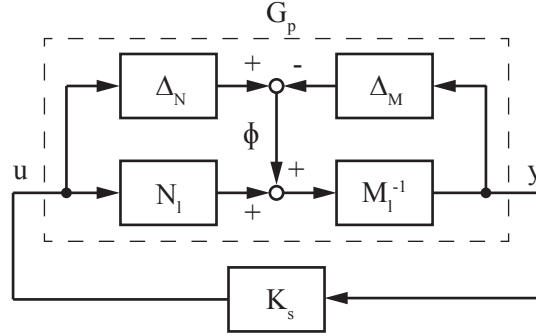


Figure 27: H_∞ robust stabilization of a normalized left coprime factor plant G

norm bound ε is necessary for a tight condition for robust stability in terms of $\|M\|_\infty$ ([32, p. 304], [28]), where M is defined as in 6.55. One advantage of the coprime uncertainty description is, that it requires no *a priori* knowledge about system uncertainties. The fact that poles and zeros are allowed to shift into the RHP accounts for the generality of this uncertainty description.

Again, the goal of robust stabilization is to find a controller K_s which stabilizes the nominal plant G and the set of perturbed plants G_p as defined in (6.54). Before we can apply the algorithm presented below, we have to rearrange the block diagram in Figure 27 to match the $M\Delta$ -structure shown in fig. 28. Reforming yields

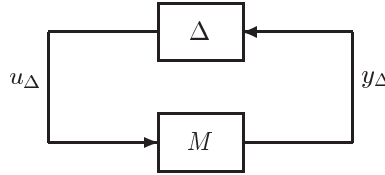


Figure 28: $M\Delta$ -structure for robust stability analysis

$$\Delta = [\Delta_N \quad \Delta_M]; \quad M = - \begin{bmatrix} K_s \\ I \end{bmatrix} (I + GK_s)^{-1} M_l^{-1}. \quad (6.55)$$

Theorem 6.1 (Robust stability for unstructured („full“) perturbations [32]). Assume that the nominal system $M(s)$ is nominal stable and that the perturbations $\Delta(s)$ are stable. Then the $M\Delta$ -system in figure 28 is stable for all perturbations Δ satisfying $\|\Delta\|_\infty \leq 1$ (i.e. we have robust stability) if and only if

$$\overline{\sigma}(M(j\omega)) \leq 1 \quad \forall \omega \quad \Leftrightarrow \quad \|M\|_\infty \leq 1 \quad (6.56)$$

When using coprime uncertainty description the tight bound in theorem 6.1 changes to $1/\varepsilon$, where ε is the H_∞ norm bound of the uncertainty

$$\|\Delta_N \quad \Delta_M\|_\infty \leq \varepsilon \quad \Leftrightarrow \quad \|M\|_\infty < 1/\varepsilon. \quad (6.57)$$

Glover and McFarlan [8] presented a method to maximize the stability margin ε . We define $\gamma_K \equiv \|M\|_\infty$ which simplifies the robust stability condition (6.57) to

$$\gamma_K \equiv \left\| \begin{bmatrix} K_s \\ I \end{bmatrix} (I - GK)^{-1} M^{-1} \right\|_\infty \leq \frac{1}{\varepsilon} \quad (6.58)$$

where γ_K is the H_∞ norm from ϕ to $\begin{bmatrix} u \\ y \end{bmatrix}$ and $(I - GK_s)^{-1}$ is the sensitivity function. The minimal achievable value of γ_K is according to Glover and McFarlan [8] given by

$$\gamma_{min} = \min\{\gamma_K\} = \frac{1}{\max\{\varepsilon\}} = \{1 - \|[N \ M]\|_H^2\}^{-1/2}. \quad (6.59)$$

$\|\cdot\|_H$ denotes the Hankel norm. A controller K that guarantees $\gamma_K \leq \gamma$ for a given $\gamma > \gamma_{min}$, was introduced by McFarlan and Glover [22]

$$K_s \stackrel{s}{=} \left[\begin{array}{c|c} A + BF + \gamma^2(L^T)^{-1}ZC^T(C + DF) & \gamma^2(L^T)^{-1}ZC^T \\ \hline B^T X & -D^T \end{array} \right] \quad (6.60)$$

$$F = -S^{-1}(D^T C + B^T X) \quad (6.61)$$

$$L = (1 - \gamma^2)I + XZ \quad (6.62)$$

where X and Z are the solutions of the following two Riccati equations

$$(A - BS^{-1}D^T C)Z + Z(A - BS^{-1}D^T C)^T - ZC^T R^{-1}CZ + BS^{-1}B^T = 0 \quad (6.63)$$

where

$$R = I + DD^T, \quad S = I + D^T D$$

and

$$(A - BS^{-1}D^T C)^T X + X(A - BS^{-1}D^T C) - XBS^{-1}B^T X + C^T R^{-1}C = 0. \quad (6.64)$$

A, B, C, D are the matrices of the state space realization of the shaped plant G_s .

Remark. By using the algorithm above, we can avoid the general H_∞ algorithm, which iteratively reduces γ to approach the optimal solution γ_{min} (γ -iteration). This is one of the advantages of the 1 DoF LSD method over the previously presented ones in section 6.5 and 6.6. Another advantage compared to the mixed sensitivity approach is that no pole-zero cancellations between the plant and the controller occurs, [32, p.372]⁴.

⁴ One exception where also pole-zero cancellation might occur are systems with all-pass behavior

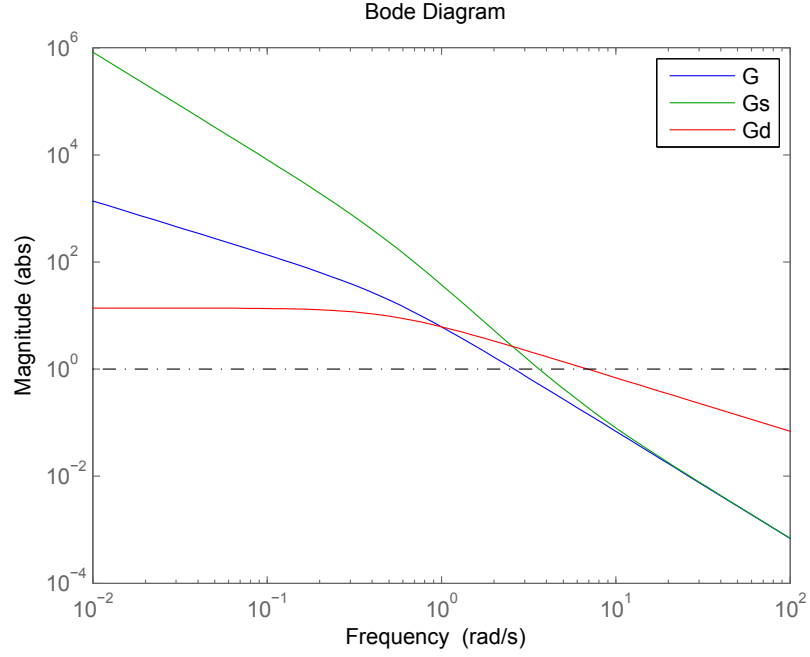


Figure 29: Singular value plots original plant G , the shaped plant G_s and the disturbance transfer function G_d

6.7.3 Plant Shaping and Final Controller

The weights are chosen as follows

$$W_1 = \frac{s+6}{s}, \quad (6.65)$$

$$W_2 = 1. \quad (6.66)$$

The integral action of W_1 ensures low frequency performance and a theoretical steady-state error of zero. The phase-advance term reduces rolloff close to gain crossover from -2 to -1 . Typically, $|L(j\omega)|$ should have a slope of -1 in the cross over region to improve transient behaviour and to achieve good GM and PM [32, p.43,49]. W_2 is usually used to define the relative importance of the controlled outputs. Since the output is one-dimensional W_2 is set to 1. Figure 29 shows bode plots of G, G_s and G_d .

Remark. Weights have to be chosen such that G_s contains no hidden, unstable modes.

The final open-loop shape $GK = GW_1K_sW_2$, achieved after robust stabilization, matches that of the desired loop shape $G_s = W_2GW_1$. More precisely, GK lies within a δ neighborhood of G_s , as can be seen in the sigma plot in figure 30. γ is an indicator for matching accuracy, Gu et al. [10, p. 179] states the following relations/estimations

$$\overline{\sigma}(GK) \geq \overline{\sigma}\left(\frac{1}{\gamma}G_s\right), \quad \forall \omega < \omega_c \quad (6.67)$$

and

$$\overline{\sigma}(GK) \leq \overline{\sigma}(\gamma G_s), \quad \forall \omega > \omega_c. \quad (6.68)$$

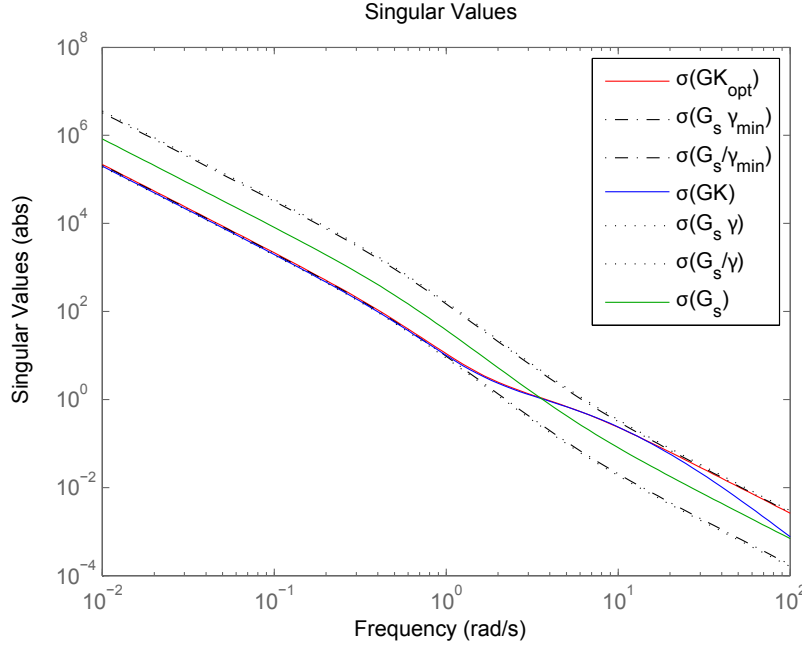


Figure 30: Singular value plots of the shaped plant G_s and the final loop transfer functions with their respective boundaries

In our case

$$\gamma = \gamma_{rel} \gamma_{min} = 1.1 * 3.1849 = \quad (6.69)$$

As desired the slope is -2 in the higher and lower frequency regions and is reduced to -1 at crossover.

Generally we want the stability margin $\varepsilon_{max} = 1/\gamma_{min}$, which defines the maximum coprime uncertainty the system can handle, to be as large as possible. Postlethwaite and Yue [28] showed that for large ε (small γ) the singular values of the final open loop resemble those of G_s . As a rule of thumb, ε_{max} should be greater than 0.25 [32] and 0.2 [10], respectively. Therefore, ε can be interpreted as an indicator of the success of loop matching and a measure of robustness.

6.8 TWO DEGREES OF FREEDOM LOOP-SHAPING DESIGN

In 1 DoF freedom design problems the desired controller shape for „optimal“ reference tracking and disturbance rejection usually differ. Both design goals cannot be optimally achieved with a single feedback controller.

One solution to this issue is to implement a 2 DoF controller which treats the reference signal r and the measured output signal y_m independently. Instead of a single controller with two inputs the controller can be split into two separate blocks. One common form is depicted in figure 31 where K_1 denotes the prefilter and K_2 the feedback part of controller. In this configuration the prefilter K_1 can be tuned to improve reference tracking performance by shaping r and the feedback controller K_2 can be tuned to alleviate the effects of disturbances and model uncertainties.

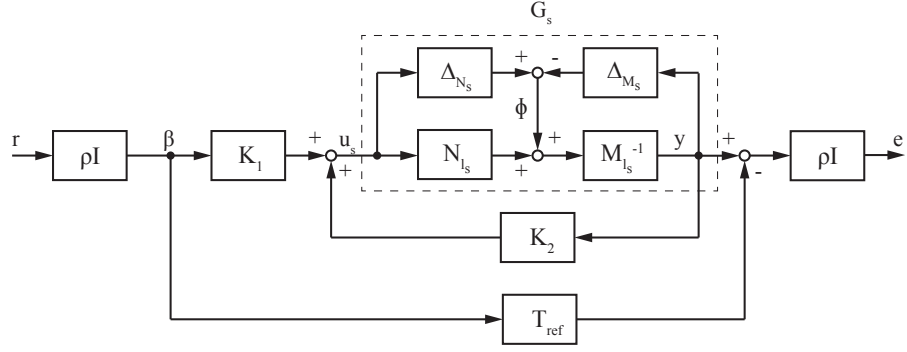


Figure 31: 2 DoF H_∞ loop-shaping design problem with prefilter K_1 and feedback controller K_2

In analog fashion to one degree-of-freedom H_∞ LSD a prefilter

$$W_1 = W_p W_a \quad (6.70)$$

is used to shape the SV of the open loop. W_p contains the dynamic shaping and is chosen to be equal to 6.65 for the same reasons given in section 6.7. The same is true for W_2 . Significant model uncertainties are expected at frequencies above about 6rad/s due to the limited description of the rotor dynamics (see 6.5.1.1). Therefore the gain crossover is set to 6rad/s by introducing an *alignment gain* W_a . The align algorithm used was first presented by Papageorgiou [26]. It basically calculates an approximate plant inverse at the desired frequency and can be used to set the 0dB crossover, [28]. The shaped plant is defined as $G_s = W_2 G W_1$.

Additionally, a *reference model* T_{ref} can be introduced to enforce the closed-loop system to behave in a desired manner. As suggested by Walker and Postlethwaite [39, p. 464] a second-order transfer function of the form

$$T_{ref}(s) = \frac{\omega_n^2}{s^2 + 2\xi\omega_n s + \omega_n^2} \quad (6.71)$$

is implemented as the reference model, also called *step reference model (SRM)*. The damping factor ξ and the natural frequency ω_n are chosen as summarized in table 5. The resulting *rise time*

$$t_r = \frac{\pi}{\omega_n \sqrt{1 - \xi^2}} \quad (6.72)$$

is given as well in table 5. As a starting point the parameters were set as suggested by Postlethwaite and Yue [28] and then iteratively adjusted until desirable reference tracking and disturbance rejection performances were achieved in simulation runs.

By adjusting the scalar parameter ρ the focus can be shifted between robustness and reference model matching. By setting $\rho = 0$ model matching is neglected and the design problem reduces to the robust stabilization problem, i.e. minimizing the H_∞ of the transfer function matrix from ϕ to $[u_s^T \ y^T]^T$. In our case ρ is set to 1.5. Skogestad and Postlethwaite [32] suggests values in the range of 1 to 3.

Natural frequency ω_n [rad/s]	Dampening factor ζ	Rise time t_r [s] ⁵
2.20	0.71	2.03

Table 5: Parameters of the desired heave dynamics response

The design problem is based on finding a stabilizing controller that minimizes the effect of the reference signal r and the uncertainty signal ϕ on the control error e , the control input to the shaped plant u_s and the output signal y . This effect is quantized by the H_∞ norm of the transfer function matrix T that maps the exogenous input signal $w = [r \ \phi]$ to the exogenous output signals $z = [u_s \ y \ e]$

$$T : [r \ \phi]^T \mapsto [u_s \ y \ e]^T.$$

T can be directly derived from figure 31. The process is demonstrated in exemplary manner on $T_{21} : r \mapsto y$

$$\begin{aligned} y &= G_s u_s = G_s \begin{bmatrix} K_1 & K_2 \end{bmatrix} \begin{bmatrix} \beta \\ y \end{bmatrix} = G_s (K_1 \rho r + K_2 y) \Leftrightarrow \\ y &= \underbrace{\frac{G_s}{I - G_s K_2} K_1 \rho}_{\substack{\text{prefilter} \\ T_{21}}} r, \end{aligned}$$

eq. (6.73) shows T

$$\begin{bmatrix} u_s \\ y \\ e \end{bmatrix} = \begin{bmatrix} \rho(I - K_2 G_s)^{-1} K_1 & K_2(I - G_s K_2)^{-1} M_s^{-1} \\ \rho(I - G_s K_2)^{-1} G_s K_1 & (I - G_s K_2)^{-1} M_s^{-1} \\ \rho^2[(I - G_s K_2)^{-1} G_s K_1 - T_{ref}] & \rho(I - G_s K_2)^{-1} M_s^{-1} \end{bmatrix} \begin{bmatrix} r \\ \phi \end{bmatrix}. \quad (6.73)$$

Its elements T_{ij} can be interpreted as follows. T_{11} and T_{21} limit actuator usage. T_{12} and T_{22} are related to robust stabilization. By comparing it with (6.58) it becomes apparent that $[T_{12} \ T_{22}]$ is equal to the transfer function of the robust stability criterion 6.58. T_{31} ensures model matching and T_{32} is related to the performance of the loop, [32, p. 374].

One way to calculate a stabilizing controller, that minimizes the H_∞ norm of the closed loop transfer function T from w to z , is to cast the problem into the general control configuration and apply the general H_∞ algorithm and γ -iteration as described in section A.1. Therefore we have to derive the generalized plant P , which is defined as

$$\begin{bmatrix} z \\ w \end{bmatrix} = \underbrace{\begin{bmatrix} P_{11} & P_{12} \\ P_{21} & P_{22} \end{bmatrix}}_P \begin{bmatrix} w \\ u \end{bmatrix}$$

At first we determine z, v, w, u and then set up z and w as functions of w and u

$$\begin{aligned}
z: \quad & \text{outputs to minimize: } [u_s \quad y \quad e]^T \\
v: \quad & \text{input to } K: [\beta \quad y]^T \\
w: \quad & \text{external input to } P: [r \quad \phi]^T \\
u: \quad & \text{input signal to } G_s: u_s = [K_1 \ K_2] \begin{bmatrix} \beta \\ y \end{bmatrix} = Kv
\end{aligned}$$

$$\begin{aligned}
u_s &= K_1\beta + K_2y = K_1\rho Ir + K_2M_s^{-1}(\phi + N_s u_s) \\
y &= M_s^{-1}(\phi + N_s u_s) \\
e &= \rho Iy = \rho IM_s^{-1}(\phi + N_s u_s) - \rho IT_{ref}\rho Ir \\
\beta &= \rho Ir.
\end{aligned}$$

Reformulating these results in matrix form yields

$$\begin{aligned}
\left\{ \begin{array}{c} z \\ v \end{array} \right\} \begin{bmatrix} u_s \\ y \\ e \\ \beta \\ y \end{bmatrix} &= \underbrace{\begin{bmatrix} 0 & 0 & I \\ 0 & M_s^{-1} & G_s \\ -\rho^2 T_{ref} & \rho M_s^{-1} & \rho G_s \\ \rho I & 0 & 0 \\ 0 & M_s^{-1} & G_s \end{bmatrix}}_P \begin{bmatrix} r \\ \phi \\ u_s \end{bmatrix} \left\{ \begin{array}{c} w \\ u \end{array} \right\}
\end{aligned} \tag{6.74}$$

Now the general H_∞ algorithm (see A.1) can be applied to the generalized plant P in eq. (6.74). γ -iteration is used to find a suboptimal controller that fulfills $\gamma > \gamma_{min}$. The truly optimal controller, i.e. $\gamma = \gamma_{min}$ is usually not desirable – mostly for practical reasons. The closer the controller moves to optimality the faster the controller poles become [32, p.507]. This can be disadvantageous if a discretized version of the controller is needed since the required sampling rates would increase. If a truly optimal controller is desired, the algorithm presented in 6.7.2 cannot be implemented; $\gamma = \gamma_{min}$ yields singular L . Two distinct approaches for solving for controllers that achieve $\gamma = \gamma_{min}$ were presented by Safonov et al. [30] and Glover [6].

6.8.0.1 Analyzing final Controller

Figure 32 shows singular value bode plots of the loop transfer function, the input (output) sensitivity $S = (I - K_2G)^{-1}$ and input (output) complementary sensitivity $K_2G(I - K_2G)^{-1}$. Note, since G and K are one-dimensional transfer functions $GK = KG$ holds true. Therefore the input and output sensitivity functions⁶ and the input and output complementary sensitivity functions are identical, i.e.

$$S_{in} = (I - K_2G)^{-1} \stackrel{SISO}{=} S_{out} = (I - GK_2)^{-1} \tag{6.75}$$

and

$$T_{in} = K_2G(I - K_2G)^{-1} \stackrel{SISO}{=} T_{out} = GK_2(I - GK_2)^{-1}. \tag{6.76}$$

⁶ S_{in} and S_{out} are the transfer matrices from d_u to u and d_y to y , respectively. For our example the following $u = z_1, y = Z_2, d_u = d_1$ and $d_y = d_2$ holds true, see also fig. 26.

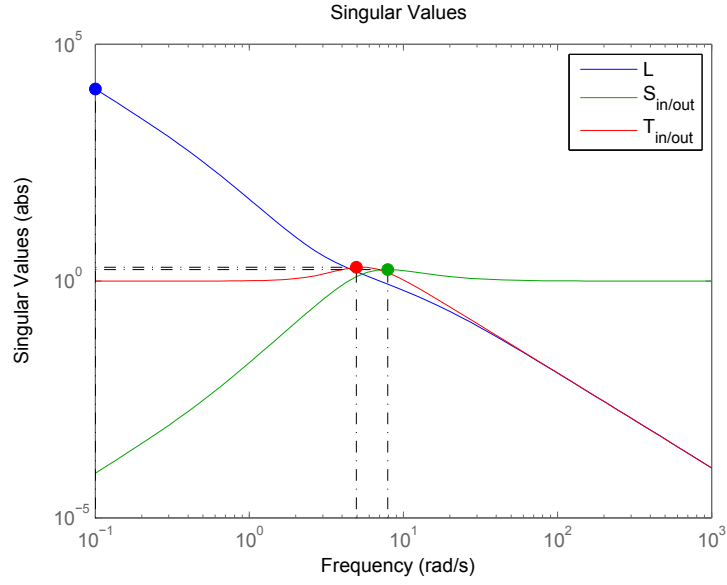


Figure 32: Singular value bode plots of the loop transfer function, the input/output sensitivity $S = (I - K_2 G)^{-1}$ and input/output complementary sensitivity $K_2 G(I - K_2 G)^{-1}$

As desired the loop transfer function has a slope of -2 in higher and lower bandwidth regions and a slope of -1 at the predefined crossover frequency of approximately 6 rad/s. The peak values of S and T are 1.75 and 1.97.

SIMULATION RESULTS (CONTROLLER COMPARISONS)

This chapter presents a comparison of the performances of the various controller designs of chapter 6. Based upon the simulation results a final controller design was picked and benchmarked in flight experiments on the HE-2 helicopter. See [Kondak et al. \[16\],\[17\],\[19\]](#) for more technical information about the helicopter and its on-board software.

7.1 SIMULINK MODEL

Figure 33 shows the Simulink Model being used to evaluate the performances of the different controllers. The model allows to impose disturbances on the system: noise on the output, wind disturbances, input disturbance and parameter variation on G_z . The results of these simulation runs are summarized in table 7.

7.1.1 Step Response

Step response performance is shown in figure 34. The maximum overshoot value $|y_{max}|$ for a unit step response and the rise-time t_r to 90% of the final value are given for each of the controllers in table 7.

7.1.2 Disturbance Rejection

To imitate the noise of the measured height signal on the helicopter under real flight conditions, the noise's frequency and amplitude was estimated and then replicated by a Band-Limited White Noise block in Simulink. The effects of vertical wind gusts on the system were also tried to replicate in the Simulink model by disturbing the vertical velocity state, see section 3.7.7. Based on the superior disturbance rejection capabilities the 2 DoF LSD controller was picked as the one to be implemented on the helicopter.

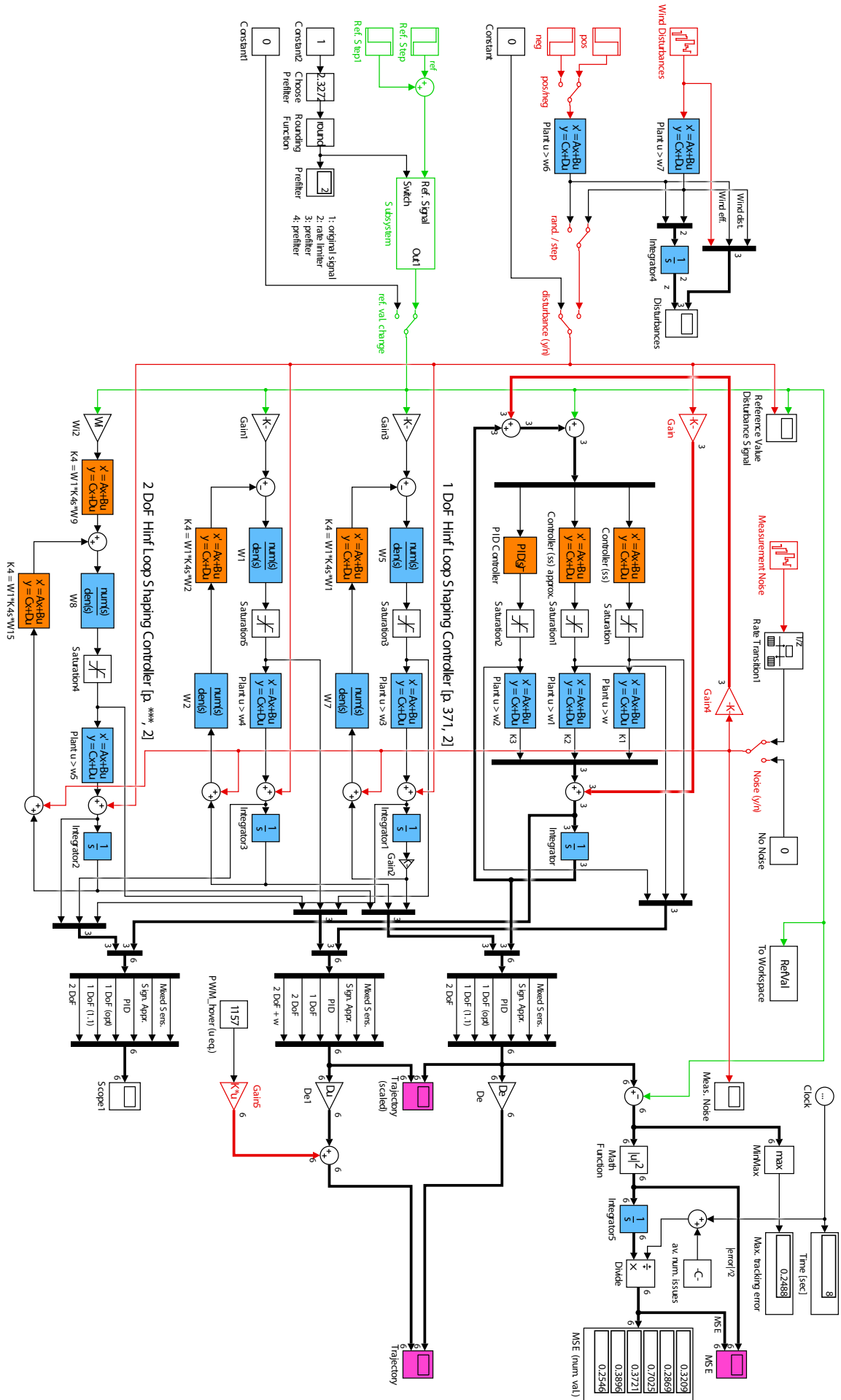


Figure 33: Simulink model for comparison of the different controller designs

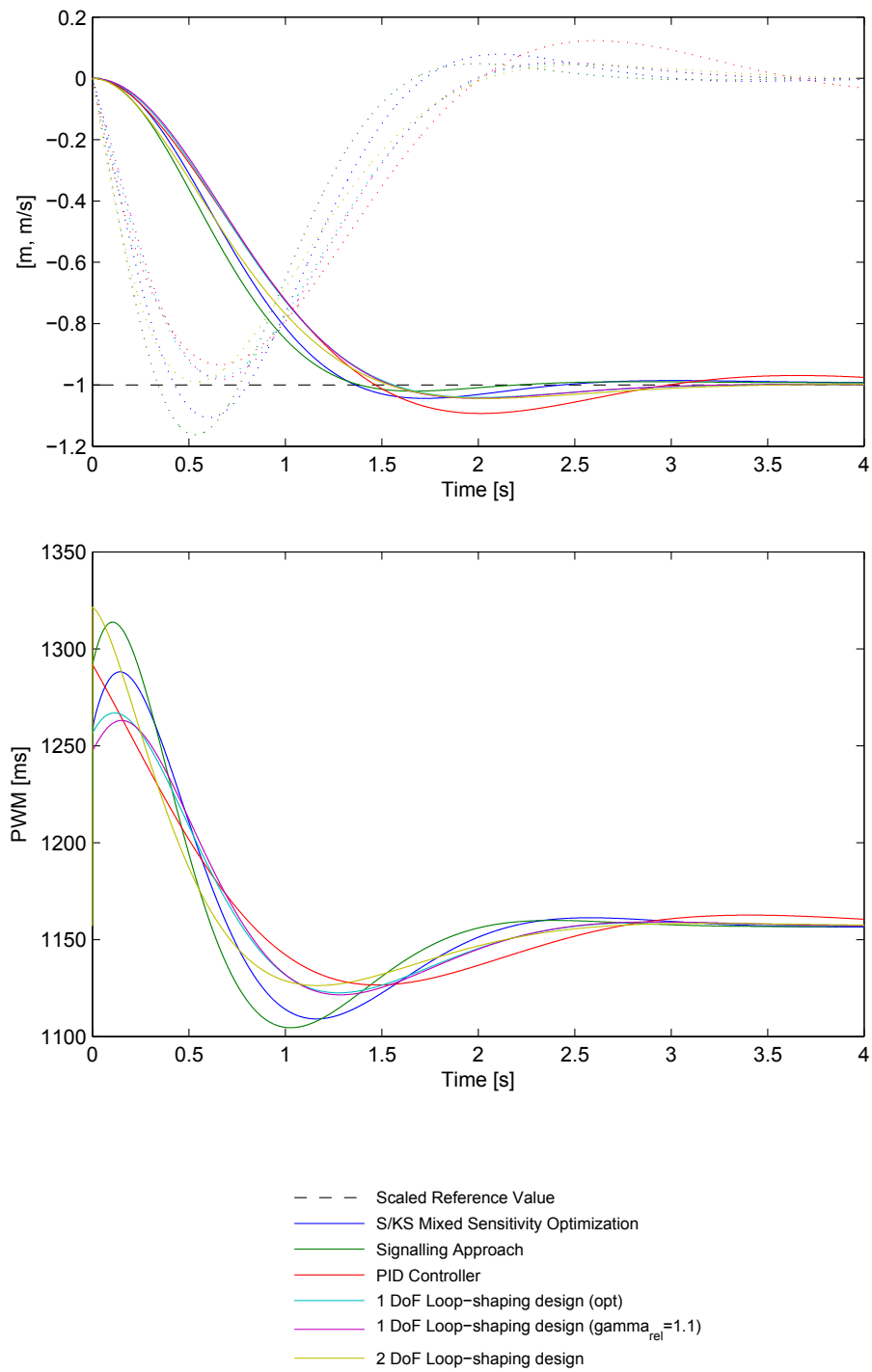


Figure 34: Unit step response and control input, climbing 1 m

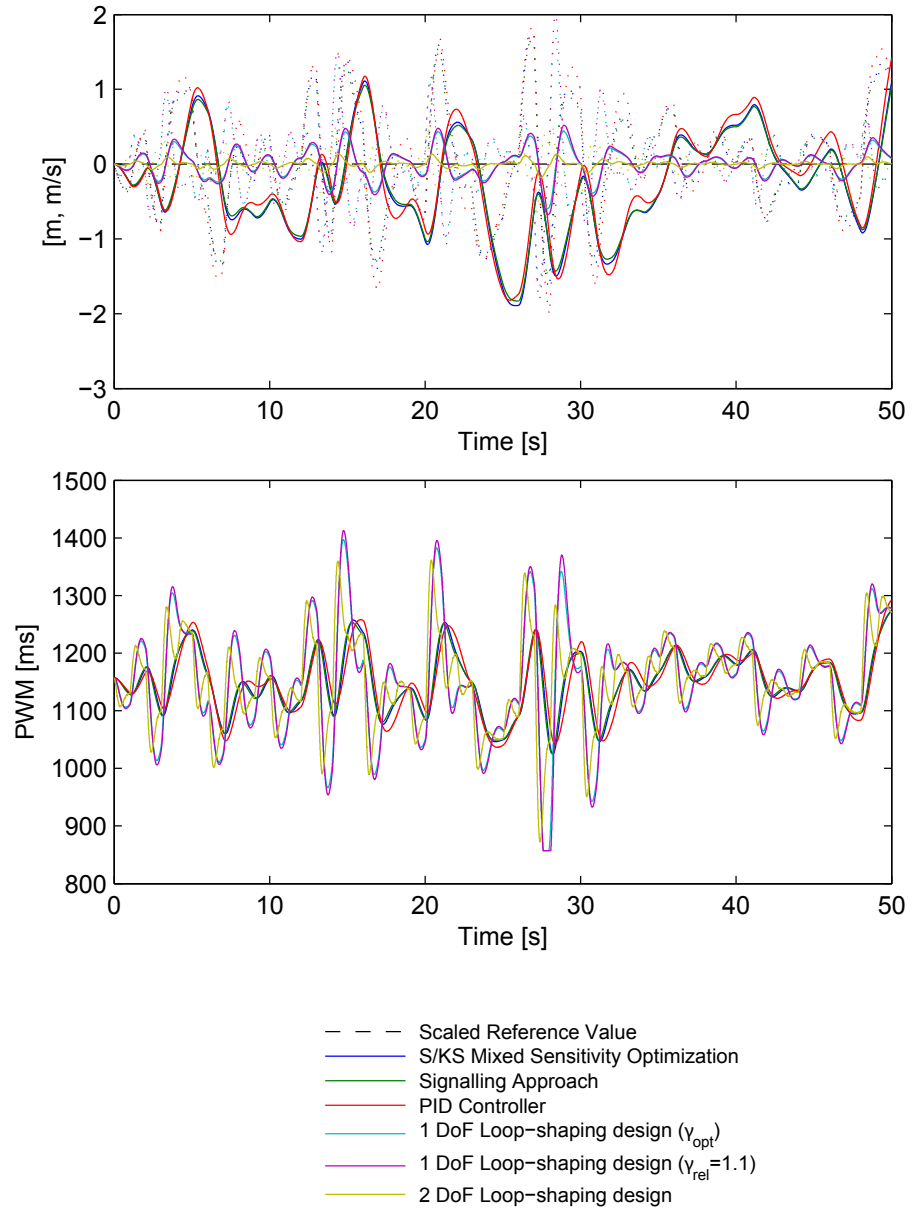


Figure 35: Comparison of the disturbance rejection capabilities; output noise, wind disturbances

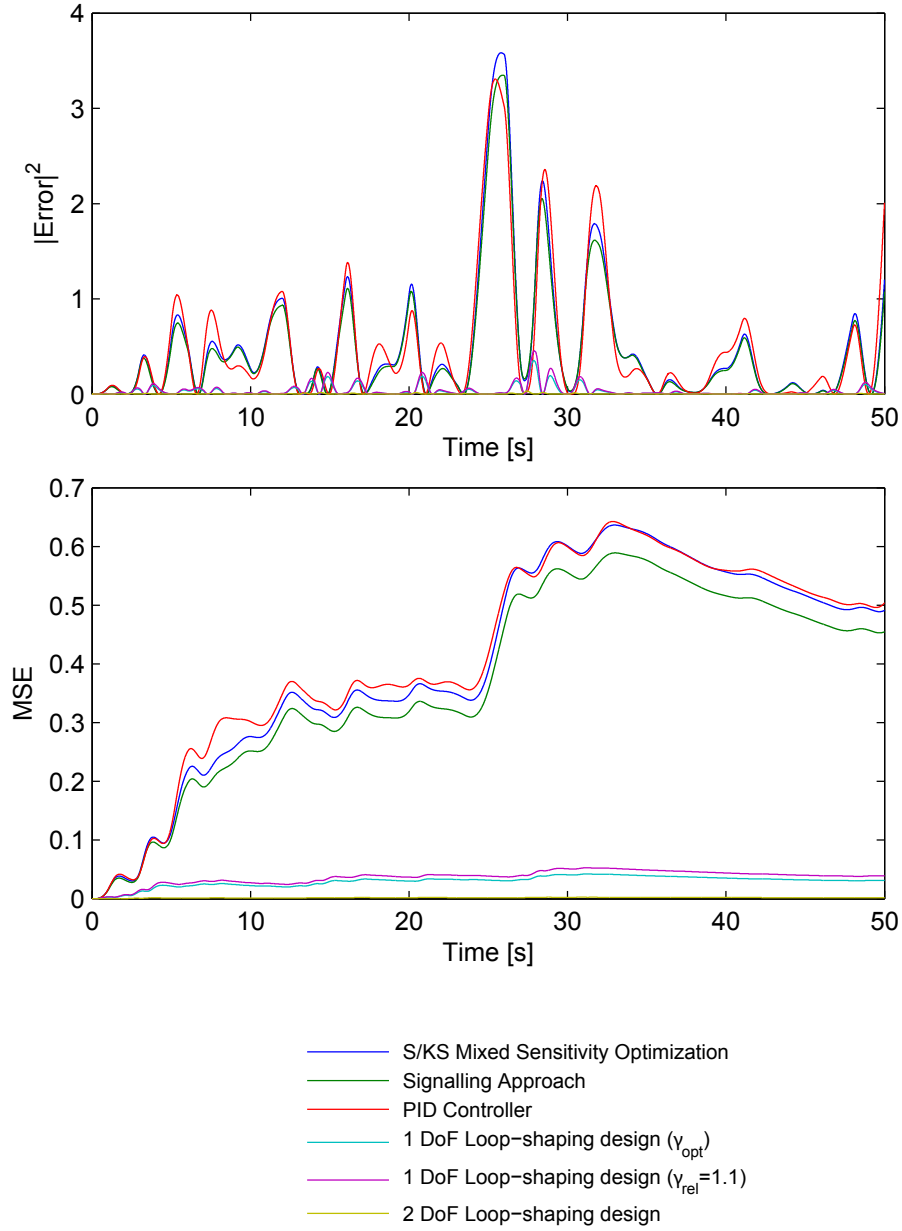


Figure 36: Temporal course of $|e|^2$ and the MSE. The helicopter system is affected by output noise and wind disturbances

Controller Design	MSE	$ e _{\max}^2$
S/KS Mixed Sensitivity Optimization	5.52×10^{-1}	4.004
Signalling Approach	4.99×10^{-1}	3.642
PID Controller	7.05×10^{-1}	3.870
1 DoF Loop-Shaping Design ($\gamma = \gamma_{\min}$)	7.02×10^{-2}	0.648
1 DoF Loop-Shaping Design ($\gamma_{\text{rel}} = 1.1$)	8.64×10^{-2}	0.807
2 DoF Loop-Shaping Design	2.91×10^{-3}	0.0407

Table 6: Comparison of the disturbance and output noise rejection capabilities of the different controller designs in terms of MSE and maximum squared error. Simulation time: 100 s.

	n	$\gamma = \ N\ _{\infty}$	ω_c [rad/s]	M_S	M_T	GM	PM	Reference			Disturbance		
								Delay	t_r [s]	$ y_{\max} $	$y(t=1)$	e_{MSE}	$ e _{\max}$
Mixed sens.	4	1.88	1.55	1.44	1.00	6.60	64.3°	0.72	1.08	1.04	0.23	5.52×10^{-1}	2.00
Sign. appr.	4	1.67	1.60	1.38	1.00	8.04	67.24°	0.74	1.20	1.01	0.22	4.99×10^{-1}	1.91
PID	-	-	1	-	-	-	-°	0.74	1.22	-	0.24	7.05×10^{-1}	1.97
1 DoF LSD	3	3.50	3.70	2.20	2.27	11.4	27.1°	0.13	1.08	1.06	0.07	7.02×10^{-2}	0.80
1 DoF LSD*	3	3.18	3.79	1.99	2.12	∞	29.7°	0.14	1.08	1.05	0.06	8.64×10^{-2}	0.90
2 DoF LSD	5	3.82	7.04	1.75	1.97	2.34	29.6°	0.074	1.21	1.01	0.002	2.91×10^{-3}	0.20

Table 7: Performance comparison of different H_{∞} -optimization based controller designs. * indicates that $\gamma = \gamma_{\min}$.

n	controller order
γ	reached H_{∞} norm of N in gamma-iteration
ω_c	gain crossover frequency
M_S	maximum singular value of S
M_T	maximum singular value of T
GM	gain margin
PM	phase margin
Delay	how much phase lag the system can tolerate, see eq. 6.19
t_r	rise-time until the system reaches 90% of its final value after a unit step
$ y_{\max} $	maximum overshoot in a unit step response
$y(t=1)$	output value after a input disturbance (10% of the maximal allowed input value)
e_{MSE}	MSE under wind disturbance and output noise
$ e _{\max}$	maximum quadratic error under wind disturbance and output noise

Part III

FLIGHT EXPERIMENTS



*"No experiment is ever a complete failure. It can always be used
as a bad example."*

— Charles Dickson

FLIGHT EXPERIMENTS

As part of the master's thesis a number of flight experiments were conducted to analyze the performance of several different H_∞ 2 DoF controller designs. Starting with a rather conservative design the parameters were adapted to slowly increase the controllers performance.

Prior to testing the flight controller airborne with the newly designed H_∞ controller implemented, extensive and thorough ground tests were conducted to minimize risks. Special focus was set on the mechanism to switch between manual and autonomous flight mode. Switching over to autonomous mode requires all the internal states of the various state space systems, constituting the controller, to be reset to zero (orange blocks in fig. 33). Other issues were concerned with CPU overload of the respective on board processor. On ground analysis of the collective pitch response to vertical steps showed the necessity for an anti wind-up mechanism, especially for the more aggressive controller versions. The pre-compensator W_1 shows integral action (one pole at zero), which is necessary for low-frequency disturbance rejection. But in case of actuator saturation it keeps integrating and thereby causing windup issues. To avoid this problem W_1 is implemented in its *self-conditioned* form.

After resolving all the issues faced, nothing stood in the way of airborne flight experiments. The original cascaded PID controller that was developed over ten years ago and has been continuously adapted and tuned through out this time span was used as reference. Figure 37 shows HE-2 in flight with controller version FE03.



Figure 37: Test flight of HE-2 with controller version FE03

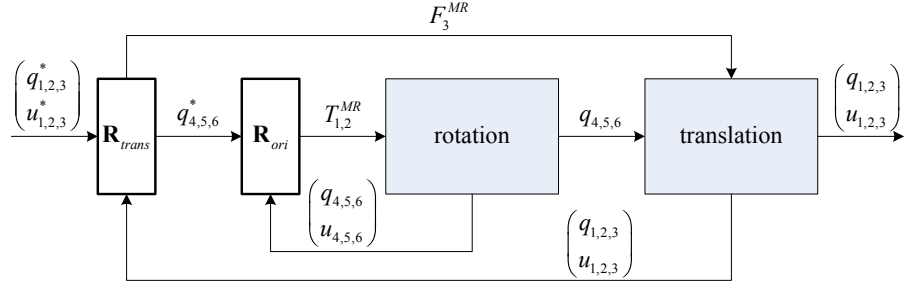


Figure 38: General scheme of the helicopter control [18]

8.1 IMPLEMENTATION OF THE H_∞ CONTROLLER INTO THE EXISTING FLIGHT CONTROLLER

The H_∞ norm based controller that showed the most promising potential in simulation was implemented in the existing flight controller framework, in its core it is based on cascaded PID controllers for orientation and position control. Solely the control part for the vertical dynamics was substituted with the newly designed controller while the rest of the control framework was left mostly unchanged (the control part for the other 5 degrees of freedoms was left unchanged). The original flight controller can be tuned by pole placement. The poles were set to standard values which are used for regular flight missions. The controller scheme is composed of an outer loop for position control and an inner loop for orientation control, see fig. 38. The outer loop controller \mathbf{R}_{trans} processes the position and velocity errors and determines the required translational accelerations to reduce these. It then determines the orientation of the main rotor plane q_4^*, q_5^* and the magnitude of the lifting force F_3^{MR} that are required to achieve these accelerations. Tracking of these desired angles q_4^* and q_5^* is ensured by the inner controller \mathbf{R}_{ori} . From the angular position and angular velocity error it computes the required angular accelerations and then derives the required torques T_1^{MR} and T_2^{MR} . The orientation about the body-fixed vertical axis \mathbf{b}_3 is controlled by a separate loop not shown here.

Detailed information about the controller scheme for attitude and position control can be found in [16], [18] and [19].

8.2 RESULTS

In total 3 different version of the H_∞ 2 DoF controller were tested in flight experiments. With safety concerns in mind, the first version was designed extremely conservatively. The first test flight was successful and the vertical performance was close to that of the PID controller. Based on the insights gained, two alternative H_∞ 2 DoF controllers variants were designed. Those will be referred to as FE02 and FE03. The according design parameters can be found in table 8.

Figure 39 shows the results of the test flight with the original PID controller. The average wind speed was 4.0 km/h and the wind gusts reached up

H_∞ contr. var.	λ	ω_a [rad/s]	ξ [kg/s]	ω_h [rad/s]	$T_{ref,rise}$ [s]
FE02	2	2	0.9	2.0	3.6
FE03	3	3	0.9	3.0	2.4

Table 8: Design parameters for the H_∞ 2 DoF controllers used in flight experiments

to 9.8km/h. During hovering phases, where good tracking performance is particularly important, the actual height stays within a 15 cm band of the reference value for most of the time. Higher deviations can be observed at the start of reference value changes where the controller reacts too slowly and the helicopter lags behind. At the end of climbing as well as descending phases, the helicopter clearly overshoots the reference height.

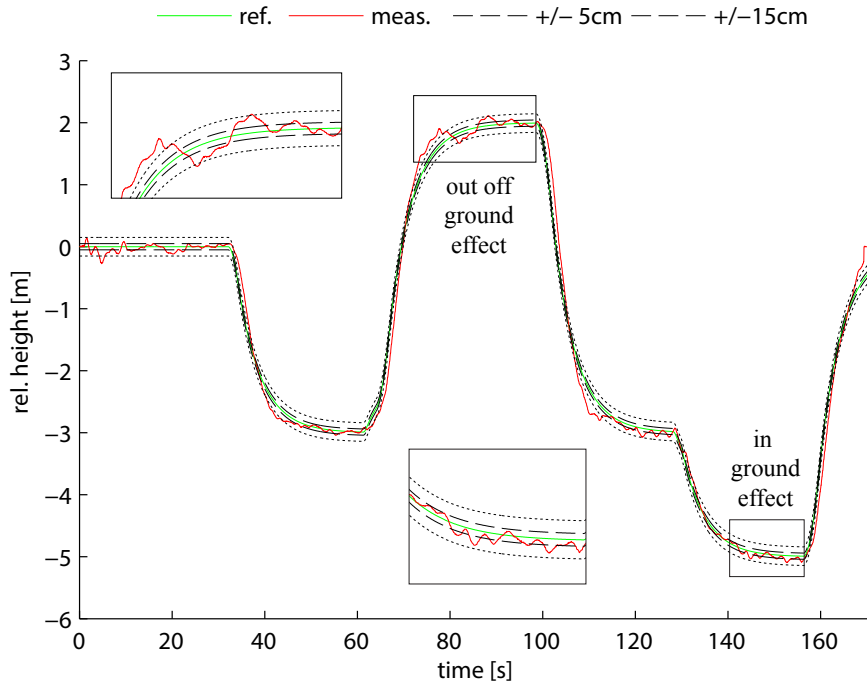


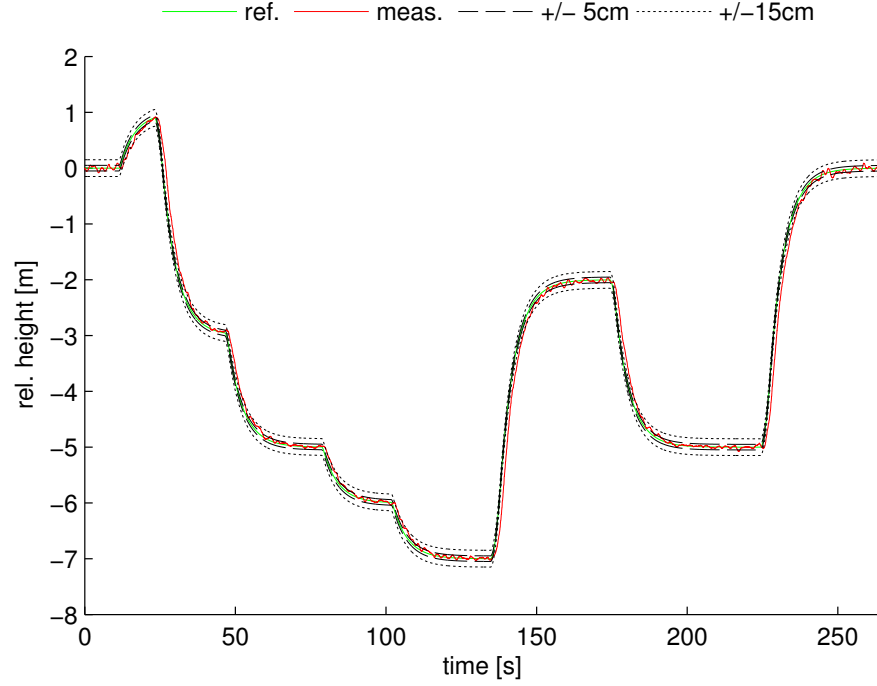
Figure 39: Flight Experiments with original PID controller

Results of test flight with controller FE02 are shown in fig. 40. There was no noticeable wind at that time.

Figure 41 shows the results of the test flight with the FE03 controller. Average wind speed was 4.8km/h and the wind gusts reached up to 15.0km/h.

$$MSE = \frac{1}{n} \sum_{i=1}^n (z_{ref} - z_{meas})^2 \quad (8.1)$$

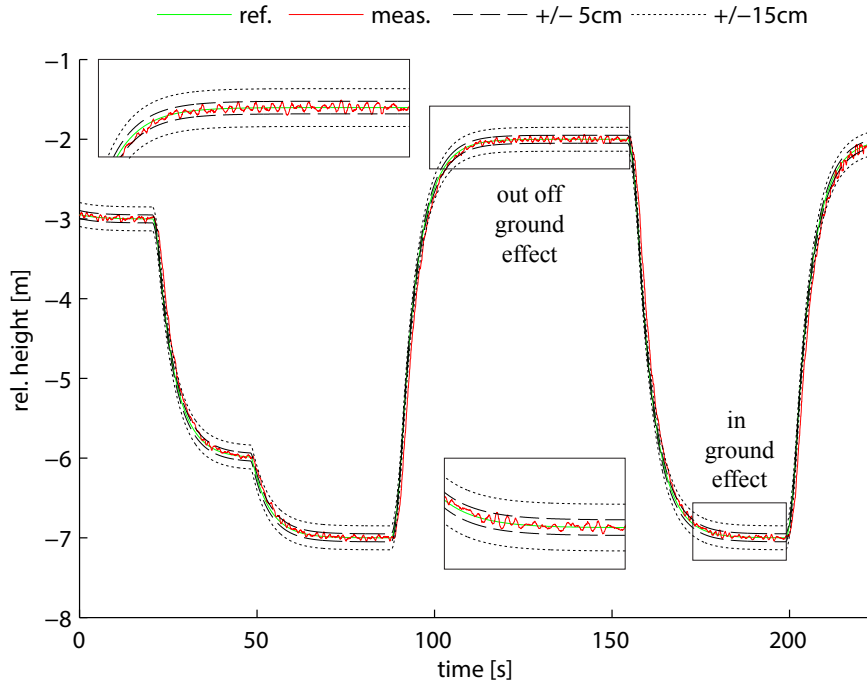
Controller FE03 shows similarly performance in hover conditions as the FE02 version, albeit slight better: $MSE_{h,FE03} = 4.3 \times 10^{-4}$ versus $MSE_{h,FE02} = 6.4 \times 10^{-4}$, see table 6, where MSE denotes the mean squared tracking error. Overall tracking performance, in terms of MSE, was increased by a factor of roughly two from 2.9×10^{-2} to 1.6×10^{-2} . Important results of the

Figure 40: Flight Experiments with H_∞ controller (FE02)

flight experiments are summarized in table 9 and visualized in fig. 42 and 43. $|z_{ref} - z_{meas}|_{max,h}$ denotes the maximum absolute control error.

During hovering phases the measured height stays mostly within a 5 cm band of the reference value. At the end of climbing and especially descending phases, shortly before the reference value flats out, the motion of the helicopter is a little jerky. When hovering the helicopter oscillates about the reference value with a period of about 2 s. The reason behind this will be subject to further investigations.

An analysis of the log data of the height and input signal suggests non-modeled delays as the reasons behind this undesired behavior. There are many sources of delays. The signal pathway of the received differential GPS to PMW servo input signal goes through many hardware components and gets processed by many processes on the on-board flight computer. Between each process the data gets written and read-out from an internal memory buffer. An estimation is hardly possible and specially designed hardware would be required to gain meaningful values. It has to measure the time an emulated GPS signal impulse takes to arrive at the Power Cube[®] output which feeds into the servo manipulating the main rotor collective pitch angle. In addition the GPS signal inherent delay itself has to be determined. Moreover, servo dynamics should be analyzed and modeled. Delay is definitely an important aspect which has to be investigated to further improve the controller performance and will be subject to future work. This behavior can be reproduced in simulation by including an output delay which supports the theory of delay induced oscillations. An input or output delay of 10 to 17 samples, which

Figure 41: Flight Experiments with H_∞ controller (FE03)

Controller	MSE [m^2]	hover	
		MSE _h [m^2]	$ z_{ref} - z_{meas} _{max,h}$ [cm]
PID	3.2×10^{-2}	3.8×10^{-3}	17
H_∞ 2 DoF LSD (FE02)	2.9×10^{-2}	6.4×10^{-4}	9.3
H_∞ 2 DoF LSD (FE03)	1.6×10^{-2}	4.3×10^{-4}	6.2

Table 9: Flight performance in terms of mean squared errors (MSE)

equals to 0.1-0.17 s, results in oscillations of the same period of about 2 s, which further supports the theory of delay-induced oscillations.

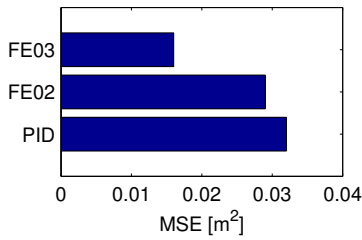


Figure 42: MSE overall

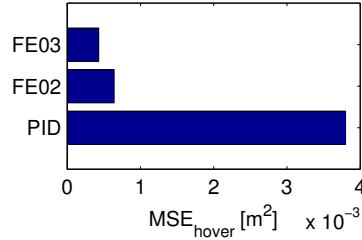


Figure 43: MSE in hovering



Figure 44: Autonomous helicopter with 7 DoF manipulator

8.3 CONCLUSION

The experimental data clearly indicate an improvement in the tracking performance. Especially in hover flight condition, when the helicopter is commanded to hold its current position the new H_∞ 2 DoF LSD outperforms the original cascaded PID controller.

Accurate tracking reference height and hovering at constant level are of utmost importance in the following scenarios that are relevant for us: (1) aerial manipulation with medium [31] and large-sized helicopters featuring a fully actuated, redundant robot arm [11], see also fig. 44, and (2) picking up ground based robotic systems in multi-robot missions [*** citation needed]. During all these operations the helicopter is required to deal with turbulences arising when operating in ground effect.

The height controller developed in this thesis can be easily adapted to other helicopters, providing that flight data exist which is suitable for system identification of the heave dynamics. It is planned to implement the new controller on all helicopter platforms of the DLR Flying Robots group in Oberpfaffenhofen. In near future more aerial manipulation missions are planned where the new controller should be able to show its benefits over the existing one.

By taking signal and servo delays into account in the model the controller is expected to be improved further.

Part IV

APPENDIX

MATHEMATICAL BACKGROUND

A.1 GENERAL H_∞ ALGORITHM

The idea behind H_∞ control is to minimize the H_∞ norm of $F_l(P, K)$, see (6.31). The most general and widely used algorithm for H_∞ control is based on the ideas presented in Glover and Doyle [7] and Doyle et al. [4]. To employ that algorithm the following assumptions have to be met

A.1 (A, B_2, C_2) are stabilizable and detectable.

A.2 D_{12} and D_{21} have full rank.

A.3 $\begin{bmatrix} A - j\omega I & B_2 \\ C_1 & D_{12} \end{bmatrix}$ has full column rank for all ω .

A.4 $\begin{bmatrix} A - j\omega I & B_1 \\ C_2 & D_{21} \end{bmatrix}$ has full rank for all ω .

A.5 $D_{11} = 0$ and $D_{22} = 0$ will simplify the algorithm formulas significantly but are not necessary conditions.

A.6 (A, B_1) is stabilizable and (A, C_1) is detectable.

The reasons behind those assumptions are given in the aforementioned papers.

Theorem A.1 (General H_∞ algorithm, Skogestad and Postlethwaite[32]). *For the general control configuration of figure 21 described by (6.27)-(6.30), with assumption A.1 to A.5, there exists a stabilizing controller $K(s)$ such that $\|F_l(P, K)_\infty\| < \gamma$ if and only if*

1. $X_\infty \geq 0$ is a solution to the algebraic Ricatti equation

$$A^T X_\infty + X_\infty A + C_1^T C_1 + X_\infty (\gamma^{-2} B_1 B_1^T - B_2 B_2^T) X_\infty = 0 \quad (\text{A.1})$$

such that $\text{Re } \lambda_i[A + (\gamma^{-2} B_1 B_1^T - B_2 B_2^T) X_\infty] < 0 \forall i$; and

2. $Y_\infty \geq 0$ is a solution to the algebraic Ricatti equation

$$A Y_\infty + Y_\infty A^T + B_1 B_1^T + Y_\infty (\gamma^{-2} C_1^T C_1 - C_2^T C_2) Y_\infty = 0 \quad (\text{A.2})$$

such that $\text{Re } \lambda_i[A + Y_\infty A^T + B_1 B_1^T + Y_\infty (\gamma^{-2} C_1^T C_1 - C_2^T C_2) Y_\infty] < 0, \forall i$; and

3. $\rho(X_\infty Y_\infty) < \gamma^2$.

All such controllers are then given by $K = F_l(K_c, Q)$ where

$$K_c(s) = \begin{bmatrix} A_\infty & -Z_\infty L_\infty & Z_\infty B_2 \\ F_\infty & 0 & I \\ -C_2 & I & 0 \end{bmatrix} \quad (\text{A.3})$$

$$F_\infty = -B_2^T X_\infty, \quad L_\infty = -Y_\infty C_2^T, \quad Z_\infty = (I - \gamma^{-2} Y_\infty X_\infty)^{-1} \quad (\text{A.4})$$

$$A_\infty = A + \gamma^{-2} B_1 B_1^T X_\infty + B_2 F_\infty + Z_\infty L_\infty C_2 \quad (\text{A.5})$$

and $Q(s)$ is any stable transfer function such that $\|Q\|_\infty < \gamma$. For $Q(s) = 0$ the so called *central controller*

$$K(s) = K_{c11}(s) = -F_\infty(sI - A_\infty)^{-1} Z_\infty L_\infty. \quad (\text{A.6})$$

The number of states of the resulting controller equal that of the generalized plant P .

A.2 ESSENTIALS OF LINEAR SYSTEM THEORY

Linear state space systems in terms of deviation variables, where x and u represent deviations from the equilibrium (trim) state, are written as

$$\dot{x}(t) = Ax(t) + Bu(t) \quad (\text{A.7})$$

$$y = Cx(t) + Du(t) \quad (\text{A.8})$$

$$(\text{A.9})$$

where A, B, C and D are real matrices.

Remark. The representation in (A.8) and (A.9) is not a unique description of a linear system.

$$x(t) = e^{A(t-t_0)}x(t_0) + \int_{t_0}^t e^{A(t-\tau)}Bu(\tau)d\tau \quad (\text{A.10})$$

$$e^{At} = I + \sum_{k=1}^{\infty} \frac{(At)^k}{k!} = \sum_{i=1}^n t_i e^{\lambda_i t} q_i^H \quad (\text{A.11})$$

A.3 COPRIME FACTORIZATION

Is a way of representing systems in transfer function form.¹ One distinguishes between the *left coprime factorization*

$$G(s) = M_l^{-1}(s)N_l(s) \quad (\text{A.12})$$

and the *right coprime factorization*

$$G(s) = N_r(s)M_r^{-1}(s) \quad (\text{A.13})$$

¹ Coprime Factorization of systems in state space representation is also possible

of G . Here N_l, M_l, N_r and M_r are stable coprime transfer functions.

Vidyasagar [38] presented a method to derive a normalized left coprime factorization of G , if G has a minimal state space realization

$$G \stackrel{s}{=} \left[\begin{array}{c|c} A & B \\ \hline C & D \end{array} \right]$$

with the coprime transfer functions given by

$$\begin{bmatrix} N_l(s) & M_l(s) \end{bmatrix} \stackrel{s}{=} \left[\begin{array}{c|cc} A+HC & B+HD & H \\ \hline R^{-\frac{1}{2}}C & R^{-\frac{1}{2}}D & R^{-\frac{1}{2}} \end{array} \right] \quad (\text{A.14})$$

where

$$\begin{aligned} H &\equiv -(BD^T + ZC^T)R^{-1} \\ R &\equiv I + DD^T \end{aligned}$$

and Z being the solution to the following algebraic Ricatti equation

$$(A - BS^{-1}D^TC)Z + Z(A - BS^{-1}D^TC)^T - ZC^TR^{-1}CZ + BS^{-1}B^T = 0$$

with

$$S \equiv I + D^TD.$$

MATLAB command `ncfmr` can be used to numerically find the normalized coprime factorization for G by using (A.14).

A.4 MATRIX NORM

Definition A.1 (Matrix Norm, [32]). For A and B in $K^{m \times n}$, $\|A\|$ denotes the norm of A if

1. $\|A\| \geq 0$ (non-negative)
2. $\|A\| = 0 \Leftrightarrow A = 0$ (positive)
3. $\|\alpha \cdot A\| = |\alpha| \|A\|$, $\alpha \in \mathbb{C}$ (absolute homogeneity)
4. $\|A + B\| \leq \|A\| + \|B\|$ (triangular inequality)
5. $\|AB\| \leq \|A\| \|B\|$ A and B in $K^{n \times n}$, (multiplicative property).

REMARK. From the second and third axiom results $\|A\| \geq 0$ (positivity).

FILE LIST

B.1 MAPLE

- [Dynamics_Kane_Basis_Vectors.mw](#) Implementation of Kane's method to derive the dynamics of a standard configuration helicopter composed of three rigid bodies.
- [Dynamics_Lagrange_euler_angles.mw.mw](#), [Dynamics_Lagrange_pqr.mw](#) Implementation of Lagrange's method to derive the dynamics of a standard configuration helicopter composed of three rigid bodies (using time-derivatives of the Euler angles and p, q, r to describe angular rotations, respectively).

B.2 MATLAB

- [align.m](#)

References:

1. Maciejowski, J.M., Multivariable Feedback Design, 1989, pp. 145–148
2. Edmunds, J., and Kouvaritakis, B., Extensions of the frame alignment technique and their used in the characteristic locus design method. Internation J. Control, 1979, 29, (5), pp.787–796

By Yi Cao, 1 May 1996, University of Exeter

Copyright 1996-2003 Sigurd Skogestad & Ian Postlethwaite

- [coprimeunc.m](#) Finds the controller which optimally robustifies a given shaped plant in terms of tolerating maximum coprime uncertainty. Used in the McFarlane-Glover H-infinity loopshaping procedure. Uses the robust control toolbox. Copyright 1996-2003 Sigurd Skogestad & Ian Postlethwaite.
- [Heave_Dynamics_02.m](#) Verification and analysis of the system identification results.
- [Heave_Dynamics_Controller_Hinf_LSD_1DoF.m](#) Algorithm to calculate the H_∞ 1 DoF LSD controller.
- [Heave_Dynamics_Controller_Hinf_LSD_2DoF.m](#) Algorithm to calculate the H_∞ 2 DoF LSD controller.
- [Heave_Dynamics_Controller_Hinf_Mixed_Sensitivity.m](#) Algorithm to calculate the H_∞ KS/S/T mixed sensitivity controller.

- [Heave_Dynamics_Controller_Plant_scaled.m](#) Scaling of the plant.
- [Heave_Dynamics_Controller_RUN.m](#) Execute this file to calculate the various controller designs presented in this thesis and to run Simulink model [SIMULINK_Controller_Comparison.slx](#) to compare them.
- [Heave_Dynamics_Parameters_Analytical.m](#) Analytical calculation of the Heave dampening parameter.
- [Hinf_mix_sens_weights.m](#) Contains definitions of the weights for the KS/S/T mixed sensitivity approach.
- [hinf2dof.m](#) synthesizes the H_∞ 2-DOF controller as described by [Skogestad and Postlethwaite](#) [32, p.375] by calling the function `hinfsyn` of the MATLAB robust control toolbox.
- [Plot_Results_of_Simulink_new.m](#) Plotting results of simulation.
- [PPWM2pitch_coll.m](#) Converts the PWM collective pitch signal into the resulting pitch angle for HE1 & HE2.
- [findGainM.m](#) Find gain at specified ω_c and inverse plant at that frequency. Copyright 1996-2003 Sigurd Skogestad & Ian Postlethwaite.

B.3 SIMULINK

- [SIMULINK_Controller_Comparison.slx](#) Model to test and compare different controller design
- [h_mech_ctrl.mdl](#) Flight controller for position and attitude control (programmed by Konstantin Kondak)
- [kalman_tmp.mdl](#) Kalman state observer (programmed by FlyRob Team)

BIBLIOGRAPHY

- [1] C. A. Desoer and M. Vidyasagar. Robust control systems design using h_∞ optimization theory. 15, July-August .
- [2] J. Doyle. Lecture notes in advances in multivariable control. ON-R/Honeywell Workshop, Minneapolis, USA.
- [3] J. C. Doyle, editor. *Synthesis of Robust Controllers and Filters*, number 22nd in IEEE. Conf. Decision, 1983.
- [4] J. C Doyle, K. Glover, P. P. Khargonekar, and B. A. Francis. State-space solutions to standard h_2 and h_∞ control problems. *IEEE Transaction on Automatic Control*, 1989.
- [5] Nichols Ean and U.S. Army. *Rotary Wing Flight (FAA Handbooks series)*. Aviation Supplies and Academics, 1992. ISBN 1560271183.
- [6] K. Glover. All optimal hanke-norm approximations of linear multivariable systems and their l_∞ -error bounds. *Internation Journal of Control*, 1984.
- [7] K. Glover and J. C. Doyle. State-space fomulae for all stabilizing controller that satisfy an h_∞ norm bound and realations to risk sensitivity. *Systems and Control Letters*, 1988.
- [8] K. Glover and D. McFarlan. Robust stabilization of normalized coprime factor plant descriptions with h_∞ bounded uncertainty. *IEEE Transaction on Automatic Control*, 1989.
- [9] K Glover, J. Sefton, and D.C. McFarlan. *A Tutorial on Loop Shaping using H_∞ Optimization Theory*.
- [10] Da-Wei Gu, Petko H. Petkov, and Mihail M. Konstantinov. *Robust Control Design with MATLAB*. Springer, 2012.
- [11] F. Huber, K. Kondak, K. Krieger, D. Sommer, M. Schwarzbach, M. Laiacker, I Kossyk, S. Parusel, S. Haddadin, and A Albu-Schaffer. First analysis and experiments in aerial manipulation using fully actuated redundant robot arm. In *Intelligent Robots and Systems (IROS), 2013 IEEE/RSJ International Conference on*, pages 3452–3457, 2013. doi: 10.1109/IROS.2013.6696848.
- [12] Ronald L. Huston. Multibody dynamics formulations via kane’s equations. *American Institute of Aeronautics and Astronautics*, 1990.
- [13] Reza N. Jazar. *Theory of Applied Robotics: Kinematics, Dynamics, and Control*. Springer Publishing Company, Incorporated, 2007. ISBN 0387324755, 9780387324753.

- [14] Thomas R. Kane and David A. Levinson. *Dynamics, Theory and Applications*. McGraw Hill, 1985.
- [15] S. K. Kim and Tilbury D. M. Mathematical modeling and experimental identification of an unmanned helicopter robot with flybar dynamics. *Journal of Robotic Systems*, 2004.
- [16] K.Konstantin Kondak, Markus Bernhard, Nicolas Meyer, and Günter Hommel. Autonomously flying vtol-robots: Modeling and control. In *IEEE International Conference on Robotics and Automation*, 2007.
- [17] Konstantin Kondak. *Modeling, simulation and motion control of complex robotic systems*. Technical University of Berlin, Berlin, Germany, 2006.
- [18] Konstantin Kondak, Bernhard Markus, Losse Nikolas, and G  nter Hommel. Elaborated modelling and control for autonomous small sized helicopters.
- [19] Konstantin Kondak, Carsten Deeg, G  nter Hommel, Marek Musial, and Volker Remu  . Mechanical model and control of an autonomous small size helicopter with a stiff main rotor. In *Proceedings of 2004 IEEE WRSJ International Conference on Intelligent Robots and Systems*, 2004.
- [20] J. Gordon Leishman. *Principles of Helicopter Aerodynamics*. Cambridge University Press, 2006.
- [21] X. P. Li, B. C. Chang, S. S. Banda, and H. H. Yeh. Robust control systems design using h_∞ optimization theory. *Journal of Guidance, Control, and Dynamics*, 1992.
- [22] McFarlan and Glover. Robust controller design using normalized coprime factor plant descriptions. *Vol. 138 of Lecture Notes in Control and Information Sciences*, Springer-Verlag, Berlin, 1990.
- [23] Bernard Mettler. *Identification Modeling and Characteristics of Miniature Rotorcraft*. Springer Science+Business Media, New York, Boston, MA, USA, 2nd edition, 2003.
- [24] Bernhard Mettler, Mark B. Tischler, and Takeo Kanade. System identification of small-size unmanned helicopter dynamics. *American Helicopter Society 55th Forum*, 1999.
- [25] Gareth D. Padfield. *Helicopter Flight Dynamics*. Blackweel Publishing, 207.
- [26] George Papageorgiou. Two-degree-of-freedom control of an actively controlled wind-tunnel model. *Journal of Guidance, Control, and Dynamics*, 25, July-August 2002.

- [27] I. Postlethwaite and D.J. Walker. Advanced helicopter flight control using two-degree-of-freedom h_∞ optimisation. *American Institute of Aeronautics and Astronautics*, 1995.
- [28] I Postlethwaite and A. Yue, editors. *Improvement of Helicopter Handling Qualities using H_∞ -Optimisation*, 1990.
- [29] A. Purushotham and Anjeneyulu J. Kane’s method for robotic arm dynamics: a novel approach. *IOSR Journal of Mechanical and Civil Engineering (IOSR-JMCE)*, 6(4):7–13, May-June 2013. URL http://www.academia.edu/4815763/Kanes_Method_for_Robotic_Arm_Dynamics_a_Novel_Approach.
- [30] M. G. Safonov, D. J. N. Limbeer, and R. Y. Chiang. Simplifying the h_∞ theory via loopshifting, matrix-pencil and descriptor concepts. *International Journal of Control*, 1989.
- [31] Marc Schwarzbach, Konstantin Kondak, Maximilian Laiacker, Chia-Yen Shih, and Pedro Jose Marron. Helicopter uav systems for in situ measurements and sensor placement. In *Geoscience and Remote Sensing Symposium (IGARSS), 2012 IEEE International*, pages 4766–4769, 2012. ISBN 978-1-4673-1160-1.
- [32] Sigurd Skogestad and I.Ian Postlethwaite. *Multivariable Feedback Control: Analysis and Design*. Wiley, 2nd edition, 2005. ISBN 978-0-470-01167-6.
- [33] Ismaila B. Tijani, Rini Akmeliawati, Ari Legowo, Agus Budiyo, and A.G. Abdul Muthalif. h_∞ robust controller for autonomous helicopter hovering control. *Aircraft Engineering and Aerospace Technology*, 2011.
- [34] Mark B. Tischler and Robert K. Remple. *Aircraft and Rotorcraft System Identification: Engineering Methods with Flight Test Examples (AIAA Education)*. AIAA Education Series, 2012.
- [35] Hannu T. Toivonen. Signal and system norms. URL <http://users.abo.fi/htoivone/courses/robust/>.
- [36] NASA Tom Benson. Lift from flow turning. Webpage, July 2014. URL <http://www.grc.nasa.gov/WWW/k-12/airplane/right2.html>.
- [37] Kimon P. Valavanis. *Advances in Unmanned Aerial Vehicles*. Springer, 2007.
- [38] M. Vidyasagar. Control system synthesis: A factorization approach for non-strictly proper systems. *IEEE Transaction on Automatic Control*, 1988.
- [39] D.J. Walker and I. Postlethwaite. Advanced helicopter flight control using two-degree-of-freedom h_∞ optimization. 1996.

- [40] Kemin Zhou. *Essentials of Robust Control*. Tom Robbins, 1998.
- [41] Ziegler and Nichols. Mathematical modeling and experimental identification of an unmanned helicopter robot with flybar dynamics. 2004.